

**Investigation of ion channel activity in alveolar
epithelial cells.**

The development of lung slice in-vitro model.

Steven Abraham Bourke BSc. (Hons).

Submitted in accordance with the requirements for the degree of
Master of Philosophy.

Cardiff University.

Cardiff School of Biosciences.

March 2010.

DECLARATION

This work has not previously been accepted in substance for any degree and is not concurrently submitted in candidature for any degree.

Signed (candidate)

Date.....

STATEMENT 1

This thesis is being submitted in partial fulfilment of the requirements for the degree of PhD.

Signed (candidate)

Date

STATEMENT 2

This thesis is the result of my own independent work/investigation, except where otherwise stated.

Other sources are acknowledged by explicit references.

Signed (candidate)

Date

STATEMENT 3

I hereby give consent for my thesis, if accepted, to be available for photocopying and for inter-library loan, and for the title and summary to be made available to outside organisations.

Signed (candidate)

Date

Summary.

Investigation of ion channel activity in alveolar epithelial cells. The development of an in-vitro lung slice model.

The alveolar epithelium maintains lung fluid homeostasis by active ion transport. The molecular machinery required to create an osmotic gradient across the alveolar epithelium, which in turn moves water out of the airspaces, has been identified by number of experimental techniques. The alveolar epithelium, which covers 95% of the surface area of the lung, is composed of two morphologically distinct epithelial cell types: alveolar epithelial type one and alveolar epithelial type two cells. The much studied alveolar epithelial type two cell, which cover <5% of the surface, contain the myriad of ion channel and transports required to undertake fluid transport. The alveolar epithelial type one cell, which covers >95% of the surface area, is less well characterised. Direct functional electrophysiological measurements from the alveolar epithelial type one cell has proved difficult to obtain.

In order to obtain novel recordings the unfilled lung slice experimental model was developed. This experimental model demonstrated excellent cellular viability. VIII B2 mouse monoclonal antibody, a specific cell marker for alveolar epithelial type one cells, was used to obtain live cell immunohistochemistry, the first such reported in peripheral tissue. The results presented in this thesis represent the first published ion channel recordings from identified alveolar epithelial type one cells within a rat lung slice (Bourke, S. *et al* 2005). Cell-attached, patch-clamp recordings demonstrated the presence of a voltage-dependant, K⁺ selective ion channel with a measured unitary conductance of 21 pS. The findings contained within this thesis present a novel experimental technique to investigate the functional physiological role of the alveolar epithelial cells.

The alveolar epithelium is reliant upon Ca²⁺ signalling mechanisms to undertake a number of normal physiological activities. The release of surfactant from the alveolar epithelial type two cell lamellar bodies relies on a Ca²⁺ dependant exocytosis step. To investigate further the function of Ca²⁺ in the alveolar cells, experiments were undertaken using Ca²⁺ fluorescent indicator dye Fluo-3. Slices demonstrated spontaneous Ca²⁺ oscillations. Application of a number of physiological and pharmacological substances failed to modulate the observed activity.

*“The unknown is not to be feared. It is to be examined, understood and
accepted.”*

“Close friends become family and family is the true centre of the universe.”

Dave Marinaccio

Dedicated to Joe and Claire.

Acknowledgments.

Over the period of this thesis there are so many people who have influenced, helped and become friends with along the way.

I want to take this opportunity to thank Professor Paul Kemp. My mentor, friend and all round “dude”. Who should be praised no end for his help, guidance, and support over all the years of lung slice fun and frolics. Paul, you asked me a question the very first day we met and as it turn out it was the most astute question you could have asked. It has taken me till now to fully understand the wisdom behind that “silly” question. Heartfelt thanks for everything and I look forward to many years of productive work and friendship.

Leeds. “Each day I wake and thank the lord I wake in Yorkshire”. To the original lab rats and bosses. Dr. Miller (squeaky and original slicing guru), Dr. Searle (climbing and questions galore), Dr. Plant (perfect dry humor), Dr. Wotton (fun beyond words), Dr. Lewis (Northern monkey), Dr. Peason (phantom chestnut neuroscientist), Professor Peers (wonderfully wicked and all round good man) there were so many fun time and productive days. You are all superstars and helped me to achieve many hangovers and lots of wonderful slice success. To the original “Chancers”, Dr. Dallas (the best beer buddy ever!) and Dr. Dr. Gillies (perfect company) God bless the grove and all who lived in her. Matty Markingson (biker god) you are still and always will be a biker GOD even if the babies now live with me. Colin Miller (weeman) rugby rules! A word also for Ammid (loss to science), rest in peace, you are remembered.

Cardiff. “Each day I wake and thank the lord I wake in Wales”. Dr. Riccardi (Italian science guru) you and Kemp make a great team, Dr. Mason (taught me a trick or two), Dr. Brazier (the quite one, always watch the quite one), Dr. Williams (Yeah MAN), Dr. Finney (superstar who can kick so high). There can be no doubt

that I shall be friends with you all for many years to come. Rhys (Plaid PC) the rugby weekend ends with Abber boys shall continue for many a year.

The Antwerp crowd should stand up and take a bow, Dr. DeProost (lung buddy), Dr. Pinton (my immuno go to girl), and Professor Adriaensen (always a gent and a lover of good beer).

There are other people who should not go unmentioned a chink of glasses and a warm thanks. Scientifica, Mark Johnson (Rodger Millie of stability), Matt Kemp (Mr. Tickle and the best sales man I know), Sias Jorrdan (perfect gent). Tomas Bayton "hyphen" Williams the Third (BW you are a legend, Nuggets!), The KK boys Deco, Marky T and Muja and all the and girls. Rob Fahy (Mr Ireland, Coo Coo Thomas) Dr. Novak (the next noble prize winner), Dundalk, Dr. DeFaoite (Buck da Hate Mac A), Dr. Large (100 cement), Dr. Bradley (Linguistic legend), Baz (football hero). Dr. Hollywood, Dr. Sergeant, Dr. Thornbury and Professor McHale (all very patient and great to work with), Ciara (Binnty Mac Ginnty a lady who lunches), Aunty Mary (lifetime of prayers), and the family members who watch over me from above.

My family (GO ON THE CATS) has always been and continues to be full of words of support, understanding, and unmerciful slugging. Ruth (scientific mother hen, SWE), Rachel (my perfect foil and good friend and lover of water features, NZ) the two best sisters a boy could have. Ken "Bozwell" Garda Bourke (the garda from TV, ROI) you are a great friend, horrid older Bro, and have been there always. I owe you lot of thanks (and money) free bike services for life! I look forward to us all being together again soon.

Mum and Dad (Claire and Joe). You never doubted me and have always supported me. I know it is in the contract but you go so far past what is required. I love you both lots, you can now have a holiday as no you longer have to light the candles.

This thesis could not have been completed with out the help, guidance, and patience of all the people mentioned above and more besides to you all I am more grateful than words can ever allow me to express.

Table of contents	Page
Title page.	1
Copyright declaration.	2
Summary.	3
Acknowledgments.	6-7
Table of contents.	8-10
Table of figures.	11-12
Chapter 1. General introduction and literature review.	14-51
1.1 Respiratory anatomy and physiology.	14-19
1.2 Epithelial tissue morphology and physiological roles.	19-20
1.3 Epithelial transport.	20-25
1.4 Alveolar epithelium	25-26
1.5 Vectorial transport across alveolar epithelium.	26-29
1.6 Fetal and neonatal lung fluid homeostasis.	29-33
1.7 Postnatal lung fluid homeostasis.	34-35
1.8 Alveolar epithelial type one cells.	36-42
1.9 Alveolar epithelial type two cells.	42-46
1.10 Organ slice models.	46-49
1.11 Summary.	50
1.12 Aims of current research.	51
Chapter 2. Materials and methods.	53-69
2.1 Tissue culture methods.	53-60
2.1.1 HEK 293 cell culture.	53
2.1.2 Long-term storage of cell lines.	53
2.2 Preparation of lung slices.	
2.2.1 Animals.	54
2.2.2 Preparation of the lungs.	54-57
2.2.3 Sectioning of lung with the Integraslice®.	57
2.3 Live cell immunohistochemistry methods.	

2.3.1 Alveolar epithelial type one cells Identified with VIII B 2 monoclonal antibody.	59
2.3.2 Alveolar epithelial type two cells identified with Nile Red.	60
2.3.3 Alveolar epithelial type two cells identified with LysoTracker ® Green.	60
2.4 Electrophysiology methods.	60-65
2.4.1 Solutions.	60-61
2.4.1.1 Extracellular bath solutions for recording currents in lung slices.	61
2.4.1.2 Extracellular pipette solutions for cell attached recording.	61
2.4.2 Maintaining lung slice position.	61-62
2.4.3 Preparation of slices for electrophysiology recording.	
2.4.4 Patch-clamp electrodes.	62
2.4.5 Cell-attached configuration of the patch-clamp technique.	62-64
2.4.6 Experimental protocol for cell-attached patch-clamp.	
2.4.6.1 Standard ramp protocol.	64-65
2.4.6.2 Gap-free voltage-step protocol.	65
2.4.7 Data analysis and presentation of cell-attached patch-clamp recordings.	65
2.4.7.1 Calculating NP_o .	65
2.5 Slice viability staining methods.	65-67
2.5.1 Propidium iodide staining.	65
2.5.2 LIVE/DEAD® staining.	66-67
2.6 Calcium imaging methods.	67-68
Chapter 3. Slice optimisation, viability and live cell identification.	71-104
Introduction	72-76
3.1 Preparation of lung slices.	77-78
3.2 Cellular viability within lung slices.	78-84
3.2.1 Propidium iodide staining.	79-80
3.2.2 LIVE/DEAD® viability.	80-81
3.2.3 Slice viability assessed via LIVE /DEAD® stain	81-82
3.2.4 Unfilled lung slice cellular viability.	82-83
3.2.5 The effect of VIII B2 live cell imaging on cell viability.	83-84

3.3 Live cell identification within a lung slice.	84-87
3.3.1 VIIIIB2 alveolar epithelial type one cell identification live lung slice.	85-86
3.3.2 Alveolar epithelial type two live cell staining.	86-87
3.4 Discussion.	88-93
3.5 Conclusion.	93-94
Chapter 4. Electrophysiological investigation of identified alveolar epithelial type one cells in a lung slice.	106-122
Introduction	106-109
4.1 Locating and positioning of patch electrode with lung slice containing identified alveolar epithelial type one cells.	110-111
4.2 Electrophysiological recordings from identified alveolar epithelium cells in lung slice.	111
4.3 Cell attached gap free patch clamp protocol in a lung slice recordings from identified alveolar epithelial type one cell.	111-112
4.4 Discussion.	113-116
4.5 Conclusion.	117
Chapter 5. Measuring calcium signals in living rat lung slices.	123-145
Introduction	123-126
5.1 Confocal scanning microscope line-scan imaging of Fluo-3 in living rat lung slices.	127-129
5.2 Time-lapse imaging of cropped regions of interest in Fluo-3 loaded rat lung slices.	129-131
5.3 Manipulation of Ca ²⁺ oscillations in a lung slice.	131-132
5.4 Discussion	135-139
5.5 Conclusion.	140
Chapter 6. General discussion.	146-151

References.	152-178
Appendix: Publications.	179-202
Figure List.	Page
Chapter 1.	
Figure 1.1 Cartoon representation of the gross anatomy of the lung.	16
Figure 1.2 Diagrammatic presentation of single alveoli.	17
Figure 1.3 Koefoed-Johnson and Ussing two membrane model.	23
Figure 1.4 Vectorial transport across alveolar epithelium.	28
Figure 1.5 Fetal lung liquid secretion.	31
Chapter 2.	
Figure 2.1 Unfilled lung slice sectioning by Intrgraslice®	58
Figure 2.2 CellMap IC™ schematic configuration.	69
Chapter 3.	
Figure 3.1 Agarose filled 200µm thickness rat lung slice.	95
Figure 3.2 Propidium iodide and VIII B2 treated agaros filled lung slice.	96
Figure 3.3 HEK 293 cell line employing Live/Dead cellular viability assay.	97
Figure 3.4 PEG 400 backfilled lung slice treated with Live/Dead® cell viability stain.	98
Figure 3.5 Confocal images of unfilled rat lung slices co-stained with LIVE/DEAD® viability/cytotoxicity assay kit for animal cells.	99
Figure 3.6 Confocal images of rat lung slice co-stained with either live or dead viability stains and specific alveolar epithelial type one cell antibody, VIII B2.	100
Figure 3.7 Graph showing quantification of dead cells per field of view in unfilled lung slices loaded with LIVE/DEAD® cell viability assay.	101
Figure 3.8 Confocal reconstructed stack of alveolar epithelial type one cells identified with VIII B2 antibody in a 200µm thickness lung slice.	102
Figure 3.9 Confocal image of lung slice treated with Nile Red vital stain.	103
Figure 3.10 A confocal image of live cell identification in a lung slice of alveolar epithelial type one and alveolar epithelial type two cells.	104

Chapter 4.

Figure 4.1 Confocal image of a cell-attached patch-clamp recording in a lung slice following identification of alveolar epithelial type one cells with VIII B2.	118
Figure 4.2 Cell attached recordings from an identified alveolar epithelial type one cell in the lung slice employing high K^+ solution.	119
Figure 4.3 Cell-attached single-channel recordings from identified alveolar epithelial type one cells in rat lung slice.	120
Figure 4.4 Current-voltage relationship from the channels identified in alveolar.	121
Figure 4.5 Voltage-dependence of the single channels recorded from identified alveolar epithelial type one cells in a lung slice.	122

Chapter 5

Figure 5.1 Confocal 0.85 μ m optical section from a 200 μ m live lung slice loaded with 5 μ M Fluo-3 Ca^{2+} indicator dye.	141
Figure 5.2 Confocal LSM410 linescan of a 200 μ m thick live lung slice loaded with 5 μ M Fluo-3 and resultant graphs.	142
Figure 5.3 Three-dimensional pseudo color graphical representation of calcium signaling events in a living lung slice.	143
Figure 5.4 Cropped region of interest from Fluo-3 loaded 200 μ m thickness lung slice.	144
Figure 5.5 Graphical representations of regions of interest from time lapse imaging of 200 μ m thickness lung slice loaded with Fluo-3 and oscillation frequency as a function of time post slicing.	145

Chapter 1

**General introduction
and literature review**

1.1 Respiratory anatomy and physiology.

The lung is designed to undertake gas exchange. This is accomplished by the passive movement of oxygen (O_2) from inspired air across the alveolar epithelial layer to the capillary bed and the movement of carbon dioxide (CO_2) contained within the venous blood in the reverse direction (Berne. and Levy 1998; Tortora and Graaboski 1996; West 2000). Cells are continually using O_2 for metabolic reactions and the waste product CO_2 is produced, which if retained would create an acidic environment that would prove toxic to cellular homeostasis. Thus, appropriate gas exchange is essential to maintain cellular homeostasis. Of crucial importance is the ability of the respiratory system to match the distribution of inspired air with pulmonary blood flow, in order to provide the necessary supply of O_2 and remove CO_2 . The unique design of the lung facilitates biological optimisation of exchange of O_2 and CO_2 between the alveolar air and the pulmonary capillary blood supply. This is carried out very efficiently with a minimum of physiological energy expenditure. CO_2 and O_2 move between air and blood by simple diffusion (Krogh 1919). The diffusion is assisted by the partial pressure differences created within the gas exchange area of the lung, the “respiratory zone”. The areas of high partial pressure of O_2 , the alveoli, allows the movement of gas to an area of lower partial pressure of O_2 , the capillary bed. The measured partial pressure of O_2 alveolar gas is ~100mm Hg while at the pulmonary capillary level the value is ~40mm Hg thus creating the required pressure gradient to allow the energy efficient movement of O_2 (West 2000).

To provide the most efficient method of diffusion, physiology subscribes to *Flick’s law* of diffusion as closely as possible. The law states that, “The rate of transfer of a gas through a sheet of tissue is proportional to the area of the tissue and to the difference in gas partial pressure between the two sides, and is inversely proportional to the tissue thickness”. The adult human lung has a surface area of between 100-150m² (about the size of a tennis court, Crapo *et al.* 1983) and the blood/gas barrier is extremely thin, being only 0.2-0.3 μm across the majority of the alveolar epithelial layer (Bastacky *et al.* 1995). The

vast surface area is created by wrapping a large number of capillaries around an enormous number of small air sacs, or alveoli.

The structure of the respiratory system can be separated into the upper and lower regions. The upper region contains the nose, pharynx, and associated structures. The lower region comprises of the larynx, trachea, bronchi, and alveoli. The airways of the respiratory system consist of a series of branching tubes which become narrower and more numerous as they penetrate deeper into the lung. The larynx is more commonly know as the voice box and is superior to the trachea. Its key function is to aid in the production of sound via the vibrations of the vocal cords. The epiglottis is located at the larynx and is crucial in preventing any large foreign substances reaching the lower respiratory regions (Berne and Levy 1998; Tortora and Graaboski. 1996).

The trachea or “windpipe” is a tubular passageway, in a human it is about 12 cm in length and 2.5cm in diameter. It is located anterior to the oesophagus and extends from the larynx to the superior border of the fifth thoracic vertebra, where is divides into right and left primary bronchi (Lumb 2005). The trachea has a number of layers of differing cells. The main body of the cell layer which is surface is exposed to the external environment is call the epithelium. One of the key functions of the trachea and terminal bronchioles is to remove any foreign bodies that may be inhaled into the lower respiratory region during inhalation. The mucosa of the trachea consists of pseudostratified ciliated columnar epithelium and this is in contact with the lumen of the airway and is involved in a protective role in conjunction with the nasal cavity and the larynx.

At the fifth thoracic vertebra, the trachea divides into the right and left primary bronchus (Lumb 2005; Tortora and Graaboski. 1996). The division of the airway continues and produces the respiratory airways. This branching is critical as it produces the vast surface area of the lung. After numerous divisions the combined structure is given the title of the “bronchiole tree”.

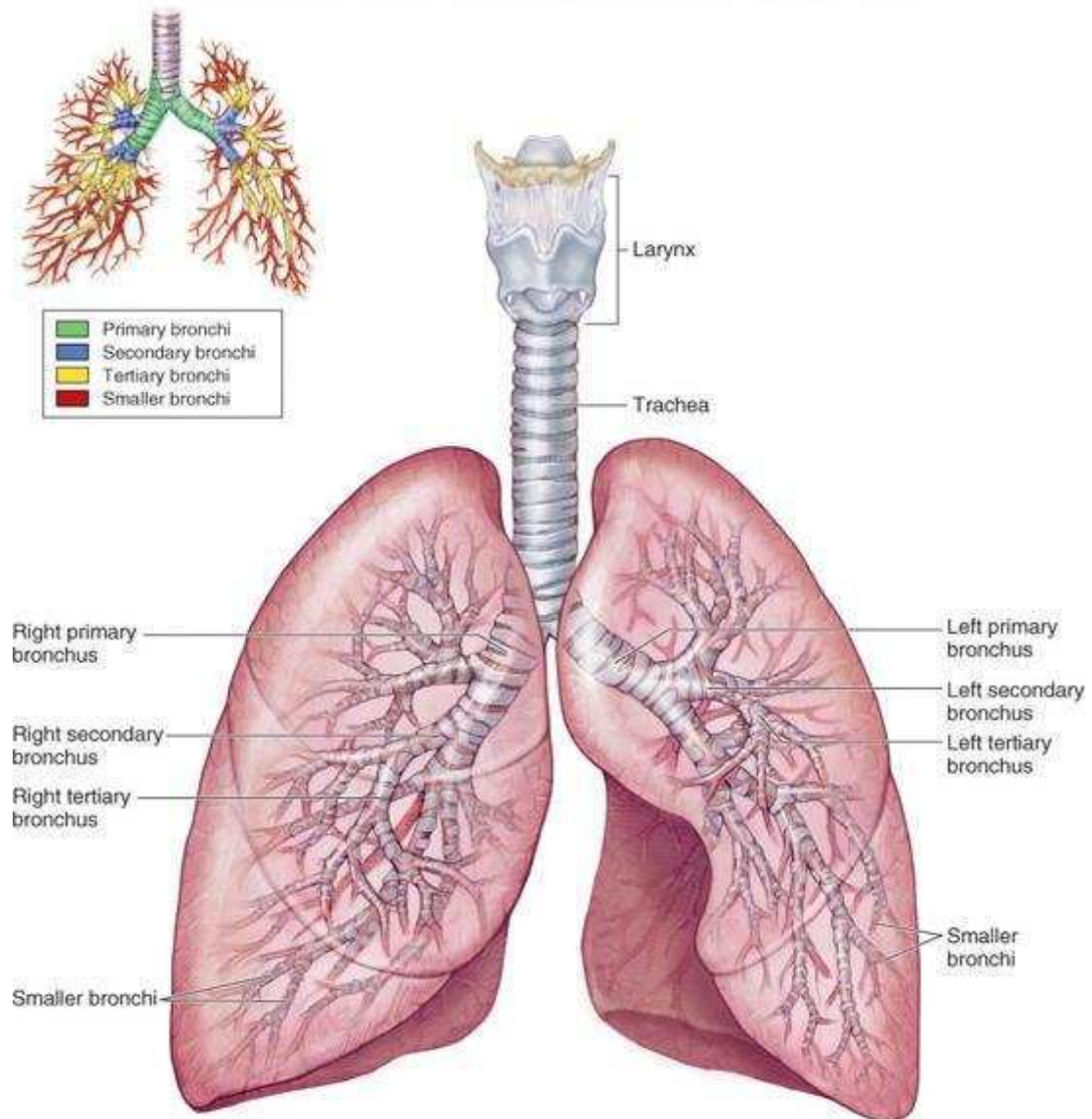


Figure 1.1 Cartoon representation of the gross anatomy of the lung.

This image shows the gross anatomy of the lung from the trachea to the small bronchi. The illustration of the bronchiolar branching is shown in the top left; the different bronchiolar regions are color-coded. This image demonstrates the lower portion of the respirator region of the lung and shows clearly the trachea, branching into the right and left lobes and continuing to the bronchi. Taken from Principles of Anatomy and Physiology, 8th Revised Edition. (1996) Tortora GJ, Graaboski S. John Wiley & Sons Inc.

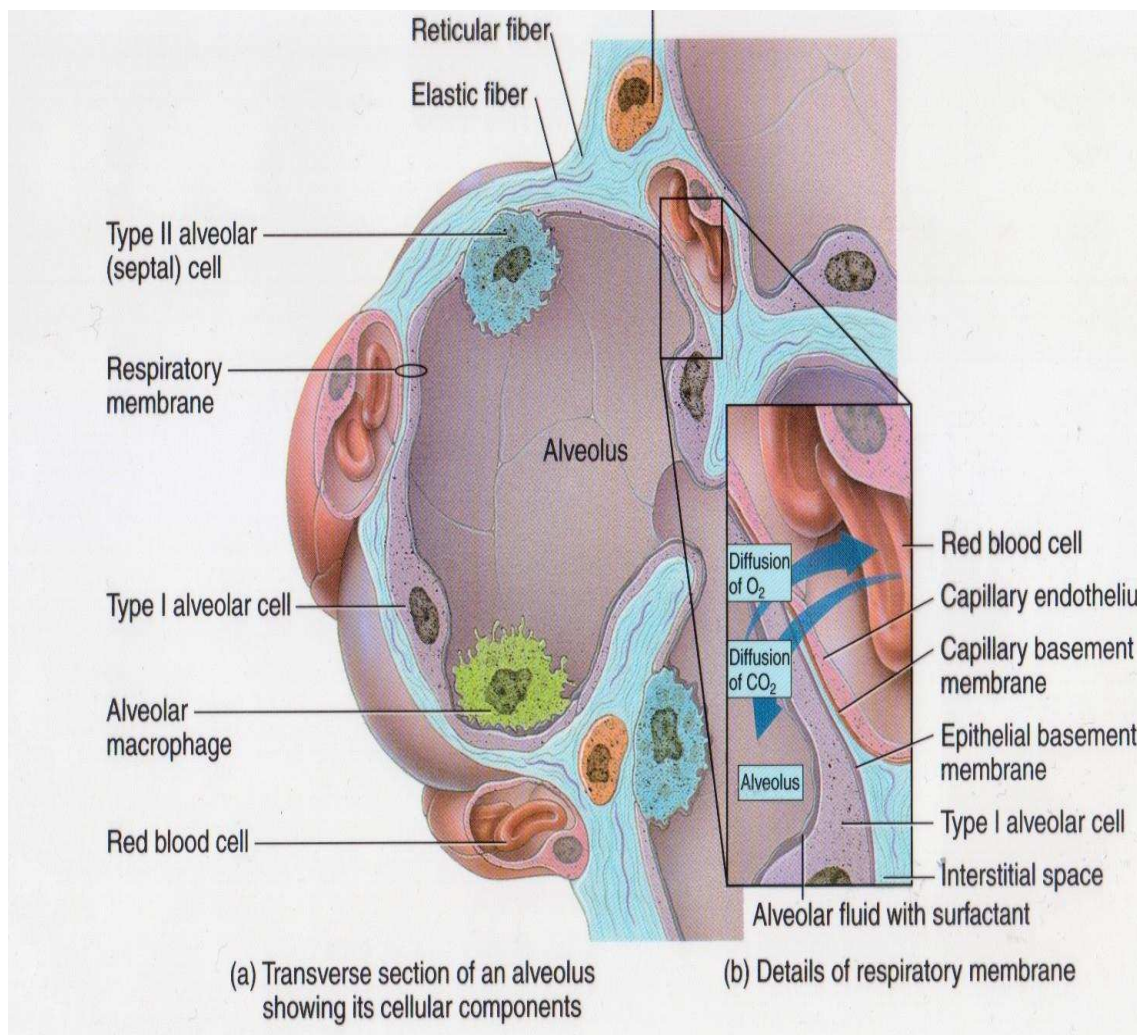


Figure 1.2 Diagrammatic presentation of single alveoli.

This diagram presents a transverse section of an intact alveolus, diagram a. It shows the cellular composition of the alveolar epithelium. Illustrated are alveolar epithelial type one cells, alveolar epithelial type two cells, alveolar macrophages, and pulmonary capillaries. The insert (panel b) details the role of the alveolar epithelium in gas exchange and outlines the layers of the respiratory membrane. Taken from Principles of Anatomy and Physiology, 8th Revised Edition. (1996) Tortora GJ, Graaboski S. John Wiley & Sons Inc.

In the human lung the primary bronchi divide to form smaller bronchi the secondary (lobar) bronchi, one for each lobe of the lung. Within the adult human lung there are three lobes contained in the right lung and two contained in the left lung. The branching of the secondary bronchi continues to still smaller branches, called the tertiary (segmental) bronchi, which divide further to create the bronchioles. The final part is the branching of the bronchioles into the terminal bronchioles. The terminal bronchioles are the smallest airway, which have no alveoli. Collectively, these airway regions are defined as the anatomical dead space, which has a volume of ~150ml. All these bronchi go to make up the conduction airway; the function of the conducting airway is to facilitate the transport of inspired air to the gas exchange regions of the lung (Berne and Levy 1998; Tortora and Graaboski 1996; West 2000, Lumb 2005).

The respiratory zone (transitional and respiratory zones) has a number of anatomically distinct areas. There are the respiratory bronchioles, so called as they have an intermittent alveoli budding from their walls, the alveolar ducts which are completely lined with alveoli. From the trachea to the alveolar ducts there is somewhere in the region of 25 orders of branching (West 2000). Around the circumference of the alveolar ducts are the numerous alveoli and alveolar sacs. An alveolus is the single terminal region of the lower respiratory region while an alveolar sac is defined as two or more alveoli sharing a common opening. This project has been focused on the alveolar region and principally on furthering our understanding of the molecular make up of the alveolar epithelial cells.

Research undertaken by the Danish physiologist August Krogh in the period from 1910 to 1920 (for review see Schmidt-Nielsen 1995) resulted in the understanding that respiratory gas exchange took place by simple diffusion across the alveolar epithelia and capillary bed. Krogh was awarded the Noble Prize for Medicine or Physiology in 1920 for these landmark discoveries. In order to maintain optimised gas exchange the lumen must maintain an extremely thin layer of liquid (Walters 2002). To sustain lung liquid homeostasis it is essential that there are methods for the removal of

excess fluid from the lung. One of the key functions of the alveolar epithelial is to maintain lung liquid homeostasis. An entire field of research is devoted to the investigation of fluid homeostasis in healthy and diseased lungs.

1.2. Epithelial tissue morphology and physiological roles.

The epithelial tissue is divided into two distinct types: A) glandular and B) lining. The glandular epithelium comprises the secreting portion of glands, such as sweat glands and the thyroid gland. The lining epithelium forms the superficial layer of skin and some internal organs (Alberts *et al.* 2002). Lining epithelial also forms the inner lining of ducts, body cavities, and interiors of the respiratory, digestive, urinary, and reproductive systems. There are a number of general features that are associated with epithelial tissue. The epithelium consists largely of closely packed cells with little extracellular material between adjacent cells (Alberts *et al.* 2002). The epithelium is arranged in a continuous sheet, and is made of either single or multiple layers. The epithelial cells have an apical surface, this can be exposed to the exterior of the body, lining of an internal organ, or exposed to a body cavity. The epithelium also has a basal surface, which is attached to the basement membrane. Cell junctions are numerous and provide secure attachment between the cells of the epithelial sheet and excellent communication between cells (Koval 2002). Epithelia are not directly supplied by the vascular system; the bordering connective tissue blood vessels supply the required nutrients and remove the waste products of the epithelium. Epithelia need to be regenerated on a regular basis and they demonstrate a high mitotic rate (Fehrenbach 2001). The functions of epithelia are wide and varied comprising of protection, filtration, lubrication, secretion, digestion, absorption, transportation, excretion, sensory reception, and reproduction.

The arrangement of the cells within the lining epithelia is dependant upon their function, either single or multiple cell layers. The layers are classified as follows: A) simple epithelium; B) stratified epithelium and C) pseudostratified epithelium. The epithelial cells are then further demarcated according to their shape, of which there are four basic types: A) squamos; B) cuboidal; C)

columnar and D) transitional. Squamos are the flat cell type, with large surface area and thin in nature. They are designed for rapid movement of substances. These cells attach to each other in a tile-like fashion. Cuboidal cells are cube or hexagon in shape. Their functions are two-fold: active physiological secretion and active physiological absorption of fluid and solutes. Columnar cells are tall and cylindrical and, in certain organs, form cilia and perform specialised secretion and absorption. The transitional cells which have the ability to change shape from flat to columnar due to distention, expansion, or movement.

1.3 Epithelial transport.

Epithelial transport involves the controlled directional movement of solutes, ions and water across the walls of the alimentary, renal, respiratory and reproductive systems. The volume of liquid transported on a daily basis is impressive with ~180 litres of liquid absorbed across the human proximal renal tubule each day (Spring 1999). A volume of $\sim 0.01 \text{ ml} \cdot \text{kg}^{-1} \cdot \text{h}^{-1}$ was reported as the measured balance rate of fluid secretion and absorption in steady state within the pleural spaces of the human lung (Wiener-Kronish *et al.* 1984). The importance of these processes to the normal physiological function of these organ systems is reflected by the pathophysiological symptoms, which manifest themselves when the regulation of the transport mechanisms regulation breaks down. Loss of normal epithelial function in the lung, can lead to pulmonary edema which if untreated will result in alveolar flooding, inability to undertake suitable gas exchange and ultimately death (O’Brodivich 2001). Despite the vast number of transport functions that are undertaken by these systems, it appears that all operate on a relatively small number of general principals. Epithelial cells contain different transport and ion channels in the plasma membranes that face opposite side of the tissue. The two classical models of epithelial transport the "tight" and "leaky" models of epithelia transport via the transcellular or paracellular pathway. These different transport mechanisms serve a number of physiological functions.

“Tight” epithelial transport is based upon observations made in frog skin, and is generally referred to as the Koefoed-Johnson and Ussing model or the two-membrane model of Na^+ epithelial transport (Koefoed-Johnson and Ussing 1958). The development of this model benefited greatly by the use of radioactive isotopic tracers for example Na^+ , K^+ and Cl^- . The precise measure and direction of flow of ionic fluxes can be determined using this experimental technique. Combined with implementation of the short-circuit measurement techniques and the design of the “Ussing” chamber allowing the recording of changes in current, voltage and transepithelial resistance across the epithelial tissue membrane. The result observed due to changes in the ionic gradients at the apical and basolateral membranes was to prove critical in the conception of the model. The 1958 paper is now recognised as a landmark paper in the epithelial transport physiology.

Koefoed-Johnson and Ussing demonstrated upon application of $10\mu\text{M}$ CuSO_4 to the outer membrane a decrease in Cl^- permeability was observed. The decrease in permeability was measured by using the $^{36}\text{Cl}^-$ isotopes. The transepithelial potential was measured in the presence of Cu^{2+} while the K^+ concentration on the inside of the membrane was increased from 2 to 80mM. The measured potential across the membrane fell in proportion to $\log [\text{K}^+]$. In order to minimize the shunt pathway Cl^- was replaced by the less permeable SO_4^{2-} and again measured when concentration of NaCl at the outer solution was reduced. The final experiment undertaken was to measure the transepithelial potential while the Na^+ concentration of the outer solution was reduced from 100mM and replaced K^+ . An increase in the concentration of Na^+ resulted in an increase in the measured voltage. These results demonstrated in the absent of shunt, the electrical properties of the two membrane become independent (see figure 1.3).

The voltages of the two membranes add as if in series to generate the transepithelial voltage. The key aspect of this model and the conclusions drawn from the results present in the Koefoed-Johnson and Ussing paper is idea that the apical and basolateral membrane have different ion selectivity.

The outer or apical, membrane demonstrated selectivity for Na^+ while the inner or basolateral, membrane is selective for K^+ . Although frog skin is composed of numerous cell layers, the concept is simplified and understood using the two plasma membranes separated by the epithelial intracellular environment model. The active transport step must be at the basolateral membrane to avoid being shunted by the high Na^+ permeability of the outer membrane. The model takes consideration for the low Na^+ concentration required at the cytoplasm of the cell and the pump will maintain this low concentration. The identification Na^+ , K^+ -ATPase further strengthened the acceptance of the model (Skou 1957), however it was not mentioned in the Koefoed-Johnson and Ussing paper directly the idea of active transport was key.

The Na^+ pump (Na^+/K^+ -ATPase) positioned at the basolateral membrane of the apical membrane exchanges the cellular Na^+ for the interstitial K^+ , with a stoichiometry of 3:2 and at the cost of metabolic energy (Skou and Esmann 1992). This active pumping results in the generation of a transepithelial gradient for Na^+ . The use of selective inhibitors confirmed this basic model. Thus, apical applications of the Na^+ channel blocker, amiloride (Palmer 1984), or basolateral application of the Na^+/K^+ -ATPase inhibitor, ouabain (Mills *et al* 1977), both resulted in disruption of the short circuit across the epithelium.

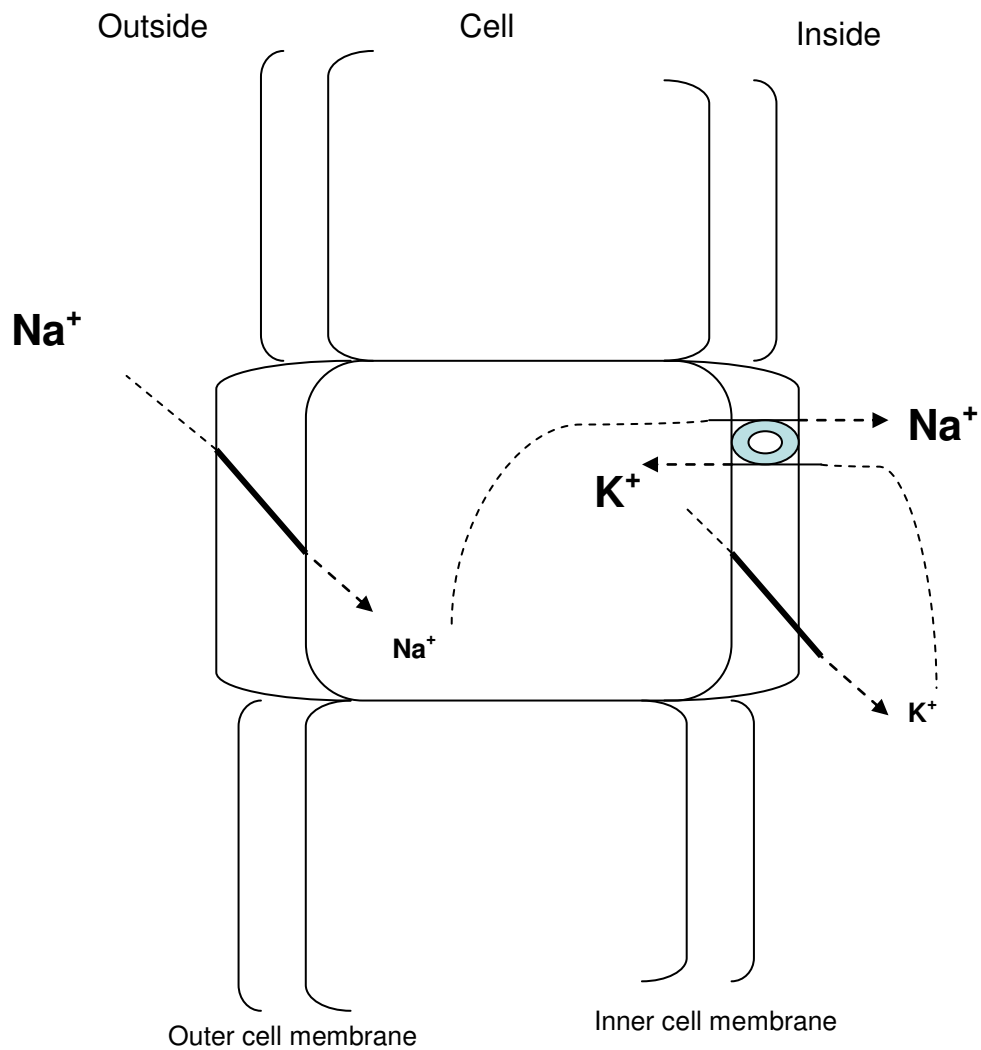


Figure 1.3 Koefoed-Johnson and Ussing two-membrane model.

Na⁺ enters the cell by electrodiffusive mechanism through the apical cell membrane and is pumped out of the cell at the basolateral membrane via the Na⁺ K⁺-ATPase pump. The K⁺ that enters the cell via the Na⁺ K⁺-ATPase pump leaves through an electrodiffusive mechanism through the inner cell membrane. The high concentration Na⁺ and low K⁺ out side the cell and low concentration of Na⁺ and high K⁺ of the cytoplasm is maintained. (Modified from Koefoed-Johnson and Ussing 1958)

More than a decade after the introduction of a model to explain solute transport across tight epithelia, Frömter proposed a refined model to explain the transport of solutes and water across 'leaky' epithelia such as the gall bladder and renal proximal tubule (Frömter, 1972). These leaky epithelia transport Na^+ vigorously however no large transepithelial voltage is recorded when compared to the ion-transport across frog skin. As in the Koefford-Johnson and Ussing model, this had the absolute requirement for epithelial polarity conferred by close cell-to-cell contact by tight junctions (Balda and Matter 2008). However, it relied on the idea that these tight junctions were, in fact, selectively permeable to certain ions and water. Frömter demonstrated directly the presence of paracellular transport (movement between the epithelial cells through these tight junctions) in an intact epithelial preparation of *Necturus* gall bladder. The Na^+ exchange in a leaky epithelium is an electroneutral process with one Na^+ exchanged for one H^+ ion (Murer *et al.* 1976). There noticeable quantitative difference between tight and leaky epithelium. With leaky epithelium demonstrating much larger conductance to that observed in the tight epithelium (Frömter and Diamond 1972). The concept of the two-membrane model is still observed with passive forces driving the Na^+ entry, however Na^+ is linked to pH differences across the apical membrane. The role of the Na^+/K^+ -ATPase is maintained at the basolateral membrane keeping a low Na^+ concentration inside the cell. Hence the distinction was made between tight and leaky epithelia (Frömter and Diamond 1972).

The movement of ions, water and solutes through the tight junctions is critical to leaky epithelial function (Spring 1983; Diamond 1979). The research into the proteins involved in tight junctions formation and regulation has advanced greatly and helped in gaining a deeper understanding of how these proteins are regulated in both healthy and diseased states (Rajasekaran *et al.* 2008; Flynn *et al.* 2008; Shin *et al.* 2006, Tsukita *et al.* 2001). The tight junctions within epithelia are formed from the protein family called the claudins (Tsukita and Furuse M 2000). The tight junctions are responsible for the formation of both the "tight" and "leaky" junctions described throughout the literature. There is a large family of claudins, 23 have been identified and other proteins such

as occluding, tricellulin- α , ZO1, ZO2 and ZO3 are involved in tight junction structure (Martin-Padura *et al.* 1998; Langbein *et al.* 2002; Morita *et al.* 2004; Schlüter 2007). Structurally the claudins are formed of transmembrane proteins that span the lipid bi-layer four times, contain two extracellular loop domains, and have an N and C termini oriented towards the cytoplasm (Van Itallie and Anderson 2006). Within lung tissue, claudin-1, -3, 4, -5, -7, -8, -18 expression has been confirmed (Daugherty *et al.* 2004; Kaarteenaho-Wiik and Soini 2008). Each of the claudins expressed in the lung have been identified at the alveolar epithelium. There is, however, a cell specific expression profile, with alveolar epithelial type one cells demonstrating increased claudin-4, -7, and -8 and the alveolar epithelial type two cells showing increased levels of claudin-1, -3, and -18. The claudins provide a barrier to the flow of fluid through the epithelium by producing selectively permeable paracellular channels (Eaton *et al.* 2008).

As with many protein families, the expression profile is crucial, *i.e.* which members are expressed together, and claudins are no different. In the lung, it has been shown that an increase in claudin-5 at the alveolar epithelium effects barrier function (Coyne *et al.* 2003). However, the expression of claudin-5 is essential for creating a normal epithelial barrier function (Nitta *et al.* 2003). The function and mechanism of the claudin protein family in paracellular channel formation and regulation is complex. The manipulation of claudin expression has allowed the investigation of their effect on epithelial tight junction permeability and selectivity (Van Itallie and Anderson 2006). The differences in expression profiles of the claudins between alveolar epithelial type one and alveolar epithelial type two cells would suggest that the ion flux across the epithelium will depend upon which cells are in contact with each other (Wang *et al.* 2003).

1.4 Alveolar epithelium.

The mammalian lung comprises of more than 40 different cell types (Weibel and Taylor 1988, Bastacky *et al.* 1995). The epithelial covering layer at the end point of the respiratory system is termed the alveolar epithelium. Within the

lung, the physiological functions of the alveolar epithelium are to maintain lung liquid fluid homeostasis, assist in gas exchange and defend against inhaled particles by creating a physical barrier. The alveolar epithelium comprises 99% of the surface area of the lung (Crapo *et al.* 1983). The alveolar epithelium comprises of two morphologically distinct epithelial cell types, the alveolar epithelial type one cells and alveolar epithelial type two cells. The alveolar epithelium is in a unique position as it is in direct contact the external gaseous and internal cellular environments. The physiological stresses encountered by the epithelial begin at birth (Olver *et al.* 2004; Wilson. *et al.* 2007) and continue each and every day of adult life (Dobbs and Johnson 2007). The lung is unique as the patterns and mechanisms of ion and fluid transport change from development and as it matures.

1.5 Vectorial transport across the alveolar epithelium.

The route of liquid flow into the alveolus differs according to the physiological situation. Under adult normal physiological circumstances the majority of the flow across the alveolar epithelium is directed via the transcellular pathway (Eaton *et al.* 2008). The basic fluid balance is driven by osmotic gradients created by active solute transport (Diamond 1979). Within the alveolar epithelium the osmotic gradients are created by vectorial transport. Vectorial transport is made possible by the non-uniform distribution of transport proteins in the plasma membranes of two faces of the epithelium (Whittham and Ager 1964). The lung is under constant liquid challenge during fetal development, at birth and to the final day of life in health and especially in disease (Wilson *et al.* 2007; Dobbs and Johnson 2007). The passive movement of fluid into the alveolar space is driven by hydrostatic pressure from the pulmonary capillaries across the airway epithelium. This is a constant figure (~15mmHg) under normal physiological circumstances and the epithelial permeability also remains constant. Therefore, it is absolutely essential that lung fluid homeostasis be carefully regulated to prevent the lung filling with liquid.

The classic experiment undertaken by Colin (1873) in the nineteenth century showed that a horse could effectively remove 25 litres of saline infused

directly into the lung luminal space over a 6-hour period (Colin 1873). This study elegantly demonstrated the ability of the lung to remove liquid from the lumen across the alveolar epithelium and into the interstitium, pulmonary vasculature and lymphatic system. The lung must maintain and balance the osmotic gradient, which is required to move fluid into, and out, of the lumen across the alveolar epithelium. The presence of the basolateral Na⁺K⁺-ATPase (Borok *et al* 1998; Schneeberger and McCarthy 1986) creates and drives a transepithelial Na⁺ gradient. In the postnatal alveolar epithelium, the presence of ENaC on the apical membranes of both alveolar epithelial type one type two cells, allows apical Na⁺ entry. Although it remains unclear if active Na⁺ transport is essential in maintaining a fluid free air space in the normal lung it has been demonstrated that Na⁺ transport limits the degree of alveolar flooding during pathological conditions (O'Brodovich *et al.* 2001). Indeed, animal studies have demonstrated that transepithelial Na⁺ transport can be inhibited by the presence of both ouabain (Olver and Robinson 1986; Olivera *et al* 1994) and amiloride (Olver and Robinson 1986).

Our understanding of vectorial Na⁺ transport at the alveolar epithelium has been further advanced by examining the electrophysiological properties of the alveolar epithelial type two cell population (Dobbs and Johnson *et al.* 2007 for review) and more recently alveolar epithelial type one cell population (Eaton *et al* 2009 for review). It is clear that the alveolar epithelium obeys the requirements to produce vectorial transport see figure 1.4 below. The particular details of the research outlining the identification and location of the ion channels mentioned in figure 1.4 are discussed later in this introduction. Isolated alveolar epithelial type two cells will form a tight monolayer under the right culture conditions and these have been shown to have tight epithelial properties, with overall resistance of $\sim 2\text{k}\Omega\text{cm}^2$, actively absorb Na⁺ from the apical fluid (Kim *et al.* 2005; Borok *et al.* 1994; Cheek *et al.* 1989).

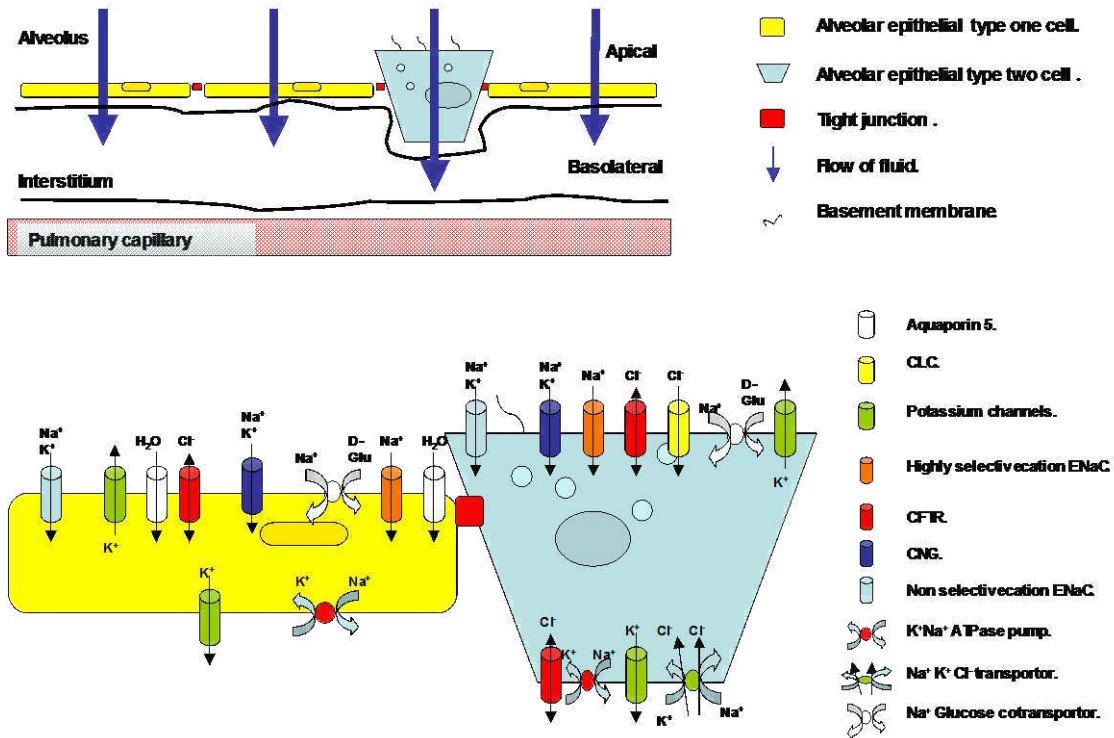


Figure 1.4 Vectorial transport across alveolar epithelium.

The top panel is a schematic depiction of transcellular epithelial transport across the alveolar epithelium. Top panel demonstrates the cellular layout of the alveolar epithelium. Representing transcellular ion transport across both alveolar epithelial type one (yellow) and alveolar epithelial type two (gray) cells. This model restricts the flow through tight junctions (red) and is considered a ‘tight’ epithelium. The fluid flows down the osmotic gradient created by the active solute transport into the interstitial space. Bottom panel is Schematic depiction of the channels and transporters involved in alveolar epithelial ion and fluid transport. The current paradigm for the vectorial transport of ion across the alveolar epithelium: Na^+ is absorbed from the apical surface both alveolar epithelial type one and alveolar epithelial type two cells via the ENaC channels (Orange, highly selective ENaC and light blue, non selective ENaC). Electroneutrality is conserved with Cl^- movement through the CFTR (Red) in type one and type two cells, and/or paracellular through tight junctions. Na^+ is transported from the basal surface of both cell types into the interstitial space by $\text{Na}^+ \text{K}^+$ -ATPase (Red/Blue). K^+ is transported from both cell populations via apical and basolateral channels (Green). CNG: cyclic nucleotide-gated channels (Dark blue) are present in both cell populations at the apical membrane. Aquaporin 5 (White) is expressed only in alveolar type one cell apical membrane allowing the movement of H_2O . The basolateral location of the glucose co-transporter (white) and the $\text{Na}^+ \text{K}^+ 2\text{Cl}^-$ (Red/Blue) combine to create a net ion movement of ions from the apical membrane to the interstitium and osmotic gradient is created. This in turn directs water in the same direction, either through the aquaporin or by diffusion. (Adapted from Johnson *et al.* 2002)

The application of ouabain to the basolateral side of the isolated cultured monolayer resulted in a rapid decrease in short-circuit current however no change in the measure transepithelial resistance was observed upon application of amiloride to the apical side of the monolayer an immediate reduction in short circuit current was observed (Cheek *et al* 1989). These and many other studies have firmly established that the alveolar epithelium is the major site of Na^+ . Fluid absorption in the adult lung and both amiloride-sensitive Na^+ channels and ouabain sensitive basolateral Na^+ K^+ -ATPase pump are critical components in this molecular mechanism.

The alveolar epithelium also expresses other co-transporters that are vital in maintaining the lung fluid homeostasis. The physiological evidence for the Na^+ -glucose co-transporters has been identified at the apical membrane of the alveolar epithelium in whole lung studies (Fisher *et al.* 1980) and isolated alveolar epithelial cells (Kemp and Boyd 1992). There is active co-transport of glucose and Na^+ , which results in a liquid absorption. The potential mechanism is as follows Na^+ enters the apical membrane of the alveolar epithelial cells with glucose (Barker *et al* 1989). The Na^+ is pumped out at the basolateral membrane via the Na^+ K^+ -ATPase that exchanges K^+ for Na^+ . K^+ is recycled via K^+ channels at the apical and basolateral membranes. Cl^- or another anion follow Na^+ transported to ensure electroneutrality. The Glucose is either metabolised or transported out of the cytoplasm via glucose transporters.

1.6 Fetal and neonatal lung fluid homeostasis.

It has long been recognised that the foetal lung is a liquid filled organ (Addison and How 1913; Potter and Bohlender 1941; Adams *et al.* 1963; Mossinger *et al* 1990). It was initially believed that the amniotic fluid was responsible for the liquid present in the lung prior to birth, however this idea was challenged only as recently as the early 1940's. Potter and Bohlender (1941) observed that obstruction placed distal to the congealed airways resulted in the lung filling with liquid and drew the conclusion that the lung produced the liquid. Further evidence to support this idea was delivered when Jost and Policard (1948),

accidental restriction of the trachea. They reported a distension of the lung, which filled with liquid. The direct measurement and comparison of amniotic fluid and fetal lung both an ionic level and measured proteins confirmed a difference in the composition of the two liquids, and confirmed beyond doubt the lung could secrete liquid in the neonatal phase (Adams *et al.* 1963; Adamson *et al.* 1969).

During the fetal period the developing lung is predominately under the influence of Cl^- secretion (for review see Olver *et al.* 2004, Wilson *et al.* 2007). The secretion of fluid into the lung lumen elegantly demonstrated in 1974 by Olver and Strange in their landmark paper. The experimental model chosen was foetal lambs of two groups were examined, 16 animals of 123-133 days gestation, described as the immature group and 46 animals of 136-144 gestation, described as the mature group. The use radioactivity labelled ions allowed the measures of bidirectional ion fluxes through the alveolar epithelium according to the Ussing flux ration equation (Koefoed-Johnson and Ussing 1958). In the discussion they drew attention to the most striking result in a modest fashion stating, "The high Cl^- concentration is probably due to the active transport of this ion from plasma and interstitial fluid into the pulmonary alveoli against an electrochemical gradient". This observation lead to a novel theory at the time in regards secondary active transport. The active transport of Cl^- would bring about the passive movement of Na^+ as a co-ion. Figure 1.5 below demonstrates how the model of lung secretion during the foetal period operates. It transpires that the observed secretion of Cl^- into the lung lumen is dependent upon basolaterally located $\text{Na}^+/\text{K}^+/\text{2Cl}^-$ co-transport system, harnesses the Na^+ gradient to transport Cl^- across the basolateral surface. The movement of the Cl^- is electrogenic and produces that electrical driving force which moves Na^+ passively into the lumen. The movement of Na^+ and Cl^- creates an osmotic gradient, which drives water into the lumen. At present the actual channel or transporter responsible for the movement of anions at the apical membrane has not been identified. The secretion of liquid has a very powerful effect in stimulating growth during the period of gestation.

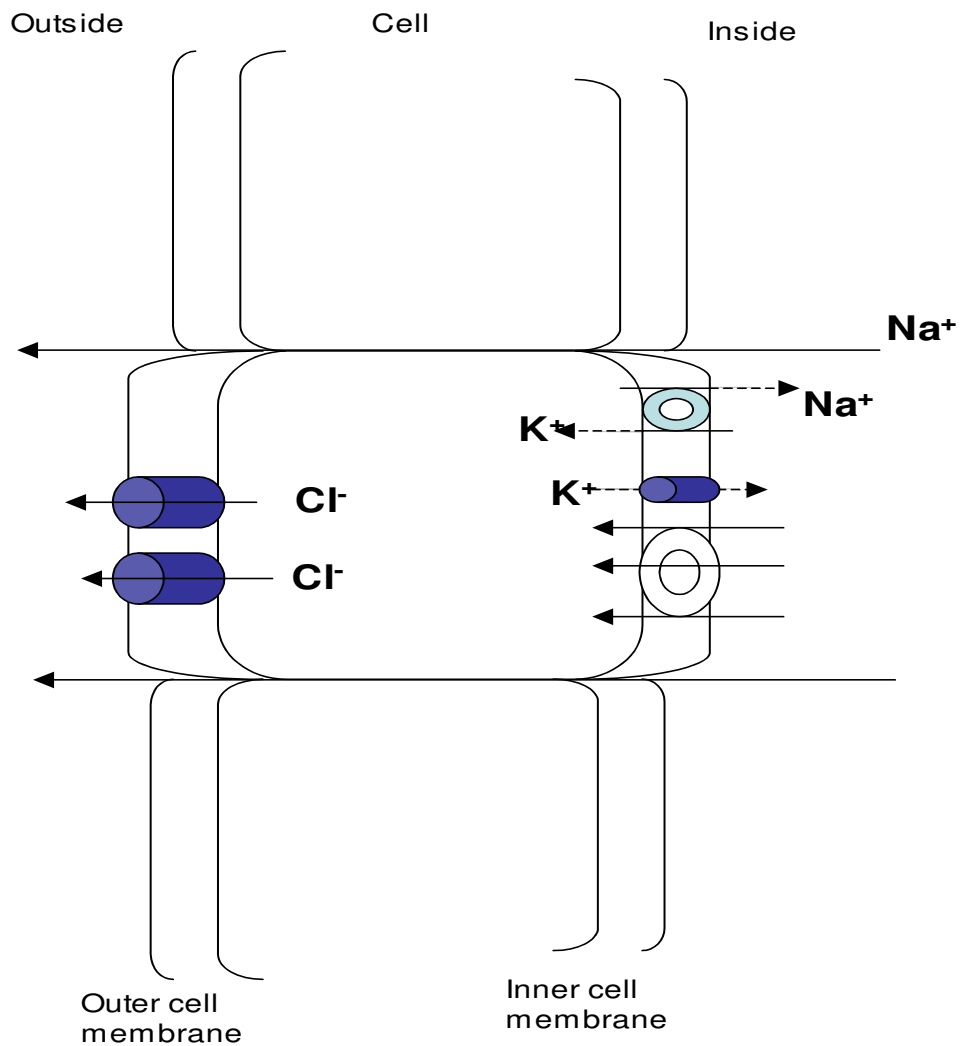


Figure 1.5 Fetal lung liquid secretions.

The present model for chloride secretion emphasises the central role of basolateral Na^+K^+ -ATPase in maintaining high intracellular K^+ and low Na^+ concentration. Na^+ re-enters the cell down its electrochemical gradient via the $\text{Na}/\text{K}/2\text{Cl}$ co-transporter on the basolateral membrane. K^+ may leave the cell through basolateral channels. The high intracellular Cl^- concentration and negative intracellular membrane potential facilitates the rise in Cl^- concentration to tally its electrochemical equilibrium. A further rise in intracellular Cl^- concentration will lead to opening of the apical Cl^- channels and flow of this anion into the lung lumen. Na^+ and water will follow Cl^- through a paracellular route. (Adapted from O’Brodivich 1996).

The developing lung requires the stretch induced by the influx of fluid into the lumen (Olver *et al.* 2004, Wilson *et al.* 2007). The interruption of the fluid influx can cause a number of developmental respiratory problems, which in turn are detrimental to whole body physiology. Two fetal pathological situations, which interrupt how the intrapleural pressure is maintained, are diaphragmatic hernia and tracheal agenesis. In the case of diaphragmatic hernia, a failure of the diaphragm to form correctly causes the internal organs to fill the chest cavity and lung development is impaired (de Buys Roessingh and Dinh-xuan 2009). In tracheal agenesis, a sealed or malformed trachea and larynx, acts as a one-way valve and causes a build up of the luminal lung fluid and disruption to normal lung development (Saleeby *et al.* 2003). The result of the occlusion is differentiation of pulmonary epithelial cells appeared to be more advanced for the gestational age in pulmonary hyperplasia with congenital tracheal agenesis. Post delivery, infants who have this pathological defect are recognised at term due to the respiratory distress, lack of crying and intubation is difficult if not impossible (Spitz 2007).

The period of weeks prior to birth (late gestation period) sees an important upregulation of the molecular machinery necessary to allow the fluid filled neonatal lung to transform from a liquid filled organ to air filled respiratory organ (Olver *et al.* 1986; O'Brodovich *et al.* 2001). The process of giving birth triggers the actual switch of the alveolar epithelium from active secretion to one of fluid absorption (Walters *et al.* 1990). This rapid removal of liquid that in later life would be considered pulmonary edema is an extremely challenging event for the neonatal physiology (Berthiaume and Matthay 2007). The large release of adrenaline at birth is the molecular switch, which is required to transform the lung from a liquid secretion to absorption organ (Walters and Olver 1978). The identification of genes for the Na⁺-K⁺-ATPase "sodium pump" and ENaC have lead to a deeper understanding of the regulation of transepithelial ion transport at a molecular level which underlie the mechanisms for fluid clearance during the perinatal period.

The clearance of lung fluid after birth is rapid. Fluid clearance was demonstrated in rabbit pups and was complete in a 2 h period (Aherne and

Dawkins 1964). The vast surge of fetal catecholamine secretion is triggered by birth (Lagercrantz and Bistoletti 1977). A critical link between the β -adrenergic stimulation and lung liquid clearance was made by Walters and Olver in 1978. Their experiments on mature fetal lambs demonstrated that when epinephrine and isoproterenol were infused directly into the lung they caused rapid absorption of lung liquid (Olver and Walters 1978). This response was not observed in the presence of norepinephrine. After advanced administration of propranolol the absorptive response was inhibited. The majority of the liquid is cleared via the pulmonary circulation with lung lymphatic's contributed only a small fraction of the removal (Chapman *et al.* 1994). The developmental period is critical in how lung fluid homeostasis is maintained in the perinatal period. This point is clearly demonstrated by the respiratory difficulties, which premature babies encounter. They lack the required molecular machinery to clear the lung fluid, which will result in neonatal respiratory distress syndrome (RDS). This is one of the most common causes of death amongst new born and premature infants in the western world as reported by the national heart, lung and blood institute (Blaisdell *et al.* 2008).

The change from a liquid-filled lung to an air-filled lung also presents an original environment to the newborn lung. Prior to birth, the lung is maintained in hypoxic surroundings and the first breath that a new born takes introduces the lung to the air environment. The regulation of ion channels by O_2 particularly hypoxia is well recognised (Kemp and Peers 2007) and there is evidence for an increase in α , β , and, γ ENaC mRNA and Na^+ transport upon stimulation with O_2 (Pitkänen *et al* 1996). An increase in α -ENaC promoter activity by increasing the P_{O_2} for 24-48 hours has also been demonstrated (Baines *et al* 2001). O_2 acts directly upon the Na^+K^+ -ATPase pump (Ramminger *et al* 2000). Hypoxia has the directly opposite effect in that both amiloride-sensitive apical Na^+ entry and basolateral Na^+ extrusion are both reduced (Mairbäurl *et al* 2002).

1.7 Postnatal lung fluid homeostasis.

Unlike other epithelial surfaces the lung is unique as the apical surface face an air filled region while the basolateral surface is in contact with the internal vascular as with all epithelial surfaces. The movement of fluids within biological systems is attained by the regulation of the salt and water balance. There is now indisputable evidence to support both constitutive and stimulated, Na^+ -driven, active vectorial transport of water from the lung lumen to interstitium in neonatal and adult lung (Folkesson *et al.* 1998; Kemp and Olver 1996; Norlin and Folkesson 2001; Eaton *et al.* 2009). Osmotically driven water movement follows the primary active transport of Na^+ and secondary active transport of Cl^- . The active transport of ions is followed by the movement of water, as there is an osmotic imbalance. It is crucial for gas exchange to be completed efficiently and correctly at the alveolar region. To aid in this there are a number of mechanisms in place to maintains liquid homeostasis. It is essential to maintain a thin liquid layer on the air surface side and this is referred to as the hypophase. This was measured at 0.37 ± 0.15 ml/kg body weight of sheep (Stephens *et al.* 1996; Walters 2002). The hypophase is essential as it acts as a “medium” for the intra-alveolar cells such as alveolar macrophages and preserves the alveolar extracellular milieu. The ability of the alveolar epithelium to strike such a fine balance between allowing the necessary amount of fluid to remain for correct physiological function shows the control tight control that the alveolar epithelium maintains. The amount of fluid present in the airspace is a balance of the passive secreted fluid from the vascular space through the paracellular space and tight junctions and the rate at which fluid is actively absorbed.

A change in the way liquid is transported in the adult lung over the neonatal and perinatal period has been observed (Junor *et al.* 1999; Ramsden *et al.* 1992, for review Folkesson and Matthay 2006). The massive upregulation of ENaC seen in late gestational period required to initiate active Na^+ transport to allow the change from secretion to absorption is essential. However, there is a defined change in the ability of the fetal hormones to affect the adult lung.

Junor et al (1999 and 2000) demonstrated elegantly the loss pharmacological function of amiloride inhibition in sheep aged 6 months and in comparison lambs aged only a few week demonstrated net secretion upon the application of amiloride at the lung lumen.

The percentage of fluid movement that can be attributed to one mode of transport over another varies across species. 30% of the ability to clear fluid from the alveolar space in rat lung is attributed to amiloride sensitive Na^+ ENaC (Li and Folkesson 2006), with similar percentages observed in sheep (Junor *et al* 1999). Other ion channels present in the lumen of the adult lung are the CNG ion channels and demonstrated at a functional level by electrophysiology (Kemp *et al.* 2001; Schwiebert *et al.* 1997) and by immunohistochemistry (Ding *et al.* 1997). The CNG have not been shown to be present in the fetal or neonatal lung, its presence in the adult lung provides an alternative mechanism for lung fluid homeostasis. The principal mechanism for the control of fluid homeostasis in the adult lung is a matter of debate. A key finding by Junior et al (1999), in the presence of both amiloride and di-chloro-benzamil (CNG-1 blocker) observed a net secretion was observed but a full block was not obtained. It is the combination of both mechanisms that provides optimal lung fluid homeostasis.

It has become more evident that the alveolar epithelial type one cells have a more active role in fluid absorption than was considered in the recent past. The molecular proteins required to move fluid in an electroneutral manner are present in the alveolar epithelial type one cells. A recent study in isolated alveolar epithelial type one cells demonstrated that the amiloride-sensitive rate of Na^+ uptake exceeds the rate of Na^+ influx measured in parallel cultures of alveolar epithelial type two cells by 2.5-fold (Johnson *et al.* 2002). The more recently electrophysiological evidence from the alveolar epithelial type one cell has demonstrated the presence of ENaC subunits α , β , γ , potassium channel, CFTR, nonselective cation channel and the presence of basolaterally Na^+K^+ -ATPase. Relative contributions of each cell type to overall ion transport had not been possible until the advent of lung slice *in situ* measurements.

1.8 Alveolar epithelial type one cells.

Alveolar epithelial type one cells are large squamous epithelial cells with a diameter of ~50 to 100 μm and a volume of ~2000 to 3000 μm^3 (Crapo *et al.* 1983, Stone *et al.* 1992). These cells have a highly flattened cellular structure and attenuated cellular extensions. There was a doubt, as recently as, 60 years ago as to the existence of an alveolar epithelium. It was believed by some investigators that the vast capillary bed of the pulmonary system lacked an epithelial covering. The existence of the alveolar epithelium was confirmed in 1952 by an investigation of the lung at the electron microscope level (Low 1952). This research showed the existence of both alveolar epithelial type one cells and alveolar epithelial type two cells. These populations of cells formed a complete epithelial lining of the peripheral lung.

Since the alveolar epithelium covers such a large surface area it is important that cell-to-cell communication is maintained for normal function and when injury occurs this can be lost. Gap and tight junctions were first identified in the lung by electron microscopy (Bartels 1979; Schneeberger *et al.* 1978). Gap junctions, a class of membrane channels, are small pores that allow the free passage of ions and small molecules between neighbouring cells (Koval 2002). The presence of the gap junction proteins (connexins) has been demonstrated between alveolar type one cells and alveolar type two cells *in situ* (Wang 2003; Isakson *et al.* 2003; Abraham *et al.* 1999; Bartels *et al.* 1980). The expression profile of the connexions has been greatly investigated in the isolated alveolar epithelia cell culture and in the in lung tissue sections and a complex pattern of expression has been show with at lease six connexins (Cxs) present (Cx26, Cx32, Cx37, Cx40, Cx43, and C46 (Abraham *et al.* 1999; Isakson *et al.* 2001; Abraham *et al.* 1999; Carson *et al.* 1998). It is clear that there is a complex interaction between the two populations of the alveolar epithelial cells. It remains to be answered and has been difficult to assess if connexins combine to form multimeric complexes (Koval 2002).

The expression profile of the connexins in lung sections and heterocellular culture of alveolar epithelial cells was investigated by Isakson *et al* (2003). Immunohistochemical treatment of lung sections showed that anti-Cx26 showed sparse staining throughout the alveolus. Anti-Cx32 and anti-Cx40 staining was relatively sparse however it was seen to accumulate with alveolar epithelial type two cells. Sections treated with Anti-Cx43 showed the strongest staining pattern and was seen throughout the alveolus. Anti-Cx46 demonstrated high immunoreactive staining throughout the alveolus. The expression profile in the heterocellular alveolar cultures was assessed in an attempt to draw comparison between an *in vitro* expression profile and an *in vivo* expression profile. Anti-Cx26 and anti-Cx32 demonstrated sparse staining across the two cell populations. No immunoreactivity was observed with Anti-Cx37 in either population. Anti-Cx40 was tightly localised to the alveolar type two cells only and no reactivity was seen in the alveolar type one cell population. Two Anti-Cx43 antibodies were used and reactivity was seen in both cell populations with each antibody. Anti-Cx46 was the most reactive in alveolar type one cell population; however, up to 20% of the alveolar type two populations demonstrated staining. The results in the heterocellular culture when compared with the slice sections demonstrate the heterocellular compared favourably as an experimental model to study connexins *in vitro* (Isakson 2003). The physiological effects of stretch and a number of pharmacological agents were investigated in the culture. In addition the immunohistochemistry was also undertaken. The cultures demonstrated propagated communication between the alveolar type one and alveolar type two cell populations. Both dye coupling and Ca²⁺ indicator dye studies demonstrated that connexins allow functional and cellular communication between alveolar epithelia type one and alveolar epithelial type two-cell population in a heterocellular culture.

The tightly coupled nature of the alveolar epithelial membrane proved, until very recently, to be a stumbling block in production of primary isolated alveolar epithelial type one cell of high purity and cellular viability. Published data from primary isolated alveolar epithelial type one cells has been confined to a

handful of laboratories (Johnson *et al.* 2006; Borok *et al.* 2002; Isakson *et al.* 2003). Once the cells have been isolated they appear fragile and are susceptible to injury. Their structure takes on a “cloud like” appearance. Improvements in the methods used to isolate the alveolar epithelial type one cells have been very productive. Chen *et al.* using a polyclonal antibody raised against T1 α were successful in producing a high yield of alveolar epithelial type one cells, a purity of over 90% was reported (Chen *et al.* 2005). T1 α was the first molecular marker to be cloned and sequenced which is specific to alveolar epithelial type one cells (Dobbs *et al.* 1985), making it a suitable candidate for the production of an antibody. Immunohistochemical investigations showed the lung as the major expression site for T1 α (Griod *et al.* 1999). The alveolar epithelial type one cell demonstrated a high level of positive signal. The molecular function of T1 α has remained quite elusive. However, a knockout mouse model (Ramirez *et al.* 2003) shows significant abnormality in the microstructure of the lung with a thickening of the alveolar septae. The homozygous KO animals die shortly after birth from respiratory failure manifested as an inability to inflate the lung. This finding suggests an important functional role for T1 α in development of alveoli or alveolar structure. It is demonstrated that T1 α is upregulated after lung injury (Williams 2003). T1 α has been shown to closely associate with macrophage accession (Girod 1999) suggesting that T1 α may have a function in accumulation of macrophages.

Studies in transgenic mice have begun to define the role of aquaporin (AQP)-type water channels in water transport in the intact lung (Verkman 1998). The AQPs are a family of small (~30-kDa monomer), integral membrane proteins and there are at least 11 homologous AQP in mammals, 4 of which are expressed in the lung. The cell lipid bilayer and cell membranes are slightly permeable to water, a number of theories have been suggested to explain the passive movement of water through lipid membranes (Nagle *et al.* 2008 for review). However, the surface area of lipid is it appears the determining factor for water permeability (Nagle *et al.* 2008). The addition of the AQP channels has a dramatic effect in increasing the water permeability of membranes. The

kidney tubular and alveolar permeability dramatically increases by 5-to-50 fold in the presence of AQP water channels (review Borok and Verkman 2002).

An active role for the alveolar epithelial type one cell in vectorial transport in the lung is beginning to emerge. Alveolar epithelial type one cells have been shown to express the molecular transporters and ion channels, the “molecular machinery”, required for fluid transport (Crandall and Matthay 2001). It was believed that the alveolar epithelial type one cells were a passive player in lung liquid homeostasis. The identification AQP on the apical surface of alveolar epithelial type one cell membrane (Dobbs *et al.* 1998) was important in advancing the understanding of how fluid homeostasis is maintained within the lung as a whole. AQP-5 has been positively identified in the apical plasma membrane of the alveolar epithelial type one cells by immunohistochemistry (Borok and Luberman *et al.* 1998). The alveolar epithelial type one cells demonstrate the highest water permeability of any measured mammalian cells membrane (Dobbs *et al.* 1998).

Immunohistochemical studies have also shown the presence of sodium potassium ATPase pump ($\text{Na}^+\text{K}^+\text{-ATPase}$) in the basolateral membrane of alveolar epithelial type one cells (Zhang *et al.* 1997). The movement of liquid across the alveolar epithelial membrane relies on the presence of the $\text{Na}^+\text{K}^+\text{-ATPase}$ at the basolateral membrane. The active transport of Na^+ via the ENaC channel combined with the $\text{Na}^+\text{K}^+\text{-ATPase}$ which pumps three Na^+ out and introduce two K^+ into the cell. This active vectorial Na^+ transport is electroneutral and produces a transepithelial osmotic gradient. There are a number of pathological situations, which see either an increase or decrease in expression the $\text{Na}^+\text{K}^+\text{-ATPase}$ and fluid transport is affected accordingly. A down regulation, or decreased function, of $\text{Na}^+\text{K}^+\text{-ATPase}$ will lead to an increase lung oedema. Concurrently the up regulation, or enhanced function, of the $\text{Na}^+\text{K}^+\text{-ATPase}$ leads to increased lung liquid clearance. $\text{Na}^+\text{K}^+\text{-ATPase}$ activity in alveolar epithelial type one isolated cells was inhibited using Rb^+ , Rb^+ can be used as a surrogate for K^+ uptake. The use of Rb^+ was inhibited by ouabain (Johnson *et al.* 2006) functionally demonstrating the presence of $\text{Na}^+\text{K}^+\text{-ATPase}$ pump. The expression of all three amiloride-sensitive epithelial

sodium channel (ENaC) subunits (α , β , and γ), has also been demonstrated from isolated alveolar epithelial type one cells at the mRNA and protein levels by northern blot, ISH and immunohistochemically (Borok and Luberman *et al* 1998; Johnson *et al.* 2002).

Electrophysiological evidence from the alveolar epithelial type one cells is a recent addition to the literature. The first study demonstrating electrophysiological data from identified alveolar epithelial type one cells in a lung slice model is presented in this thesis and has been published by us (Bourke *et al.* 2005). Following this study, there have been three further publications that have demonstrated electrophysiological data from alveolar epithelia type one cells, all originating from the Eaton laboratory (Johnson *et al.* 2006; Helms *et al.* 2008; Helms *et al.* 2006). Results obtained from isolated adult rat alveolar epithelial type one cells demonstrated highly selective cation and non selective cation channels, cyclic nucleotide-gated cation channels, potassium channels, and CFTR channels (Johnson *et al* 2006). The electrophysiological data have been confirmed by other molecular techniques by a number of studies (for review Dobbs and Johnson 2007). The ability to manipulate the cellular activity of the alveolar epithelial type one cells both physiologically and pharmacologically is an important advancement in uncovering their function. Subsequent investigations using the lung slice model were undertaken and have yielded interesting observations (Helms *et al.* 2006; Helms *et al.* 2008). They demonstrated the presence of a number of functional ion channels in both alveolar epithelial type one and alveolar epithelial type two cells from an agarose-filled lung slice model. Recordings from alveolar epithelial type one cells demonstrated the presence of ENaC, both highly selective and non-selective cation channels and support the observations made in the isolated single cell model. The alveolar epithelial type two recordings from the slice model demonstrated the presence of ENaC, again both the highly selective and non-selective cation channels. The data presented further strengthen the hypothesis that alveolar epithelial type one cell play an active part in lung fluid homeostasis.

P2X receptors are extracellular ATP-gated, calcium permeable, non-selective cation channels that are modulated by extracellular Na^+ , Mg^{2+} , Ca^{2+} , and H^+ (North 2002). When activated by ATP, the P2X receptors allow the non-selective movement of cations across the cell membrane, producing an increase in intracellular calcium and depolarization of the cell membrane (Ralevic. and Burnstock 1998). P2X receptors are expressed throughout the body and have been shown to be involved in inflammation and pain, neurotransmission, and regulation of endothelial smooth muscle cell metabolism (Khakh and North 2006). Studies have identified seven P2X receptors (P2X₁₋₇) in mammals, and they form a number of homomeric and heteromeric ion channel assemblies (North 2002). Within the lung, P2X receptors have been shown to be expressed in a number of lung cell types.

Of particular interest is the demonstration that rat alveolar epithelial type one cells express P2X₄ and P2X₇ ion channels in the apical membrane (Qiao *et al.* 2003; Chen *et al.* 2004). As yet, P2X expression has not been observed in the alveolar epithelial type two cells. The precise role of P2X receptors in the alveolar epithelial type one cell population has not been explained and is plausible that they do not contribute to fluid homeostasis. A number of different cellular functions are associated with the P2X receptor (for example, differentiation, migration, and proliferation) that could explain their presence in the alveolar epithelium. P2X receptors have also demonstrated a close relationship between caveolin and the P2X₇ at the membrane of the alveolar epithelial type one cell. A knockout mouse strain with genetic deletion of caveolin-2 demonstrated that P2X₇ expression was strongly downregulated in alveolar epithelial type one cells (Razani *et al.* 2002). The high density of caveolae with alveolar epithelial type one cells suggest an important physiological function (Gumbleton 2001; Park *et al.* 2003) and probing the close interaction of caveolin and P2X receptor ion channels may provide some answers to their respective physiological function in the alveolar epithelial type one cell population.

Cystic fibrosis transmembrane conductance regulator (CFTR) is a membrane protein expressed in epithelial tissue. Functionally, it is involved in

transepithelial fluid and ion transport. CFTR acts as a cyclic adenosine monophosphate (cAMP)-activated Cl^- channel. The functional expression of CFTR has been demonstrated in cell-attached patch-clamp recordings in alveolar epithelial type one cells (Helms *et al.* 2006). Mutations in the gene encoding for CFTR protein cause cystic fibrosis, which exemplify the importance of the CFTR in lung liquid homeostasis. In whole isolated lung studies imaged alveolar wall liquid (AWL) was blocked by the addition of the CFTR by bumetanide (Lindert *et al.* 2007). CFTR knockout mice were investigated and the AWL was not present. Experiments capturing image in wild type mice demonstrated that removing the Cl^- from the circulating solution also caused a block of the AWL. They concluded that there was a CFTR-dependant liquid secretion in alveoli of adult mice.

K^+ channels have also been demonstrated at a functional level in the alveolar epithelial type one cell population (Johnson *et al.* 2006; Bourke. *et al.* 2005). Multiple K^+ channels are expressed with almost 40 being recognised across the lung tissue (O'Grady and Lee 2003). The function of the K^+ channels within the alveolar epithelium is not well understood. However, it is postulated that one of the main functions is to control membrane potential to maintain the electrochemical gradient driving ion and fluid transport.

1.9 Alveolar epithelial type two cells.

The alveolar epithelial type two cells have been extensively studied and have earned the title “defender of the alveolus” (Mason and Williams 1977). These epithelial cells make up ~60% of the alveolar epithelium by volume however, they only constitute ~5% of the entire surface area of the alveolar epithelium of the adult lung. The alveolar epithelial type two cells are cuboidal in shape, with a measured diameter ~10 μm and a surface area ~ 450 to 900 μm^2 (Crapo 1983). Primary isolations of this cell type can now routinely be undertaken with a very high purity can be achieved (Chen *et al.* 2004). The alveolar epithelial type two cells have a very important function in keeping the air space open and available for gas exchange, they produce and secrete the

lipid rich surfactant. Von Neergaard hypothesized it as early as 1929 that the lung contained a surface-active agent. The existence of surfactant was confirmed and created a new area of respiratory research was born (Pattle 1955). Surfactant is composed of 90% lipid and 10% proteins. The surfactants four constitute proteins were decided upon to provide a standard identification; SP-A, -B, -C, and -D, with agreement being arrived upon at the consensus-conference in 1988 (Possmayer 1988). The function of surfactant is valuable to lung homeostasis and physiology. The main function is to act as the “anti-glue” to prevent adhesion of surfaces of gas containing organs, such as swim bladders and lungs, which might occur during collapse. The increased surface tension at the alveoli infers they are more likely to collapse at end-expiration; this is a direct result of their size and shape. Surfactant has also been shown to contribute to the pH of the alveolar environment (Lubman *et al.* 1998). Another function surfactant is that of host defence, both SP-A and SP-D have demonstrated an ability to bind to the surface of certain pathogens. The alveolar epithelial type two cells secrete other products involved in host defence such as bacteriolytic lysozymes (Katyal *et al.* 1992; Haller *et al.* 1992).

The ENaC channel expression and function in the alveolar epithelial type two cell has been demonstrated across the myriad of experimental models and techniques (for review Eaton *et al.* 2009). Absorption of lung fluid from the lung is driven by the active absorption of Na⁺. However, the identity of the proteins responsible remained unknown until the identification of the three genes that encode the ENaC subunits α , β , and γ (Canessa *et al.* 1993). In the majority of epithelial tissue the ENaC is formed from three protein subunits: α , β , and γ ENaC. The differing assembly of these proteins creates ion channels with differing regulatory mechanisms and biophysical properties. The ENaC channels play an important role in lung fluid sodium transport however this was confirmed beyond any doubt with the targeted inactivation of the mouse α ENaC gene (Hummler *et al.* 1996). This study demonstrated the functional significance of the channel in the neonatal period with the α ENaC (-/-)

neonates dying within 40 hours of birth from failure to clear their lungs of liquid.

A function of the alveolar epithelial type two cells, which is of significant importance, is their role as progenitor cells in alveolar epithelium (Evans *et al.* 1975; Lui *et al.* 2006). The type two alveolar epithelial cells can be considered to be the “stem cells” of the alveolar epithelium. The alveolar epithelial membrane if damaged needs to undergo repair in order to carry out the function of gas exchange and lung fluid homeostasis. In the adult lung the repair of the alveolar epithelium is undertaken by post-proliferative alveolar epithelial type two cell progeny acquiring alveolar epithelial type one cell characteristics and result in a loss of their type two attributes (Evans *et al.* 1975). During the period of transition the alveolar epithelial cells go through a transition stage and can be considered intermediate cells. There are a number of morphological changes seen in this period. These changes can be observed under the correct conditions in a tissue culture situation (Jain *et al.* 2001). However, in culture, the genetic transformation is not completed in its entirety (Gonzalez *et al.* 2005). This suggested endogenous substances that may trigger alveolar epithelial type two cell division are likely to be FGF-7, hepatocyte growth factor (Panos *et al.* 1993), and HB-EGF (Leslie *et al.* 1997).

The lamellar bodies of the alveolar epithelial type two cells have long been recognised as the storage compartments for surfactant (Andreeva *et al.* 2007). The lamellar bodies maintain internal acidic pH and this particular characteristic allows them to act as markers for alveolar epithelial type two cell (Haller *et al.* 1998; Haller *et al.* 1999). The release of surfactant from the lamellar bodies is by exocytosis and can be stimulated by various physiological and pharmacological stimuli acting via the β -adrenergic receptors (epinephrine, terbutaline, isoproterenol), P1-purinoreceptors or P2-purinoreceptors (for review Bucheimer and Linden 2004). Ventilation and increase in pressure have been shown to stimulate the release of surfactant (Nicholas and Barr 1983; Ashino *et al.* 2000). Real time imaging of a whole

lung experimental model has shown that there is a Ca^{2+} dependant step in release of surfactant upon expansion of the lung (Ashino *et al.* 2000).

A purinergic component has also been identified within the alveolar epithelial type two cell population. The purinoceptors have an important functional role in the regulation of fluid transport of epithelial transport (Bucheimer and Linden 2004). The purinergic receptors are divided into two subclasses P1 and P2 receptors. The alveolar epithelial type two cells do not express the P2X receptors. Addition of ATP to bath perfusion of isolated alveolar epithelial type two cells rat cell model demonstrated the activity of purinergic response (Griese *et al.* 1991). The addition of ATP caused a rapid increase in IP_3 levels suggesting the release of Ca^{2+} from IP_3 stores. The purinergic receptors have also been identified alveolar epithelial type two cells by molecular biological techniques (Rice *et al.* 1995). The A549 cell line, which is derived from lung airway epithelium displays properties of alveolar epithelial type two cells, has demonstrated the presence of purinergic receptors both at molecular (Communi *et al.* 1999) and functional level (Clunes and Kemp 1996). P2Y receptors are expressed on the apical membrane of many epithelial cell populations (Pediani *et al.* 1996).

The functional expression of G-coupled prostaglandin receptors (PG) on the apical membrane of alveolar epithelial type one cell isolated from late gestation guinea pig lung has been demonstrated (Mukhopadhyay *et al.* 1998). The binding of PG E_2 subtype plays an important role in perinatal lung alveolar Na^+ . The potency of binding of the PG in alveolar epithelial type two cells was utilised to classify the receptor type present and is shown to be the EP_3 subtype. This study was the first to demonstrate the presence of PG receptors in the alveolar epithelial type two cell population and they conclude an important function for the PG involvement in the G protein-mediated upregulation of Na^+ transport.

Cl^- channels were first identified in the alveolar epithelial type two cells in the mid-80's by single channel patch clamp recordings (Schneider *et al.* 1985).

These channels had a very high measured conductance ~350-400pS and were located in the apical membrane. The channel was found to be selective for anions relative to Na⁺ ($P_{Na}/P_{Cl} = 0.015$) and demonstrated anion selectivity of $I^- > Br_3^- > Cl^- > NO_3^-$. A high conductance Cl⁻ (375pS) was identified in guinea pig alveolar epithelial type two cell (Kemp *et al.* 1993). The expression of a number of K⁺ channels has been demonstrated also within alveolar epithelial cells including Kir channels, Ca²⁺-activated K⁺ channels, and Kv channels (O'Grady and Lee 1993.). There is still debate as to the functional role of these K⁺ channels within the alveolar epithelium.

The cyclic nucleotide-gated cation channels (CGN) are a family of channels that have been quite recently establish. Their discovery came about as a direct result of the investigation into the intracellular messenger for retinal photoreceptors (Fesenko *et al.* 1985) and as their name suggests they are stimulated directly by cyclic nucleotides cAMP and cGMP. CNG channels have been identified in a number of organs and species. A number of studies have identified nonselective cation channels in the air epithelium (Matalon *et al.* 1992, MacGregor *et al.* 1994). The CNG 1, has been demonstrated in rat lung both histologically (Ding *et al.* 1997) and electrophysiologically (Kemp *et al.* 2001; Schwiebert *et al.* 1997). The importance of the CNG channel was also demonstrated in a whole animal study (Junor *et al.* 1999). The role of a non-amiloride blockable component was in postnatal lung fluid homeostasis was introduced which was a novel observation for this class of ion channel.

1.10 Organ slice models.

The organ slice model provides biomedical research with a valuable tool to investigate *in vitro* cellular communication and interaction within an experimental model that is close to *in vivo* situation. The knowledge gained from single isolated cells and molecular biological experimental approaches can be tested to ascertain their relevance in an experimental model that retains much of the complex biological infrastructure seen in the whole organ. It is essential that we confirm and challenge our present understanding of

biological systems by using as many viable experimental techniques as possible. This in turn will provide a more informed understanding of the system as a whole. A number of key factors were considered in choosing the slice as an experimental model: the facility to represent the complexity of the intact organ; methodology that allowed easier cross-species comparison; the potential to use many organs from the same donor; the ease of histological evaluation as an alternative to, or as a complement to, biological/physiological assays and; the possibility to investigate regional physiology.

Organ slice technology has been providing answers to biological questions since the 1920's (Parrish *et al.* 1995 for review; Vickers *et al* 2004). The organ slice was developed principally as a tool to understand further the fields of pharmacology, toxicology, physiology, organ preservation and metabolism. Slices of tissue from brain, kidney, liver, lung, cardiac and smooth muscle, lymphatic tissue, placenta, mammary gland, thyroid, and gastrointestinal tract from a number of species have provided valuable information of many biological systems. In early studies, slices were produced by hand and even the most highly skilled operator had difficulties in producing highly reproducible organ slices.

The necessity to provide reproducible organ slices has lead to the development of a number of specially designed machines, which allow the automated production of precision cut tissue slices. There are a number of design and engineering aspects that allow the researcher to produce the highest quality slices on a routine basis. A fundamental requirement by the research community is the ability of the machine to preserve slice viability. It is essential that the researcher has the options to sterilise all the key components of the slice chamber, to reduce possible routes of infection, should the slices be required to be maintained in culture. The researcher should be provided with the option to autoclave any of the items that may be in contact with the tissue or bath solution, to reduce the possibility of infection or contamination. However, it should be pointed out that however sterile the procedure it is difficult to prevent against any intrinsic infections already present in the organ. Key also is the selection of materials to be used as

components; certain components will have to resist the corrosive nature of the high salt solution in which organ slices are produced. They should have a reasonable life span and replacement parts should be available.

In the production of high quality organ slices, the facility to control the temperature of the specimen bath is critical. Slices should be produced at temperatures in the region of 4-5°C to retain good viability. At this temperature, the rate of metabolic processes is reduced and will in turn see a reduction of deleterious effects at a cellular level. It is important that certain criteria are under the control of the operator; the approach speed, frequency, amplitude, and section height of the cutting blade all require fine-tuning. Each of these specific cutting profiles will need optimisation as per the organ type to be sectioned, age of the animal, and required orientation of the organ slice. However, all this is ineffectual if the blade technology is not of the highest standard. Traditionally, the use of stainless steel blades with a ground edge has been employed and these have been adequate in producing slices of quality in certain organs. To achieve a superior section from some of the more challenging tissue/organs, the use a ceramic blade is required. This provides a very sharp single bevelled edge and, combined with the greater rigidity of the blade cutting edge, this can allow the production of slices from even the most challenging tissues.

Acute organ slices have an advantage over primary cell isolations in that they are less susceptible to changes in gene expression. A recent study has demonstrated considerable differences in genetic expression profile between cultured alveolar epithelial type two cells and freshly isolated alveolar epithelial type one and alveolar epithelial type two cells (Gonzalez *et al.* 2005). Isolated alveolar epithelial type two cells have been the experimental system of choice in studying the alveolar epithelial mechanisms and functions and have provided much valuable information. However, the cell culture conditions selected to maintain primary isolated alveolar epithelial cells have been shown to have dramatic effects on the expression profiles of certain ion channels within alveolar epithelial type two cells (Jain *et al.* 2001). It is clear that the

microenvironment plays an important role in genetic expression. The microenvironment will also have an effect on results obtained from the slice experimental model. However, the genetic expression profile is less likely to be changed as dramatically as in primary cell isolation. The enzymatic reactions and mechanical separation required to obtain a primary isolated cell population can cause a disruption to certain proteins and, in turn, affect function. A multidiscipline approach has, and continues to provide, the greatest prospect of advancing our understanding of the alveolar epithelium in healthy and diseased situations. Observations and conclusions drawn should also take into account the methodological approach used, as certain methods would prove more advantageous in replicating a healthy or diseased state. The lung slice model offers a real alternative to investigate alveolar epithelial cell physiology.

1.11 Summary.

The information presented above provides a summary of the current knowledge from anatomy to molecular physiology of the respiratory system, with particular focus on the alveolar epithelial cell population. There is a distinct difference in the physiology of fetal, neonatal, perinatal and adult lung. The neonatal lung secretes fluid into the lumen by active transport to allow appropriate growth. An upregulation of ENaC ion channel expression from the third trimester, coupled to the massive increase in adrenaline at birth facilitates in the switch from liquid-secretion to liquid absorption. As the lung develops into adulthood, the reliance on ENaC for Na⁺ absorption wanes and other mechanisms become more important to overall alveolar fluid homeostasis. The unique epithelial covering of the lung is composed of two morphologically distinct cell populations. The alveolar epithelial type one cell and the alveolar epithelial type two cell. The alveolar epithelial type two cell has been the model of choice for the study of ion channel activity within the alveolar epithelium but there has been a lack of functional information as to the role of the alveolar epithelial type one cell in fluid homeostasis. Since they cover the majority of the alveolar surface area, it is critical to gain an understanding of their function at the molecular level. The fragile nature and difficult isolation of alveolar epithelial type one cells has hindered the ability to undertake such functional studies. The organ slice has proved to be a constructive research tool across a range of physiological experiments. It would be perfect to be able to collect functional experimental data from the alveolar epithelia type one cells *in situ*.

1.12 Aims of current research.

The primary aim was to obtain functional ion channel recordings from identified alveolar epithelial type one cells from a lung slice model. The objective was then to allow a full characterisation of the myriad of ion channels present in the intact alveolar epithelium. It was essential to optimise the technique of lung slicing to produce viable slices that would allow clear access to the alveolar epithelium. Following on from this it was important to assemble evidence as to the viability of acute lung slice. The understanding of the physiological role the alveolar epithelium was also investigated by means of live cell imaging using confocal microscope with fluorescence Ca^{2+} indicator dye.

Materials and methods

Chapter 2.

Material and methods in rat lung slice.

2.1 Tissue culture methods.

2.1.1 HEK293 cell culture

Human embryonic kidney 293 (HEK 293) cell line was used as a control cell population for the LIVE/DEAD® experiments. These cells stably expressed rat purinergic (P2X₂) receptors, full detail of expression can be found in Mason *et al.*. HEK 293 cells were maintained in Dulbecco's Modified Eagle's Medium supplemented with 10% fetal calf serum, 2mM L-glutamine, 1% antibiotic antimycotic, 100µg.ml⁻¹ gentamicin and 300µg.ml⁻¹ geneticin (all purchased from Invitrogen Ltd., Renfrew, Renfrewshire, U.K.) in a humidified incubator gassed with 5% CO₂ 95% air. Cells were *passaged* every 7 days using Ca²⁺ and Mg²⁺ free phosphate buffered saline (-Ca²⁺/ Mg²⁺ PBS, Invitrogen Ltd.). For the LIVE/DEAD® staining experiments described in 2.5.2, HEK293 cells were plated onto glass coverslips and cultured as above for at least one day prior to experimentation.

2.1.2 Long-term storage of cell lines.

Cryopreservation was undertaken of ~1x10⁶ cell.ml⁻¹. The cells were suspended as described above, 2.1.1. The cell suspension was then spun down, for 5 minutes at 3000 rpm, to allow the formation of a cellular pellet. The cell medium was removed and the cells were resuspended in the cryopreservation medium containing bovine serum albumin (BSA) supplemented with 10% (v/v) DMSO. The cells were aliquoted into cryotubes (BDH, Alderstone, Berkshire, U.K.) in 1 ml volumes. To prevent cryodamage the cells were allowed to freeze slowly. This was achieved by placing the cryotubes onto a cryocane, which was placed in a polythene jacket and then wrapped in 1.5 inch lagging; this was then placed in an -80°C freezer. This method allows the temperature of the cells in the freeze medium to decrease slowly, approximately 1°C/min. The cells were stored at -80°C for a period of twenty four hours. They were then transferred to a liquid nitrogen store where they were held until required.

2.2 Preparation of lung slices.

2.2.1 Animals.

In the following studies, the Wistar rat strain was used as the experimental model. Pre-weaned rat pups aged between six and eight days old were used throughout. The pups and dam were housed in acrylic cages with wood shavings in an acclimatised room (12/12 hours light/dark cycle; $21\pm 3^{\circ}\text{C}$) and provided with water and food *ad libitum*. Pups were killed in accordance with Home Office guidelines using schedule one protocol.

2.2.2 Preparation of the lungs.

During the progression of this project, a series of experimental protocols underwent optimisation to meet the demands of the evolving project. Such optimisation was necessary was to establish a method of slicing that would facilitate functional ion channel recordings from identified alveolar epithelial type one cells from within a lung slice. Specifically, three techniques were investigated: A) low melting point agarose filling and mounting of lobes, B) polyethylene glycol filling and C) unfilled lungs.

Prior to dissection of the lungs, the immediate area was thoroughly cleaned with 70% ethanol (EtOH) solution. Surgical equipment was also swabbed in 70% EtOH and allowed to air dry to maintain the sterile environment. Gloves were worn at all times and the exterior of the animal was wiped with 70% EtOH following sacrifice. The slicing procedure was carried out in a vertical flow hood (Edgegard, The Baker Company, Sanford, Maine, U.S.A.) reducing any air borne infection.

The animal was pinned out with the abdominal surface facing upwards and an incision was then made from the base of the mandible to the midline of the abdomen. The skin and visceral peritoneum was cut open to allow access to the abdominal cavity. An incision was then made below the sternum and continued

on both sides around to the dorsal side; care was taken not to puncture the organs. This allowed full access to the diaphragm, which was carefully dissected away. The rib cage was dissected by cutting along the length of the sternum, from the body of the sternum to the manubrium of the sternum. The rib cage was pinned back and the mesenteries attaching the internal organs to the dorsal body wall, along with the connective tissue around the clavicles, were carefully detached. Care was taken not to puncture the lung. The trachea was cut above the larynx and the heart and lungs were removed *en bloc*.

A 2% (w/v) solution of low melting point agarose (Sigma-Aldrich Company, Poole, Dorset, U.K.) was dissolved in fresh sterile extracellular bath solution containing (in mM): 140 NaCl, 5 KCl, 10 HEPES, 1 CaCl₂, 1.2 MgCl₂, 5 D-glucose pH 7.4, 300mOsM, by heating to ~55°C, whilst being continuously stirred. This solution was allowed to cool to 37°C and maintained at that temperature in a water bath. A catheter was fed down the trachea, a suture was tied tightly to hold the catheter in place, and another was placed just below the end of the catheter (around the trachea) and left loose. The liquid agarose was smoothly injected into the lung until each of the lobes was fully inflated. The remaining suture was tied off to prevent the agarose leaking from the airways. To avoid damage to the alveolar epithelium, the lungs were not over filled and only gentle pressure was used to fill the airspaces.

The filled organ was then gently washed with extracellular solution and the agarose allowed to solidify whilst the tissue was immersed in physiological bath solution cooled to ~4°C using an ice bath. A single dissected lobe was then removed and placed in a 5% agarose solution, maintained at 37°C. The mounting agarose, which contained the lobe, was then cooled in ice-cold physiological bath solution, which allowed the agarose to reach set point and solidify. The agarose-encased lobe was trimmed of excess agarose and mounted for slicing (see section 2.2.3).

In the case of PEG 400-filled lungs, the dissection proceeded as above except that the lung was injected with a bolus of PEG 400 via the tracheal catheter.

PEG 400 is liquid at room temperature. However, when it is cooled to 4°C, it becomes a solid and provides stability for precision sectioning of the lobe.

In experiments where unfilled slices were chosen, the lungs were again dissected as above, but the lobes were mounted immediately and directly on the jig of the slicer prior to slicing (see section 2.2.3 and fig. 1.1).

2.2.3 Sectioning of lung slices with the Integraslice®

For filled lungs, the agarose blocks were fixed to the jig with cyanoacrylate adhesive gel. For PEG 400 filled and unfilled lungs, lobes were individually dissected and fixed directly to the jig of an Integraslice® (7550 PSDS, Campden Instruments, Leicester, Leicestershire, UK) by cyanoacrylate adhesive gel; this is shown in fig. 1.1. Slices were cut at a constant temperature of 4°C (± 0.3) and were immersed in extracellular physiological bath solution. The temperature was maintained by utilising a temperature-controlled specimen bath, fig. 1.1 A (HP 756; Campden instruments). 200µm thick slices were cut across the transverse plane of the lobe. Once cut, each slice was transferred to a separate well of a 24 well plate containing 2ml of extracellular bath physiological solution (as above), and held at 37°C in a humidified incubator which was supplied with a 5% CO₂, 95% air gas mix (Sanyo MCO 15AC, Sanyo Electrical Co. Ltd, Tokyo, Japan) until they were required for further experimentation. The Integraslice® allowed the production of reproducible, viable lung slices. Quality and accuracy were greatly augmented by the use of ceramic blades, fig. 1.1 C (7550/1/C; Campden instruments).

The Integraslice® also allows the user precise control over the frequency, amplitude, and speed of advance of the blade, which are essential in production of high quality slices. Unfilled lungs were sectioned at a frequency of 96 Hz, an amplitude of 1.1 mm, and an advance speed of between 0.10 and 0.04 mm.s⁻¹. Whilst PEG 400 filled lungs were sectioned at the same frequency and amplitude, but the advance speed was increased to 3mm.s⁻¹, agarose filled lobes were cut using an advance speed of 7mm.s⁻¹.

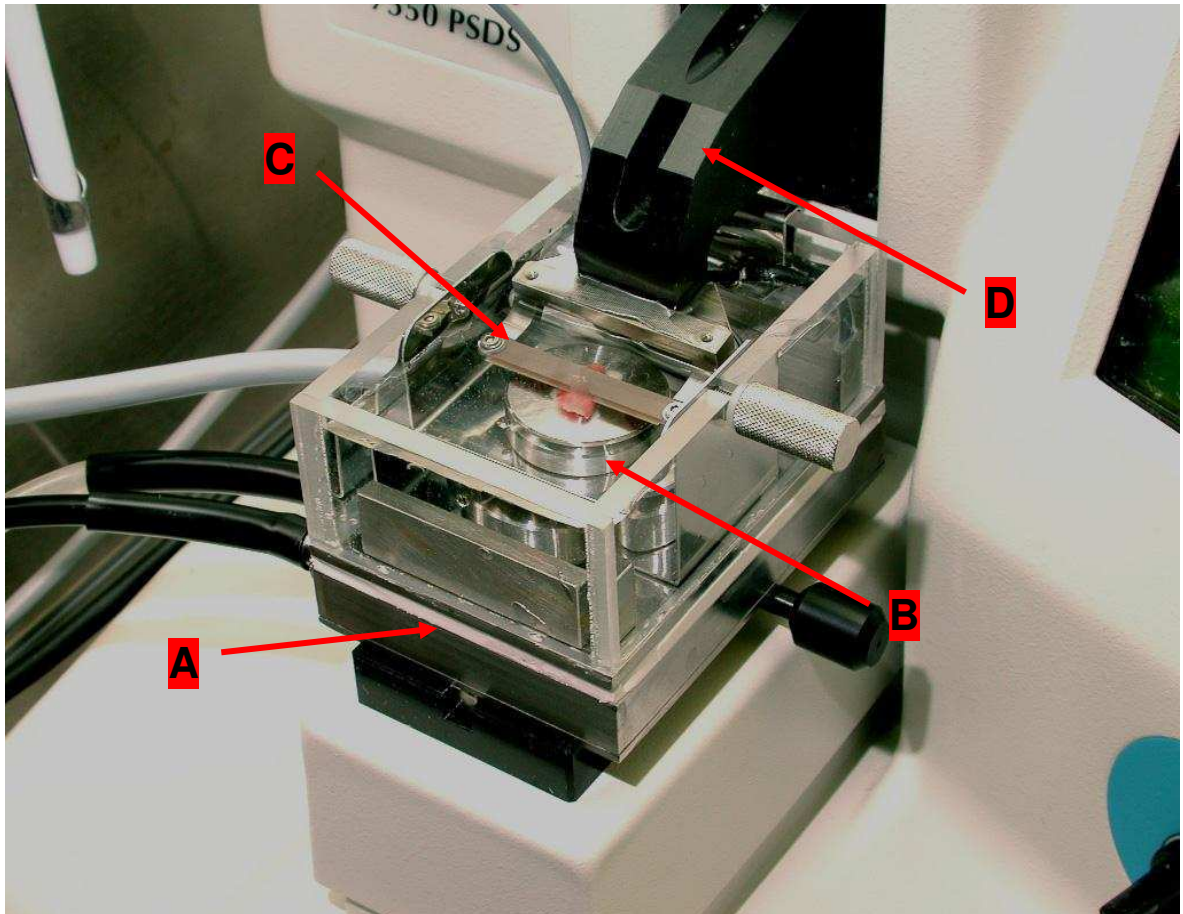


Figure 1.1 Unfilled lung slice sectioning by Integraslice®.

Whole lung lobe fixed in position on a stainless steel jig by cyanoacrylate adhesive gel. This image demonstrates production of a 200 μ m thick lung slice. The image shows the slice being cut across the transverse plane of the lung lobe. Here also can be seen the temperature controlled specimen bath A, jig B and ceramic blade C. The specimen remained in a fixed position on the jig while the sectioning arm D controlled the speed of approach, amplitude and frequency of the blade.

2.3 Live cell immunohistochemistry methods.

2.3.1 Alveolar epithelial type one cells identified with VIIIIB2 mouse monoclonal antibody.

VIIIB2 is a mouse monoclonal antibody which binds specifically to an extracellular epitope on the plasma membrane of the alveolar epithelial type one cell (Danto *et al.* 1992). Currently, the identity of the epitope is unknown. Lung slices were washed three times for five minutes with 2ml of warmed physiological extracellular bath solution. Lung slices were then incubated at 37°C for 1.5 hours in the presence of VIIIB2 (1:5 dilution). VIIIB2 was stored in hybridoma medium and this was diluted to the required concentration as necessary. Lung slices were washed three times more for five minutes each in warm physiological extracellular bath solution and then incubated in physiological extracellular bath solution containing 5% (w/v) BSA for 15 minutes at 37°C, followed by washing three times for five minutes in warmed physiological extracellular bath solution. Slices were then labelled with an anti-mouse IgG, secondary antibody (Alexa Fluor 488 or Alexa Fluor 546, Molecular Probes, Strathclyde, Paisley, U.K.) at a 1:500 dilution and incubated for 30 minutes at 37°C. Immediately prior to imaging, the lung slices were washed once again with warm physiological bath solution to remove any unbound antibody. In experiments where lung slices underwent a co-staining procedure, the choice of secondary antibody was dependant upon the excitation wavelength of the vital dye selected. In the situation where a dye with excitation of 488nm was chosen, the secondary antibody selected was a 1:500 dilution of mouse Alexa Fluor 546 secondary antibody (Molecular Probes).

The VIIIB2 antibody was a generous gift from Drs. Edward Crandal and Zea Borok, (Will Rogers Institute Pulmonary Research Center, Division of Pulmonary and Critical Care Medicine, Keck School of Medicine, Los Angeles, U.S.A.).

2.3.2 Alveolar epithelial type two cells identified with Nile Red

Lung slices were washed three times for five minutes with 2ml of warmed physiological extracellular solution. Lung slices were then incubated in Nile Red solution at 37°C for 10 minutes (1 µg.ml⁻¹). Lung slices were washed three times more for five minutes each in warm physiological extracellular solution. Slices were held at 37°C in a humidified incubator which was supplied with a 5% CO₂, 95% air gas mix (Sanyo, Japan) until they were required for further loading procedures or experimentation. Fluorescent imaging by exciting at 546nm showed the Nile Red fluorescence signal and allowed identification of alveolar epithelial type two cells.

2.3.3 Alveolar epithelial type two cells identified with LysoTracker® Green

Lung slices were washed three times for five minutes with 2ml of warmed physiological bath solution. Lung slices were then incubated at 37°C for 10 minutes in LysoTracker Green (50nM). Lung slices were washed three times more for five minutes each in warm physiological extracellular bath solution. Imaging was undertaken immediately after the wash periods as the probes may increase lysosomal pH (Molecular Probes, technical notes MP0525, April 2001 revision). LysoTracker Green is a fluorescent dye which is excited at 504 nm and emits at 511 nm.

2.4 Electrophysiology Methods.

Electrophysiological experiments were carried out at room temperature (21± 1 °C), and all solutions were equilibrated at room temperature.

2.4.1 Solutions.

All compounds were of analytical grade and were purchased from Sigma-Aldrich Laboratory Supplies (Poole, Dorset, U.K.) unless otherwise stated. Sodium isethionate, N-(2- Hydroxyethyl) piperazine-N'-(2-ethanesulfonic acid) 4-(2-Hydroxyethyl)piperazine-1- ethanesulfonic acid (HEPES), tetraethylammonium

chloride (TEA), amiloride and potassium isethionate were obtained from Fisher Scientific (Loughborough, Leicestershire, U.K.).

2.4.1.1 Extracellular bath solutions for recording currents in lung slices.

In cell-attached patch-clamp experiments, a standard bath recording solution was used to mimic normal extracellular physiological conditions. Slices were perfused under gravity (4-6 ml.min⁻¹) with extracellular bath solution composed of (in mM): 140 NaCl, 5 KCl, 10 HEPES, 1 CaCl₂, 1.2 MgCl₂, 5 D-glucose). The osmolarity of the solution was measured using a freezing point depression osmometer and adjusted to 300mOsm with sucrose. The pH of the solution was measured and adjusted to 7.4 with NaOH. Once the patch electrode was within micromanipulator range of the cell of interest, the perfusion flow was stopped to achieve a “stop bath” configuration.

2.4.1.2 Extracellular pipette solutions for cell attached recording.

Cell-attached patch clamp experiments used a high K⁺, low Cl⁻, pipette solution, which contained (in mM): 145 K Isethionate, 10 HEPES, 1 CaCl₂, 1.2 MgCl₂, 5 D-Glucose, 10mM TEA, 100µM niflumic acid, 10µM amiloride. The osmolarity of the solution was measured and was found to be 317mOsm; no adjustment was undertaken. The pH of the solution was measured and adjusted to 7.4 with KOH.

2.4.2 Maintaining lung slice position.

Slices had to be held in a secure manner to allow the formation of giga Ohm seal and to avoid movement artefacts. Two methods were employed, platinum C-ring and an in-house designed “*concentric ring slice holding sandwich*”. The platinum C-ring consisted of a 10 mm platinum wire which was fashioned into a “C” shape with individual nylon threads were spread and fixed tight over the frame with cyanoacrylate adhesive gel. This created a non-reactive, weighted net, which would allow access to alveolar epithelium by a patch electrode. The “*concentric ring slice holding sandwich*” consisted of two stainless steel rings

(larger ring: outer diameter 20mm, inner diameter 15mm, smaller ring outer diameter 14.5 mm inner diameter 13 mm; both rings were 2mm high). Within the arrangement there was a sandwich, which was composed of a cotton ribbon material, a lung slice, then nylon netting with a mesh diameter of 1.5 mm. This configuration allowed slice access to the physiological bath solution, held the slice firmly in place and, most importantly, allowed access of the patch electrode to the alveolar epithelium. The sandwich was assembled as follows: the outer ring was placed upon a flat surface; the slice was positioned on the ribbon, which was saturated in physiological bath solution, this was centred over the outer ring the nylon mesh was placed on top and then inner ring was pushed into place making sure the netting was taught, in order to keep the slice in position. Excess of ribbon and netting was trimmed and the *holding sandwich* was placed in a custom bath, which was just over 20mm in diameter also holding the slice firmly in place. This allowed the slice to be perfused with physiological bath solution.

2.4.3 Preparation of slices for electrophysiology analysis.

2.4.4 Patch-clamp electrodes.

Patch-clamp electrodes were prepared from thin-walled, filamented, borosilicate glass capillaries (Clark GC 100F-15, 1.0 mm outside diameter, 0.58 mm inside diameter (Clark Electromedical Instruments, Berkshire, U.K.), using a two stage pulling process on a Narishige PP-83 puller (Narishige, Japan). Electrodes were heat-polished to aid in seal formation (Hamill, O.P. *et al.*, 1981) using a Narishige MF-83 microforge (Narishige, Japan). Patch-clamp electrodes were 7-15 mega ohms resistance for cell attached recordings when filled with pipette solution as described.

2.4.5 Cell-attached configuration of the patch-clamp technique.

Secured lung slices (see section 2.4.2) were positioned in the perfusion chamber (produced in-house) mounted on the stage of Olympus BX50WI inverted microscope (Olympus Optical Co. (Europa) GmbH, Hamburg,

Germany). The microscope was positioned on an anti-vibration table (TMC, MA, U.S.A.) and the entire apparatus was surrounded by a Faraday cage (Scientifica, U.K.) to reduce electrical interference. Slices were initially perfused at a rate of 4-6ml.min⁻¹. The perfusion system was gravity-feed and consisted of a six reservoirs, each made from the barrel of a 50ml disposable syringe (Monoject, UK) feeding to a six way tap (Hamilton GB Ltd., Carnforth, Lancashire, UK) via gas impermeable Tygon tubing (VWR, Lutterworth Leicestershire, U.K.). The tap was connected to perfusion chamber, again using Tygon tubing. The perfusate was continuously removed by suction, provided by a vacuum pump connected to a Buchner flask reservoir.

Slices were viewed at 10x magnification (LUMPLFL 10xW, Olympus) via transmitted light using phase contrast in order to align initially the slice and patch pipette to the centre of the field of view. Pipette solution was injected through a sterile 0.22µm pore filter (Whatman® International Ltd, Maidstone, England), the filled pipette was placed in an electrode holder (Axon Instruments, Molecular devices, Forseter City, CA, U.S.A.) which was connected in turn to a CV7A amplifier headstage and MultiClamp 700A amplifier (Axon Instruments, Molecular Devices, U.S.A.). The MultiClamp system allows the user to control the amplifier via computer; this is achieved by using Programme Commander software (Axon Instruments, Molecular Devices, U.S.A.). The connection between the intracellular solution and the CV7A headstage was achieved via a silver/silver chloride (Ag/AgCl) wire. The amplifier was connected to the MultiClamp amplifier. To allow the circuit to complete an Ag/AgCl pellet (Havard Apparatus Ltd., Edenbridge, Kent, U.K.) provided the 0 V bath reference electrode, which was connected directly to the headstage. In order to create a giga seal between the patch electrode and the cell membrane, positive pressure was usually required. A side port from the pipette holder allowed the attachment of tubing and positive and negative pressure could be applied through the patch pipette.

Electrodes were manoeuvred into close proximity of the slice using a three plane mechanical macromanipulator (PCS-5000 Series, Scientifica, UK). The seal test

function in Clampex 9.1 software (Axon Instruments U.S.A.) was used to drive a 10 mV square wave test pulse and this provided an on-line calculation of the electrode resistance. The objective lens was changed to 60x magnification water immersion (LUMPLFL 60xW, Olympus), to allow very fine positioning of the electrode tip just prior to seal formation. The fluorescent VIII B2 labelling was used to identify type one alveolar epithelial cells. The microscope was fitted with a Mercury/Xenon Short Arc Lamp (Olympus, Germany) and FITC filter cube (Chroma) allowed visualisation of alveolar epithelial type one cell membrane fluorescence. To reduce photobleaching or phototoxic effects, the exposure time of the slice was kept to a minimum and a polarizing neutral density (ND) filter (ND6 or ND25 Olympus) was employed in the light path to further reduce photodamage.

A seal was formed between the patch electrode and the cellular membrane by manoeuvring of the pipette into an alveolar airspace region. The final movements were controlled by a piezoelectric micromanipulator (PCS-5000 series, Scientifica, U.K.). Gentle suction was applied when there was an increase in pipette resistance; this indicated the tip of the pipette has come into contact with the cellular membrane. On achievement of seal resistance > 1 giga Ohm, transient current deflections due to capacitance of the glass wall of the electrode were compensated for using the automatic fast and slow capacitance functions provided in the MultiClamp software. The cell-attached configuration was now achieved (see fig. 4.1)

2.4.6 Experimental protocol for cell-attached patch-clamp.

2.4.6.1 Standard ramp protocol

The protocol used for cell-attached patch clamp experiments using the identified alveolar epithelial type one cells in a lung slice used a resistive feedback voltage clamp. Ionic currents were evoked in cells by using a pre-programmed ramp protocol where the cells were held at 0mV before and after the ramp. Currents were evoked by stepping voltage from a holding potential to -70 mV and

ramping to +90 mV over a 2 seconds period, see fig.4.2. This protocol was repeated at a frequency of 0.1 Hz.

2.4.6.2 Gap-free voltage-step protocol

Cells were held at potentials ranging from +30 to -90 mV (V_m , assuming resting potential of -40 mV). Voltage protocols were generated and currents recorded using pClamp 9.0 software, employing a Digidata 1322 A/D converter (Axon Instruments). Data were filtered (4-pole Bessel) at 2kHz and digitized at 5kHz. Data analyses were performed using the pClamp 9.0 suite of software (Axon Instruments).

2.4.7 Data analysis and presentation of cell-attached patch-clamp recordings.

2.4.7.1 Calculating NP_o

The product of channel number and open state probability (NP_o) at any voltage was calculated from 20 seconds of current recording using the following equation;

$$NP_o = I/i$$

Where I is the mean patch current calculated from the whole recording and i is the single channel amplitude.

2.5 Slice viability staining methods.

2.5.1 Propidium iodide staining

Lung slices were washed three times for five minutes with 2ml of warmed physiological bath solution. Slices were added to 1.5 ml of pre-warmed

physiological extracellular solution containing propidium iodide (PI 3 μM). The specimen was incubated for 30 minutes at room temperature, and was light protected. The slices were washed three times more for five minutes each in warm physiological extracellular solution. Staining with PI was performed after all other immunohistochemical staining.

2.5.2 LIVE/DEAD® staining.

To maintain the reactivity of the kit, both reagents were stored sealed, protected from light, frozen at -20°C , and desiccated. Before experimentation, the agents were allowed to warm to room temperature. A $4\mu\text{M}$ working concentration of EthD-1 was prepared in sterile physiological solution. A vortex mixer was used to ensure that the solution was uniformly mixed. To the same solution, calcein AM was added to give a resultant working solution of 2 μM .

1.5ml of the combined solution was added to a 35mm Petri dish in the case of the HEK293 cell line. Culture medium was aspirated away prior to loading and cells were washed twice in 3ml of warmed physiological extracellular bath solution. The 35mm Petri dish containing the 1.5 ml of LIVE/DEAD® combined solution was placed at 37°C in a humidified incubator, which was supplied with a 5% CO_2 95% air gas mix (Sanyo, Japan). The cells were incubated for 30 minutes. The cells were then removed from the staining solution and washed three times for five minutes with 2ml of warmed physiological extracellular bath solution. The cells were then ready for imaging; Calcein is excited optimally at 485 ± 10 nm. EthD-1 is optimally excited at 530 ± 20 nm. The cells were imaged in extracellular bath solution. In order to confirm performance of the assay, HEK293 cells were imaged under normal conditions. Cells were then treated with physiological extracellular solution containing 1% (v/v) Triton X-100 for 10 minutes washed three times for five minutes, the combined LIVE/DEAD® solution was re-applied and cells were incubated as above.

The slice was loaded with the same concentration of LIVE/DEAD® solution. A slice was then placed in one of the well of a 24 well plate. The slice was

sectioned as described above (section 2.2.3) and this was placed at 37°C in a humidified incubator, which was supplied with a 5% CO₂ 95% air gas mix (Sanyo, Japan). The specimen was incubated for 30 minutes in 1.5ml of extracellular solution containing 4µM EthD-1 and 2µM Calcein-AM, LIVE/DEAD® solutions. The slice was then removed from the staining solution and washed three times for five minutes with 2ml of warmed physiological extracellular solution. The slice was then ready for imaging.

Lung slice viability was assessed under a number of conditions. All analyses were conducted on a Zeiss CellMap IC™ (Zeiss, Germany, fig. 1.2) confocal imaging station, which was mounted on the Olympus BX50 WI (Olympus, Germany) water immersion upright microscope. Slices were positioned in a perfusion chamber (see sections 2.4.2), which held the specimen firmly in place during experimentation. Samples were imaged having undergone: A) slicing alone, B) slicing and addition of 1% (v/v) Triton X-100 for 10 minutes and; C) slicing and VIII B2 loading protocol (see section 2.2.1). Calcein was imaged with the 488nm laser and the 520/40 emission filter set of the CellMap. EthD-1 was excited with the 532nm laser and imaged with the aid of a 560 long pass emission filter of the CellMap. To assess the viability of the lung sections, the number of EthD-1 positive nuclei (*i.e.* dead cells) per field (105 µM x 105 µM) under each of the three conditions was counted in at least three independent, random fields.

2.6 Calcium imaging methods.

Slices were cut following agarose backfilling (see section 2.2.2) and transferred to a physiological solution containing 5µM Fluo-3 AM (Molecular Probes) and 0.1% (w/v) Pluronic acid (Sigma-Aldrich) for 30 minutes at 37°C in a humidified incubator which was supplied with a 5% CO₂ 95% air gas mix (Sanyo, Japan). The slice was then washed with extracellular physiological bath solution to remove any of the unbound Fluo-3 AM for 10 minutes at 37°C. Slices were then transferred to perfusion chamber as outlined above in section 2.4.2; in these

particular experiments the weighted C-ring was used and was placed on the stage of inverted LSM 410 confocal microscope. Lung slices were constantly perfused with bath extracellular solution, with a flow rate of 4-6ml.min⁻¹. To capture intracellular calcium dynamics, two imaging techniques were employed: A) time course line scanning and B) region of interest time course scanning. Utilizing the Zeiss LSM, software line scans were captured every 3 seconds with 600 scans per time course. The region of interest scans were carried out by cropping a small area from the entire image ~100µm x 100µm field of view. The time-course was 200 scans, once every 3 seconds. Analyses were conducted off-line with the Zeiss LSM software.

A number of pharmacological agents were used in conjunction with the Ca²⁺ imaging A) Slices were perfused under gravity (4-6 ml/minute) with a high K⁺ extracellular bath solution composed in (mM) 90 NaCl, 50 KCl, 1.2 MgCl₂, 5 CaCl₂, 2.5 HEPS, 10 D-Glucose, 10 Sucrose; B) slices were also perfused with extracellular bath solution which contained of 10µM A23187 Calcimycin (Alomone Labs, Israel); C) 100µM adenosine triphosphate (ATP), and; D) 50µM muscarine chloride.

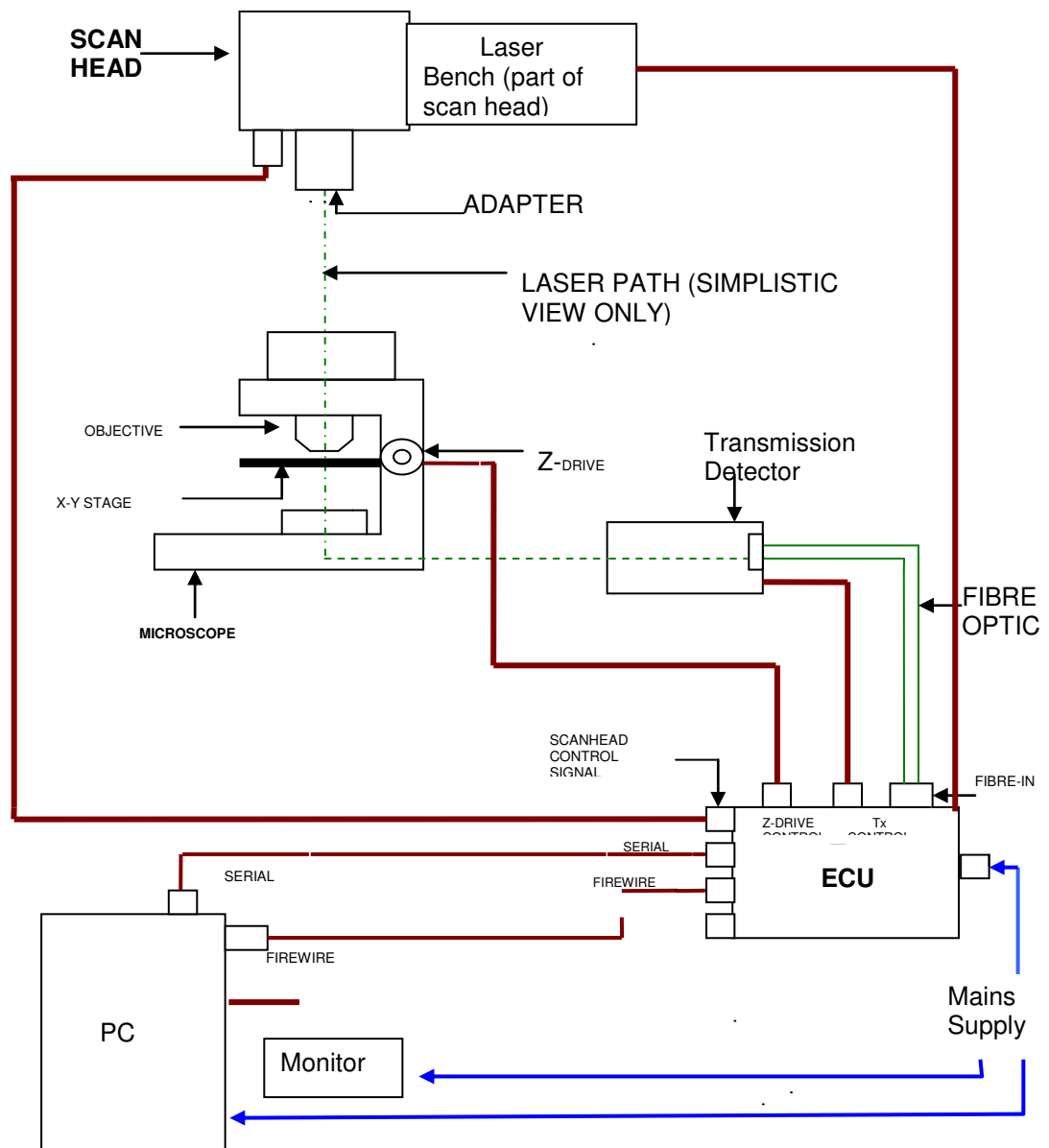


Figure 2.2 CellMap IC™ schematic configuration.

The system is designed to be mounted directly to the microscope. A fully automatic Z-drive allows precise z-stack confocal optical sections. The system is a closed system; in that it can no additional laser lines can be added. CellMap

IC™ captures confocal images of fluophores who have an excitation 488nm and 546nm. The system also contains filters.

Results

Chapter 3.

**Slice optimisation, viability and live cell
identification.**

Introduction.

The successful development of a suitable experimental model to examine the physiological properties of alveolar epithelial type one cells has been hampered due to the delicate anatomy of the postnatal lung. The introduction of a lung slice experimental model has created a number of exciting opportunities to investigate respiratory alveolar physiology at a molecular level. However, the development of this novel preparation has also introduced many technical challenges. This chapter describes the experimental optimisation which has allowed the first recording of functional ion channel activity from alveolar epithelial type one cells *in situ* (Bourke *et al.* 2005).

The alveolar epithelium plays a fundamental physiological role throughout life in both gas exchange and fluid clearance (Williams 2003; Olver *et al.* 2004; Wilson *et al.* 2007; Eaton *et al.* 2009). While the isolation of alveolar epithelial type two cells (Dobbs 1990) is by no means trivial, it has become a routine preparation in a number of research laboratories and has provided invaluable information about their role in lung fluid homeostasis and an insight into the molecular nature of paracellular fluid movement. Alveolar epithelial type one cell isolation has proved to be much more demanding due principally to the fragile nature of these cells; this difficulty is compounded by the complex nature of the tight junctions which are present between both alveolar epithelial type one and alveolar epithelial type two cells (Borok/Lubman *et al.* 1998; Chen *et al.* 2004; Dobbs *et al.* 1998; Isakson *et al.* 2001). The large surface area, extremely thin nature of the epithelium, and the close relationship to the vast pulmonary capillary network had until recently combined to thwart functional ion channel recordings from isolated alveolar epithelial type one cells (Johnson *et al.* 2006). As a result, many aspects of the alveolar epithelial type one cell function remain unresolved. In order to further our understanding of alveolar epithelial type one cell function within the epithelium, an unfilled slice model was developed and optimised making it possible to record ion channel events from identified alveolar epithelial type one cells.

It was essential to provide consistent and reproducible tissue slices, which retained a high cellular viability, were precision cut, and relatively straightforward to generate, allowing daily acute slice production. It was essential to keep cellular damage to a minimum, so that critical cellular and intracellular interplay, along with normal tissue micro-architecture, remained intact. This presented clear advantages over isolated cell preparations. A substantial quantity of the direct electrophysiological evidence from alveolar epithelial preparations has relied on recordings made from isolated alveolar epithelial type two cell preparations. The list of research investigations looking at the cellular function of isolated alveolar epithelial type two cells is extensive (for review see Kemp and Kim 2004; Eaton *et al.* 2009) and there is an ever-expanding pool of information pertaining to alveolar epithelium type one cell function (Dobbs 2007). However, although there is general considerable consensus that active transport is the critical underlying mechanism of lung fluid homeostasis, the contribution of differing ion channel families responsible for adult lung fluid clearance is still strongly debated. This is due in part to the species variations and the choice of experimental model.

A valid argument as to why there is such range of differing information has been suggested by Gonzalez *et al.* (2005), who examined the gene expression of primary isolated alveolar epithelial type one cells and compared it to that of alveolar epithelial type two cells which had morphologically differentiated into alveolar epithelial type one *like* cells after seven days in culture. Comparisons were also made between freshly isolated alveolar epithelial type two cells and alveolar epithelial type two cells in culture for seven days. A comparison was also carried out between freshly isolated alveolar epithelial type one cells and freshly isolated alveolar epithelial type two cells. Gonzalez used isolated rat cells as the experimental model and analyzed the differences in gene expression using gene chip technology.

Comparison between freshly isolated alveolar epithelial type one cells versus alveolar epithelial type two cells identified 190 unique genes associated with type one cells and 411 unique to type two cells. 52 genes, 26 each in type one and type two cells, exhibited the highest fold differences. In the comparison of

freshly isolated type two and cultured type two cells, they identified 332 unique genes to freshly isolated type two and 357 unique to cultured type two cells. They reported a similar number of differences between freshly isolated type one and cultured type two cells, with type one showing 195 different genes and cultured type two showing 503 different genes. Although the cultured type two cells lost various morphological and biochemical characteristics associated with type two cell phenotype and acquired some of the characteristics of the type one cell phenotype, it was unclear how similar a cultured type two model was to native type two cells. However, it seems apparent that type two cells in culture are substantially different from freshly isolated type one cells. The cultured type two cells have the ability to dedifferentiate, but seem unable to fully transdifferentiate at the genetic level, in culture. These data provide good rationale to investigate fully the possibility of using the lung slice as a model to examine type one alveolar epithelial cell function with the knowledge that function and gene expression would more closely resemble that seen *in vivo*.

For this model to gain universal acceptance, it was vital to provide an accurate evaluation of cellular viability within the lung slice. This required an assay that could provide clearly defined and well-recognised parameters of cell viability and would demonstrate simply and quickly that alveolar epithelial membrane integrity had not been compromised. The list of apoptotic cellular markers is substantial (Lu *et al.* 2005). In choosing an assay, it was imperative to undertake staining of living tissue in conditions matching those in which the recording of ion channel activity was undertaken. It was essential the assay could be employed in a slice model, taking full consideration of potential problems, including access of substances throughout the slice and the ability to gather high-resolution images from within the slice. Assay Kit (LIVE/DEAD®, Molecular Probes) provided the opportunity to perform a simultaneous two-colour fluorescent assay to determine cell viability by intracellular esterase activity and plasma membrane integrity. Calcein AM and ethidium homodimer (EthD-1) provide two recognised parameters of cellular viability. Calcein can be used as a marker for “live” cells while EthD-1 as a marker for “dead” cells.

In order to achieve unique electrophysiological investigation from the alveolar epithelium within a lung slice, it was crucial to have unquestionable cellular identification of the cell population being studied. To produce a lung slice in which identified alveolar epithelial type one cells and alveolar epithelial type two cells could be identified was a challenging undertaking. There are a number of distinct molecular markers which are present within alveolar epithelial type one and alveolar epithelial type two cells that could act as markers to allow specific identification (McElroy and Kapser 2004; Williams 2003). It was key to find a cell-specific marker that could be employed and which would concurrently allow functional electrophysiological recordings without disrupting the physiology of the slice. Live immunohistochemistry was the method chosen to identify the alveolar epithelial type one cell population by utilizing the VIIIIB2 mouse monoclonal antibody (Danto *et al.* 1992). Prior to this study, the use of live immunohistochemistry was limited to the central nervous system (Richmond *et al.* 1996; Pickard *et al.* 2001). This study is the first published research to utilize this technique within peripheral tissue. Following the publication of Bourke *et al.* (2005) there have been two further studies using the lung slice model with a vital stain for the identification of alveolar epithelial type one and two cells (Helms *et al.* 2006; Helms *et al.* 2008) and combined electrophysiological recordings.

In order to differentiate between alveolar epithelial type one and alveolar epithelial type two cell population a selection of vital stains were employed. Nile Red (9-diethylamino-5H-benzo, also known as Nile Blue oxazone) is formed by boiling Nile Blue with sulphuric acid. This produces a mix of Nile Red and Nile Blue. Nile Red is a lipophilic stain; it accumulates in lipid globules inside cells. An advantage of Nile Red is that it can be used with living cells. In the case of alveolar epithelial type two cells, Nile Red has previously been used to recognise the lamellar bodies (Liu *et al.* 1996). Alveolar type two epithelial cells store and release surfactant via intracellular vesicles termed lamellar bodies. LysoTracker® Green DND-26 (LTG, Molecular Probes, Eugene, OR, U.S.A.) is an acidotropic agent that selectively accumulates in cellular compartments with low pH. LysoTracker® Green has also been used to investigate pulmonary surfactant lamellar bodies in isolated alveolar type two epithelial cells (Haller *et al.* 1998) with excellent success.

The combination of these techniques allowed the first functional ion channel recordings from identified alveolar epithelial type one cells from a live lung slice. This technique provides a necessary additional experimental tool to further our understanding of alveolar epithelial physiology.

Results.

3.1 Preparation of Lung slices.

The architecture of the lung is such that it can expand and contract during the inspiration and expiration of breathing. The result is an organ that must retain a vast amount of elasticity to cope with the specific rate of ventilation, from shallow restful breathing to “lung busting” physical exercise. The lung’s unique structure and delicate nature make generating slices of 200µm thickness challenging. The traditional manner of producing precision cut lung slices has been to inject a bolus of low melting point agarose into the lung lobe (Youngson *et al.* 1993). Once the set point of the agarose is reached, the resulting stability attained by the solidified agarose within the lung lobe facilitates relatively straightforward slicing. This was the primary method employed for the production of lung slices.

Lung slices cut by this method (section 2.1) produce slices of very high and reproducible quality. In fig. 3.1, a transmitted light image of an agarose filled 200 µm thickness slice is shown. The lobe retained a suitable stiffness to allow slicing and the slice could be manoeuvred with ease between slicing and specimen baths. Good identification of the airway was also possible and, on close inspection, airway cilia were observed to be beating (data not shown), also demonstrating good slice viability. The presence of the agarose provided additional weight to the slice making it less likely to float in the specimen bath, thus reducing movement artefacts.

The next method investigated employed polyethylene glycol 400 (PEG 400). PEG comes in a range of molecular weights, the higher the molecular weight the greater the viscosity at room temperature. PEG is water soluble and described as non-toxic. PEG has been used in the pharmaceutical industry as a base material for creams and lotions. Famously, the timbers of the Mary Rose underwent PEG preservation whereby the water was removed and replaced with liquid PEG200. Once the PEG leaches into the timbers, it returns the stability to the timbers and preserves them for future generations. PEG 400 has some very

unique properties, which provided an alternative solution to the problem of lobe stability during slicing. PEG 400 is liquid at room temperature, yet solid at 4°C. This was critical as 4°C is the temperature at which the slices were cut. As PEG 400 is water-soluble, once the slice was transferred to the perfusion chamber, which is at room temperature, the flow of extracellular bath solution removed it from the alveolar air space allowing the required access to the air space. This solved the issues that the agarose-filled lung slices presented of blocked airspace and by comparison the access to the alveolar epithelium was immeasurably improved. However, PEG 400 proved unsuitable as the cellular viability of the slice was found to be unsatisfactory (see fig. 3.4).

The final, and most successful method was to section unfilled lungs. This novel production method for lung slices was only possible by using the Integraslice® high precision oscillating microtome from Campden Instruments. This microtome provided the required control, flexibility, accuracy, engineering and design to overcome the challenge of sectioning unfilled lungs. The unfilled lung slice proved a suitable model to allow the undertaking of live immunohistochemical staining and this was combined with the recording of ion channels in cell attached configuration (see fig. 4.1). The time between production of the slice and recording of electrical activity was reduced to a minimum with slices ready for patch clamping in less than 3 hours. The physical interference that agarose presented and the reduced cellular viability that PEG 400 imparted on the alveolar epithelium was consequently removed.

3.2 Cellular viability within lung slices.

It was important to address the issue of cellular viability, by use of a biological assay, before introducing the unfilled lung slice as a suitable model for recording ion channel activity at the alveolar epithelium. It was essential to demonstrate suitable cellular viability under the experimental conditions employed, as both PEG and unfilled lung slices were novel methods of sectioning lungs. The choice of assay had to demonstrate viability, taking into consideration the 3D structure of the slice. Research studies to investigate agarose filled lung slice cellular

viability was undertaken for both rat and human lung slices (Vickers & Fisher, 2004; Umachandran *et al.* 2004; Fisher *et al.* 1984; de Graaf 2006) the primary focus of these studies was to demonstrate suitable viability of the agarose filled slice for toxicological investigations. Visualization of the identified alveolar epithelial type one cells with a fluorescent secondary antibody (see section 2.2.1, fig. 3.6, and fig.4.1) was very beneficial and allowed collection of confocal images. The use of a fluorescent assay complimented the collection of fluorescent viability information from within the slice. It was also important to demonstrate that undertaking the live immunohistochemical identification of alveolar epithelial cells would not unduly affect the cellular viability of the slice.

3.2.1 Propidium iodide staining

The initial cellular viability assay undertaken made use of propidium iodide (PI). PI (Molecular Probes, Netherlands) is a nucleic acid stain which binds to DNA by intercalating between the bases, with little or no sequence preference, and with a stoichiometry of one dye per 4-5 base pairs (Vornov *et al.* 1991). The binding of the dye to the nucleic acids causes an increase of some 20-30 fold in fluorescence signal with a peak excitation at 535nm. PI is a membrane impermeable dye and is excluded from viable cells. However, cells whose membrane integrity has been disrupted allow the transport of the dye across the membrane where it is internalised within the nucleus and can be visualised by fluorescent imaging techniques. An exemplar image of PI staining can be seen in fig 3.2. This image represents a 200 μ m thickness, lung slice from an 8 day old rat. The slice firstly underwent live immunohistochemical staining with VIII B2 alveolar epithelial type one cell antibody, panel A. After the VIII B protocol, the slice was subsequently loaded with PI in order to investigate viability (panel B fig.3.2). The resultant overlay image can be seen in panel C fig. 3.2. Looking closely at panel B, it is evident that there are cells that have had their cellular membrane compromised allowing the entry of PI and binding to the DNA. It is evident that it was possible to gain good access of the dye throughout the slice and this in turn allowed image acquisition deep into the slice, it was possible to confocal images ~20 μ m into the slice. The results of the PI staining showed

cellular viability had been compromised. However, it was not possible to confirm if presence of the compromised cells were a result of the slicing processing, the agarose backfilling, or a combination of both or the natural cellular turnover.

3.2.2 LIVE/DEAD® Viability

In order to assess further the cellular viability of the lung slice, the LIVE/DEAD® viability/cytotoxicity kit, a product developed by Invitrogen Molecular Probes, was also employed. The advantages of this cellular assay kit are that it provides a two-colour fluorescence viability assay that is based on the simultaneous determination of both live and dead cell populations. A further beneficial aspect of this kit is that it uses two well recognised cell viability markers, intracellular esterase activity is measured by Calcein AM, and plasma membrane integrity is measured by ethidium homodimer (EthD-1) (Papadopoulos *et al.* 1994). The LIVE/DEAD® stain is applicable to most types of cells. The images shown in fig. 3.3 and fig. 3.5 were captured from the HEK 293 cells line and rat lung slices, respectively.

Within viable cells, where the cellular membrane has not been compromised, intracellular esterases cleave the nonfluorescent cell-permeant Calcein AM and by this enzymatic process produce the intensely fluorescent calcein. Calcein is well retained within “healthy” cells due to its polyanionic properties. Once internalised within the cytoplasm it produces an intense uniform green fluorescent signal (ex/em ~495nm/~515nm). The EthD-1 enters cells with compromised and damaged membranes, and upon binding to the DNA, it undergoes ~40 fold increase in fluorescent intensity; this means that dead cells can be identified by red fluorescence (ex/em ~495/~635). The cells with intact and uncompromised membranes will exclude the EthD-1 dye. In order to optimise LIVE/DEAD® stain to the CellMap IC™ confocal system and confirm loading protocols, HEK 293 stably expressing P2X₂ ion channels were used as a control system (fig. 3.3).

These images provide an example of the intensity and localisation of staining that can be achieved within a cell monolayer. Cells were concurrently loaded

with both Calcein-AM and EthD-1. Fig.3.3 panel A shows a monolayer of cells whose membranes are intact with the bright green fluorescent label (Ex488nm) achieved by the enzymatic conversion of Calcein AM to calcein. The fluorescent label is dispersed throughout the cell cytoplasm. When the same cells are imaged via the red excitation channel (Ex543nm) there is no visible signal in panel B, which indicates all cells in the field of view have their cell membranes intact. Panel C shows the digital overlay of both images.

In order to compromise the cellular membranes of the cells and gain a baseline reference level for the EthD-1 stain, cells were treated with a 1% (v/v) Triton X-100 in physiological solution for 10 minutes. The effect of this was quite striking, with the images collected via the 488nm excitation (panel D of fig. 3.2) exhibiting no fluorescent signal. Examination of panel E (fig. 3.3) shows that all of the membranes have been entirely compromised as the signal gathered by excitation with the 532nm channel is especially intense and the nuclei of the cells are clearly distinguishable.

3.2.3 Lung slice viability assessed with LIVE/DEAD® stain.

PEG provided a very suitable structural stability to make 200µm lung slices while offering the clearance within the alveolar airspace that was essential to provide good access to the alveolar epithelial membrane for patch clamp experiments. However, it was only towards to edge of the slice, where the morphology of the epithelium had the characteristic 'halo' in transmitted light, that is associated with healthy cells. Thus, it was decided to investigate the cellular viability, within the PEG 400 filled slice using LIVE/DEAD® staining. The results are seen in fig. 3.4, and it is clear from these images that there is a reduced staining towards the middle of the slice. The addition of PEG 400 demonstrated a clear reduction in the cellular viability towards the centre of the slice (fig. 3.4. panel A).

Access of the dye within the slice was not problematic for either LysoTracker Green or EthD-1. There were a small number of "healthy" green cells and a small number of compromised red cells seen within the interstitium that exhibit a fluorescent signal. The population of green cells seen in panel A, is less than

would be expected of a “healthy” slice. In panel D, the overlaid image demonstrates the pattern of staining achieved with the LIVE/DEAD® cell viability stain within a PEG filled lung slice. The reduced population of viable cells points towards the lack of suitability of PEG 400 backfilled slices as a physiological experimental model. These data concur with the findings from patch clamping investigations from PEG slices. The population of cells with viable ion channel activity were only observed towards the edge of the slice where the perfusion of PEG had not reached (data not shown).

3.2.4 Unfilled lung slice cellular viability.

The slicing of a 200µm thickness unfilled lung slice was made possible primarily by the addition of the Campden Integraslice® to the laboratory. This high precision oscillating microtome coupled with the ceramic blades, slow advance speed, optimisation of amplitude and frequency of the cutting blade allowed the first reported unfilled lung slice preparation (Bourke *et al.* 2005). It was clear that this method of slice preparation would offer an experimental model as near to *in vivo* as possible in which to record ion channel activity at the alveolar epithelium. However, the question remained as to the effect of VIII B2 antibody labelling on the cellular viability of the alveolar epithelium.

The results provided in fig. 3.5, and fig. 3.6 and fig 3.7 addresses the question directly with regard to the cellular viability of an unfilled 200µm thick rat lung slice. Firstly, it was necessary to investigate the cellular viability in such an unfilled slice. There was no evidence to suggest the LIVE/DEAD® stain would work satisfactorily in an organ slice. However, the reservation that there would be difficult in the probe gaining good access deep within the slice was unfounded. Fig 3.5 panel A shows a typical example of an unfilled 200µm thick lung slice which has been treated with LIVE/DEAD® and the resultant calcein fluorescence signal collected by excitation with the 488nm laser line.

There are a plentiful number of cells, which exhibit good cellular viability and demonstrate a high fluorescence signal. The image is captured by 60X water dipping objective and the central black space is the unfilled alveolar airspace,

hence, no staining is observed. Fig. 3.5 panel B is the same field of view excited by the 543nm laser line. There are a number of red nuclei visible, this equates to cells that have had their cellular membranes compromised and are classified as dead cells.

The results of these experiments illustrate clearly that there was excellent viability within an unfilled lung slice. A direct comparison between panel C and F of fig. 3.5 illustrates that there is a high degree of cellular viability. This method is superior to the PEG 400 back filled-slice (compare between fig. 3.4 panel A and fig 3.5 panel A). Upon treatment with Triton X-100 for 10 minute and subsequent loading with the LIVE/DEAD® cellular viability stain, there was a complete loss of calcein fluorescence signal, (panel F fig 3.5). Inspecting panel A of fig.3.5 shows that there is large number of viable cells present within the lung slice and this demonstrates clear cytoplasmic localization. These images are in stark contrast to the increased number of red nuclei present in fig.3.5 panel F.

Upon detailed inspection of the images, it is possible to make out the alveolar airspace region (fig.3.5 panel E). There are some points of interest when looking at the final image. It is very clear that the alveolar region has remained open and that access is no longer an issue. The Triton X-100 allows the leaching of the EthD-1 stain into the connective tissue of the lung and as a result the background signal is somewhat higher. Although the Calcein AM is present, there is no signal present with the 488nm excitation, because the metabolic reaction within the cytoplasm was unable to occur as the membranes of all cells within the slice were compromised.

3.2.5 The effect of VIII B2 live cell identification on lung slice viability.

The effect of slice viability was assessed in the presence of VIII B2 type one alveolar epithelial cell specific antibody live labelling and the results are seen in fig. 3.6. This is an exemplar image set of a rat lung slice of 200µm in thickness. The slice was treated with VIII B2 followed by treatment with a secondary antibody (Alexfluo 488/546). This was followed by treatment with the

LIVE/DEAD® stain. In the case where VIII B2 and Calcein AM live staining was examined, a 543nm anti mouse secondary antibody was used as the fluorescent marker. In the situation where the VIII B2 and EthD-1 was examined, a 488nm anti mouse secondary antibody was used as the fluorescent marker. Fig. 3.6 panel A is the live cell stain of calcein which shows good cellular viability in the alveolar epithelial region. Fig. 3.6 B is the VIII B2 antibody with AlexFluo 546 secondary antibody. The antibody has remained specifically located to the alveolar membrane region. Fig 3.6 panel C illustrates the overlay of both the calcein and the VIII B2. This demonstrates the abundance of viable cells within the unfilled lung slice following the VIII B2 protocol.

Fig 3.6 panel D shows the VIII B2 with the AlexFluo 488 secondary antibody, which again is localised to the alveolar epithelial membrane, and fig. 3.6 panel E provides evidence for compromised cells within an unfilled lung slice following the staining with VIII B2.

Quantification of the mean number of EthD-1 positive nuclei showed that Triton-X-100 treatment resulted in a significant, 4-fold increase in the number of dead cells per field from 18.0 ± 0.9 ($n = 41$ slices) to 78.1 ± 3.3 ($n = 30$ slices; figure 3.7). Thus, before such treatment, the majority of cells within the slice were alive, whilst permeabilization with detergent resulted in cell death throughout the lung slice. A modest, but significant 1.4-fold increase in cell death evoked by live immunohistochemistry is quantified in figure 3.7, which shows that VIII B2 treatment resulted in 25.3 ± 1.7 dead cells per field ($n = 31$) compared with 18.0 ± 0.9 in untreated slices ($n=23$).

3.3 Live cell identification within a lung slice.

For the success of this project, it was essential to master the production of live-labelled alveolar epithelial cells within a lung slice. This would not have been possible had it not been for the unique characteristics of VIII B2 antibody. It was also critical to investigate the most suitable method of creating dual labelling with

type one and type two markers which would prove useful in further understanding the particular role the cell population play in the alveolar function.

3.3.1 VIIIB2 alveolar epithelial type one cell identification live lung slice.

The slice was labelled as outlined in section 2.3.1 and this allowed the visualisation of the alveolar epithelial type one cell membrane within in the slice. The image presented in fig. 3.8 demonstrates membrane specific localisation of the VIIIB2 antibody staining of the alveolar epithelial type one cells. It also demonstrates very elegantly the expanse of the type one cells within alveolar epithelium. This image is of an unfilled lung slice and is the first live-labelling to show the alveolar epithelium. In order to investigate non-specific binding of the fluorescencent antibody, slices were treated as described in section 2.3.1, but with primary antibody (VIIIB2) excluded. No fluorescent signal was observed in these control slices (data not shown).

The images presented throughout this thesis when placed in a side-by-side evaluation against the published data from fixed immunohistochemical from our collaborators using VIIIB2 antibody (Danto *et al.* 1992, Borok/Danto *et al.* 1998, Bourke *et al.* 2005) clearly demonstrate the retained ability of this monoclonal antibody to recognise an extracellular apical membrane epitope specific to alveolar epithelial type one cells. The combined z-stack confocal image in fig. 3.8 provides suitable “three dimensional” representation of the specificity of binding that was achieved with the VIIIB2 antibody. When the slice was viewed by epi-fluorescence, the staining gave a 3 dimensional pattern that is in part conveyed by the confocal images displayed here. The difference in the access of the antibody can be clearly seen by comparing the VIIIB2 staining in fig. 3.2 with that in fig. 3.8.

The staining is exclusively membrane bound, and there is a reduction in the non-specific binding allowing a much less unambiguous staining pattern. The increase in blocking solution concentration from 3% to 5% also contributed to the specificity of binding. A major factor in achieving a suitable staining was the

use of the unfilled slice model. This allowed greater penetration of the primary antibody. The binding of the secondary antibody was also made easier and as a result the concentration could be reduced even further to 1:500 from the initial 1:200. This in turn, decreased the possibility of non-specific binding of the secondary antibody.

3.3.2 Alveolar epithelial type two live cell staining.

It was important to consider the possibility of live staining alveolar epithelial type two cells. There were a number of possible candidate stains that have previously demonstrated good success within primary isolated cell populations. The initial choice of vital stain was Nile Red. Nile Red is strongly fluorescent, but only in the presence of a hydrophobic environment. Nile Red can be applied to cells in an aqueous medium and has been shown to localise selectively within the lamellar bodies of the alveolar epithelial type two cells (Lui *et al.* 1996). The lipophilic environment of the lamellar bodies has allowed reliable specificity in identifying isolated alveolar type two cells. The use of Nile Red in the lung slice preparation is illustrated in fig. 3.9. The dye is localised to a number of lipid containing cellular compartments. A number of optimisation procedures were investigated, including periods of loading and differing concentrations of dye. However, all yielded a somewhat diffuse staining pattern within the alveolar region. The alveolar epithelial type two cells have retained the Nile Red within the lamellar bodies of these cells (Lui *et al.* 1996). However, due to the non-specific nature of the loading within the slice preparation it was not deemed a suitable cellular marker for the slice preparation. Stained cells were localised to the “corner of the alveoli” and show a punctuate staining and have the classical lamellar body staining pattern. These cells are identified in fig 3.9 by white arrows.

Due to the low level of specificity demonstrated by Nile Red, it was necessary to investigate other options for the identification of live alveolar epithelial type two cells. One option was to try the styryl dye LysoTracker® Green DND-26 (Invitrogen, Molecular Probes). This type of probe has been used with good success both in isolated type two alveolar epithelial cells (Haller *et al.* 1998) and in whole organ lung preparations (Ashino *et al.* 2000), although in the latter

study, LysoTracker green FM1-43 was employed. Both of these studies demonstrated the specific localisation of the fluorescence signal to the lamellar bodies of the alveolar epithelial type two cells.

Fig. 3.10 demonstrates the localization of the LysoTracker Green DND 26 within the lamellar bodies of a single alveolar epithelial type two cell. The confocal image seen in panel A was captured at a high resolution and, combined with optical zoom, allowed single lamellar body vesicles to be resolved within the alveolar epithelial type two cell. The ability to co-stain the lung slice with the specific alveolar epithelial type one cell antibody (VIII B2) provided a vivid image overlay. Panel C reveals the specificity of each of these particular live staining methods. The red signal represents the type one specific staining and it is seen localised to the apical membrane of alveolar epithelial type one cell. The localisation of the DND-26, (green signal), is tightly confined to the type two alveolar epithelial cell lamellar bodies. However, the most striking aspect is how the VIII B2 ceases directly where the DND-26 starts, indicating that there is absolutely no overlap between these two specific identification protocols.

3.4 Discussion.

The ability to produce viable and reproducible slices was essential to the success of this project. As described above, a number of methods were investigated in order to produce slices that would be suitable to allow the functional recording of electrophysiological data from identified alveolar epithelial cells in a precision cut lung slice. In the past, the method of choice, which is still favoured by a number of investigators (Fu *et al.* 2000; Helms *et al.* 2008), is the agarose backfilled lung slice, as seen in fig. 3.1. Although this has proved valuable as a research tool, inspection of fig. 3.1 demonstrates a clear definition of the air space of the alveolar region. The agarose-filling method of slice preparation has also proved valuable for a number of previous studies. For example, Fu *et al.* (1999, 2000) have been able to record voltage-activated K⁺ and Na⁺ currents in neuroepithelial bodies (NEB) of lung slices cut from an agarose-filled neonatal rabbit lung. Further, a large number of toxicology studies have used the agarose-filled slice as the experimental model of choice (de Graaf 2006; Parrish *et al.* 1995) and, as mentioned above, the more recent use of agarose backfilled lungs has allowed the recording of electrophysiological results from both alveolar epithelial type one and type two cells (Helms *et al.* 2006; Helms *et al.* 2008)

The ease of cutting agarose-filled slices is clear, and a single rat lung lobe can yield between 12 and 20 slices of 200µm thickness with any of the commercially available vibrotomes. The slices are very robust and are easy to transfer between culture medium and microscope chamber. In addition to the mechanical stability advantages, agarose-filled slicing also provides a method for studying intracellular Ca²⁺ homeostasis with Fluo-3 AM indicator dye. The results from agarose filled lungs are discussed in chapter 5 of this thesis.

The agarose filled lungs have one significant drawback, which is that the alveolar airspace was not easily accessible since it remained filled with solidified agarose. There was visible evidence of this, and when a patch electrode was positioned in the alveolar air space of the lung and the electrode was moved downwards, the microstructure of the lung could be seen to move. Attempts either to clear completely or soften the agarose, in order to gain better access to the membrane, saw the use of very low melting point agarose (Sigma-Aldrich, U.K.). This product has a melting point of $\leq 65^{\circ}\text{C}$ and a gel point of $26\text{-}30^{\circ}\text{C}$. The results were unsatisfactory as the agarose still remained within the alveolar air space.

PEG 400 did not prove to be an optimal method for the production of viable lung slices. Fig. 3.4 shows an image of a $200\mu\text{m}$ lung slice which had been cut with a PEG 400 backfill at 4°C . Panel C shows that the morphology of the alveolar airspace is markedly changed, compared to figure 3.1. However, it was clear that the alveolar membrane was fully accessible. Panel A and B demonstrate the cellular viability. What became immediately clear was there was only a small area of viable lung available for experimentation and this would prove unsuitable as an experimental model. The large extent of cell death would have detrimental effects upon the living cells. The release of cellular apoptotic signals may affect the remaining live cell population. Since the only aspect of the preparation which was changed was the PEG 400 backfill, it became apparent that PEG 400 was the cause of the cell death.

The advantage of using PEG 400 was that it provided good stability to the lung structure during slicing. The PEG 400 was chosen as it provided an airspace that was free of obstructions allowing clear access of a patch clamp electrode to the alveolar epithelium. However, PEG 400 had a less than suitable reaction with the live tissue and the viability of the lung slices was not acceptable. Certain aspects did, however, prove to be quite positive. It was clear that the alveolar air space of the lung did not collapse after removal of PEG 400. The region at the edge of the slice that had not come into contact with PEG 400 during the

perfusion demonstrated good viability and cell-attached recordings were possible. Fig 3.4 shows the viable “band of cells” around the edge of the slice.

It is important to outline there was more than one vibrotome used during this project and also a number of other vibrotomes were tested prior to the purchase of the Integraslice®. I shall outline quickly the vibrotome history within the laboratory, and deal with the positive aspects that the Integraslice® has over the competitors. The original vibrotome on which slices were cut was the Vibroslice™ (MA 752, Campden Instruments, U.K.). The unit has control of the speed of advance with a fixed lateral displacement of 1.0mm and allows the frequency to be set by the user. The stainless steel blades (752/1/SS Campden instruments, U.K.) were only available for this machine. A limiting factor was the inability of the vibrotome to cut lung slices from organs of older animals. The connective tissue of mature animals was a confounding factor for the vibrotome in the production of precision cut lung slices. This vibrotome required the stability offered by the agarose backfill and agarose block. Also, it was not possible to use animals older than 10 days as the slices were not of a suitable quality. Slices cut from animals of a later age were variable in thickness. This machine did not have the option of a temperature-controlled specimen bath and required the addition of bath solution ice cubes to reduce the temperature; hence bath temperature was not accurately controlled.

Each manufacturer (Leica Campden Instruments, Krumdieck, EMS, Vibratome), who produce a precision cut vibrotome, were individually trialled. The decision was to opt for the Integraslice® from Campden Instruments, see figure 2.1. There were a number of features associated with the Integraslice® which made this the most suitable machine for this application. One aspect that was of crucial importance was the ability of the user to control in a precise manner the advance speed of the cutting blade ($-1.0\text{mm}\cdot\text{s}^{-1}$ to $+3.0\text{mm}\cdot\text{s}^{-1}$ in 10 micron steps), the amplitude of the cutting blade (0.5mm to 1.5mm), and the oscillation frequency of the blade (20Hz to 115Hz). This precise control, coupled with the use of precision ceramic blades (Model 7550/1/C, Campden Instruments, UK), made the production of unfilled lung slices possible. The ceramic blades are precision engineered, manufactured from ultra hard zirconium and honed by a process of

'lapping'. This 'lapping' allows both sides of the blade to meet at single bevel cutting edge which is machined to micron flatness. These factors combine to make an ultra sharp durable cutting edge essential in the production of "healthy" slices. These blades are reusable and allow the cutting of thin precision cut slices from tissue that in the past had proved difficult to cut, such as rat lung and airway. The superior engineering mentioned above made it possible to cut unfilled lung slices. This was to prove an important breakthrough as it solved problems of cellular viability and access to the alveolar air space.

The optimal position for the left superior lobe, the lobe of choice, was the apex of the lobe facing the blade with the posterior of the lobe facing upwards. This offered the cutting blade a sufficient surface to start the sectioning and also an increased distance until the airway was reached. The lobe was individually sectioned away following *en bloc* heart and lung dissection (see section 2.1.2). The lobes were held in position on the jig of the Integraslice® with methyl alpha-cyanoacrylate gel; this option proved more suitable as the lobe was held firmly in position and the gel remained at the base of the tissue. Liquid has a tendency "creep up" around the lobe, reducing the life time of the blades and making sectioning more problematic.

The question of cellular viability arose due to the fact that prior to Bourke *et al.* (2005), unfilled lung slices had not been used as an experimental model. The ability to demonstrate a large population of viable cells would add strength to the arguments in support of this experimental method by which to investigate the alveolar epithelium. The examples shown of unfilled lung slices in fig.3.5 and fig 3.6 when compared to the control HEK 293 images in fig 3.4 leave no doubt as the vast number of viable cells present when using the unfilled lung slice experimental model. The addition of the VIIIB2 antibody was shown to increase the numbers of compromised cells over that in the non-treated slice (fig3.6) but the difference was not significant. The true nature of the viability is seen in the large numbers of nuclei seen by the addition of Triton X 100. It was essential to fully optimise the slice preparation and provided 'healthy' slices which would allow the first reported electrophysiological recordings from identified alveolar epithelial type one cells.

The data as presented in figure 3.7 lacked a key component, sound statistical analysis. It could have been strengthened in a number of aspects. Firstly, standardization of the regions to be investigated would aid in presenting a more balanced data set. The number of slices and fields of view should have been standardized. Each specific treatment should have had the same number of slices and a standard number of fields taken from each individual slice. The data would present the same story in that the treatment with the VIII B2 antibody increased the number of dead cells present in the selected field of view. It is not clear if this is significantly different as demonstrated by a statistical method. Upon reworking of the experiment it would provide a stronger data set if a student T test were undertaken upon the data. To undertake this statistical analysis data would be grouped as per control, triton X 100 and VIII B2 experimental procedures. However, would be analysed as unpaired experiments unless slices from each animal underwent the same procedure and were imaged and data collected on a particular animal. I feel confident the outcome would have been similar; comparisons made in a statistical manner would demonstrate that although VIII B2 caused an increase in cell death. The increase still provided a larger population of healthy cells.

Key to the success was the ability to identify with unquestionable specificity the cell population. The use of a monoclonal antibody as a live label provided this opportunity. It is the basic interaction of the antibody with the antigen which forms the basis of all immunohistochemical techniques. We can break down the properties of the antibody-antigen interaction into three sections, structure of the antibody-antigen bonds, strength of the interaction i.e. the affinity, and the overall stability of the immune complex, the avidity the number of antigen binding sites present. In selection of a suitable antibody each aspect in turn is considered. Preservation of the epitope which the antibody is to bind is critical. The use of the VIII B2 antibody (Danto *et al.* 1992) as a live cell marker relied on the epitope being extracellular. This antibody also demonstrated very high specificity and avidity essential for live cell imaging as the binding of the antigen to the epitope should be both rapid and retain good avidity throughout the experimental process. A number of methods were developed to investigate both

the viability and the characteristics of the lung alveolar epithelium within live lung sections. Live immunohistochemistry was undertaken to allow the identification of both alveolar type one cells and alveolar type two cells. Live immuno-staining in peripheral tissue has not until now been described although limited information is available for this technique in central nervous system (Richmond *et al.* 1996; Pickard *et al.* 2001)

The use of the LysoTracker® Green DND-26 proved the most suitable of the alveolar epithelial type two live cell stains for use in an unfilled lung slice. DND-26 yielded very convincing results allowing the identification and electrophysiological recording of ion channels within a lung slice in the recent publication (Helms *et al.* 2008). The images collected in that study using LysoTracker® red in a slice model are very similar to that seen in figure 3.10 panel B demonstrating the suitability of this vital dye as a marker for alveolar epithelial type two cell population in a slice model. The ability to combine precise identification of alveolar epithelial type one and alveolar epithelial type two cells in the same slice has and will continue to provide a beneficial advancement of our understanding of alveolar epithelial physiology.

3.5 Conclusion.

The initial section of this chapter described the preparation of the lung slice. The correct choice of method was critical for the success of this project. The traditional agarose backfilled slices were successful but did not allow suitable access to the alveolar epithelial type one cell membrane. The next option was to investigate the use PEG 400 as a stabilizing medium. The slices produced were of very high quality and removal of the PEG 400 allowed access to the epithelium. Upon closer inspection, the PEG 400 backfilled lungs proved not as successful as originally thought. They lacked the required cellular viability. This was confirmed with the use of the LIVE/DEAD® viability stain. The most successful and suitable option was production of unfilled lung slices. The viability of the slices was without question and I was able to provide the evidence required regarding the suitability of the unfilled lung slice as an experimental model. The unfilled lung slice was made possible by the precision engineering and control provided by the Integraslice® from Campden instruments.

As it was now possible to produce acute slices that were of the highest quality and viability, attention turned to the live cell identification of the two cells alveolar epithelial cell populations. It was essential that the selection of marker had unquestionable specificity. The alveolar epithelial type one cells were identified by the mouse monoclonal antibody, VIIB2, which binds to an extracellular epitope on the apical membrane of the alveolar epithelial type one cells. The selection of alveolar epithelial type two cell marker was equally important. Although Nile Red had proved suitable for single cells, it was not ideal for the slice model. However, LysoTracker® Green DND-26 however did prove a suitable candidate for the specific identification of alveolar epithelial type two cell within an unfilled lung slice.

In conclusion, the optimisation of production of viable acute slices, and the combination of specific cellular identifications, will allow the recording of functional ion channel recordings from identified alveolar epithelial cells within a lung slice. It was also possible using this model to obtain calcium imaging measurement using a fluorescent Ca^{2+} indicator dye

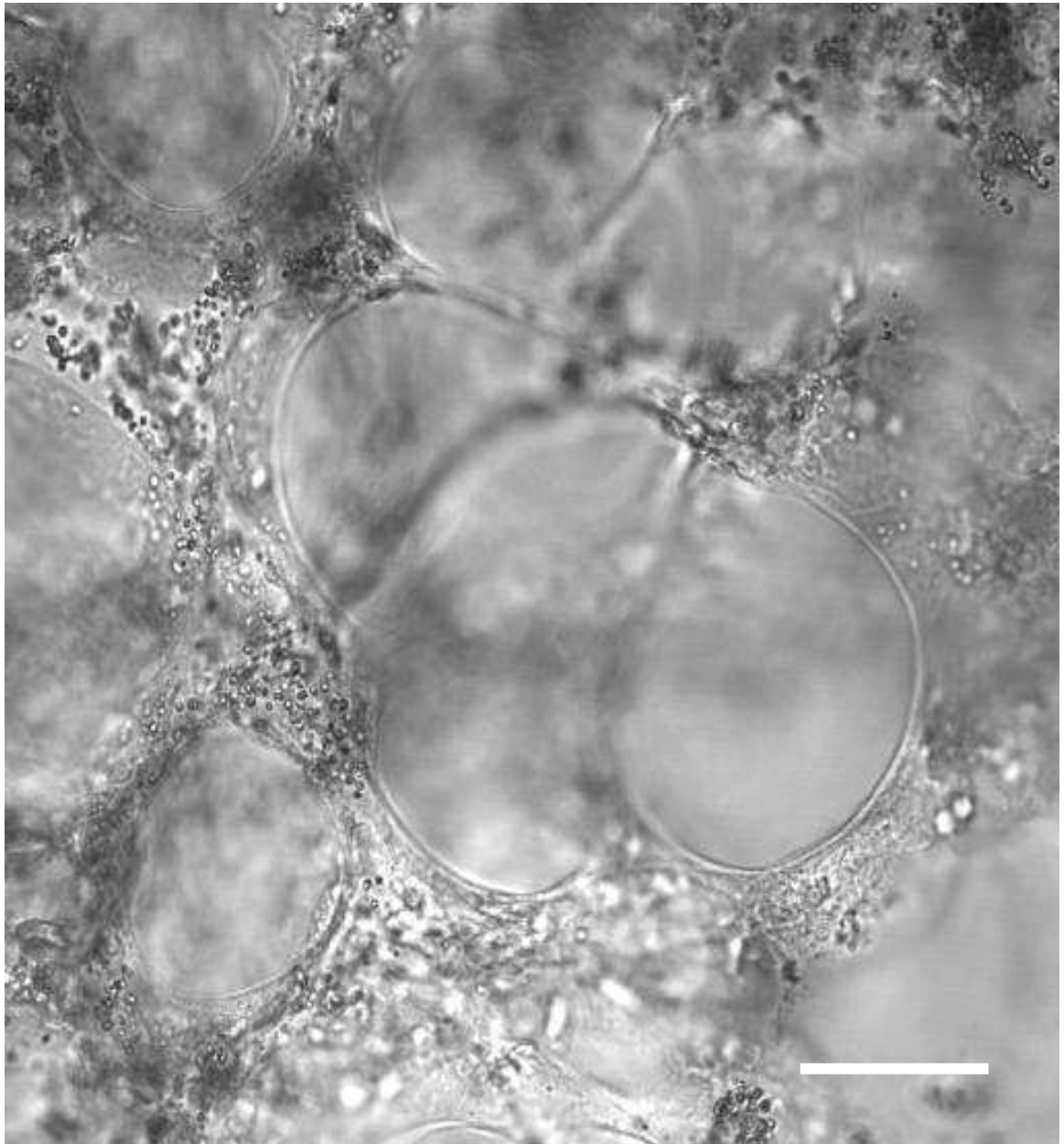


Figure 3.1 Agarose filled 200 μm thickness rat lung slice.

The image above was captured on an inverted Zeiss 410 LSM confocal microscope. This image was captured using a 63 X oil objective and excitation was via the 488 nm laser. This transmitted light image was acquired from lung slice of a 7-day-old rat. The white scale bar represents 30 μm . The alveolar region can be clearly distinguished from the interstitial region.

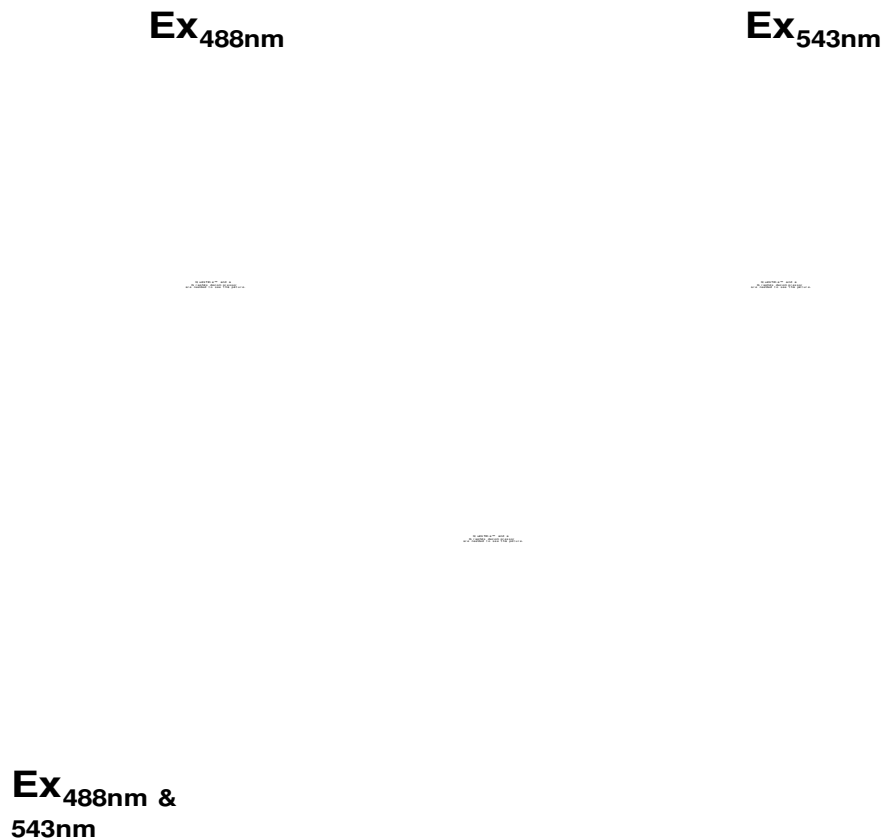


Figure 3.2 Propidium iodide and VIIIB2 treated agarose filled lung slice.

This image demonstrates a 200 μm thickness agarose filled rat lung slice. Panel A is the result of VIIIB2 alveolar epithelial type one specific live cell antibody binding. Panel B is a representation of PI staining within the lung slice. Red

nuclear stain corresponds to cells with compromised plasma membranes. Panel C is the overlay of both images. Images were captured with a Zeiss LSM410 microscope. PI was excited with a 543nm laser line and the VIII B2 was excited by the 488nm laser line.

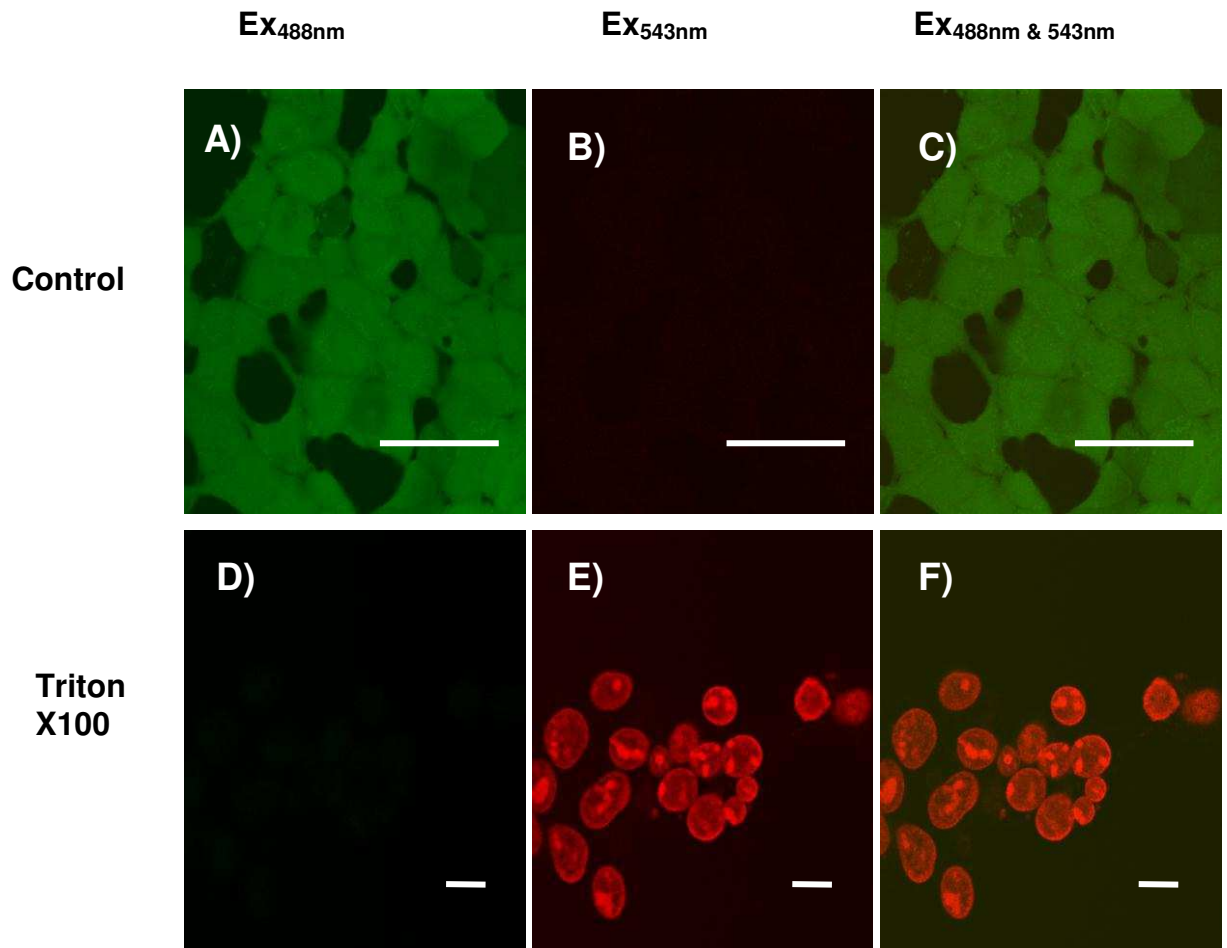


Figure 3.3 HEK 293 cell line employing LIVE/DEAD® cellular viability assay.

The above images were captured on a CellMap IC confocal attached to an upright Olympus BX50WI microscope. Excitation by the 488nm and 543nm laser lines were captured sequentially. The HEK 293 cells were treated with the LIVE/DEAD® viability stain as described in section 2.5.2. Panel A demonstrates HEK 293 cell loaded with LIVE/DEAD® vital stain. The green signal represents cells that show cellular viability, calcein is excited by the 488 laser line. Panel B

is the image captured by excitation via the 543 laser line. Panel C is the overlay of both images. The white scale bar represents 20 μm . The cells displayed in panel D,E, and F have been treated with a 1% Triton X100 containing bath solution. Panel D displays no signal. Panel E demonstrates EthD-1 nuclear fluorescence Panel F is the overlay of both images. The white scale bar represents 5 μm .

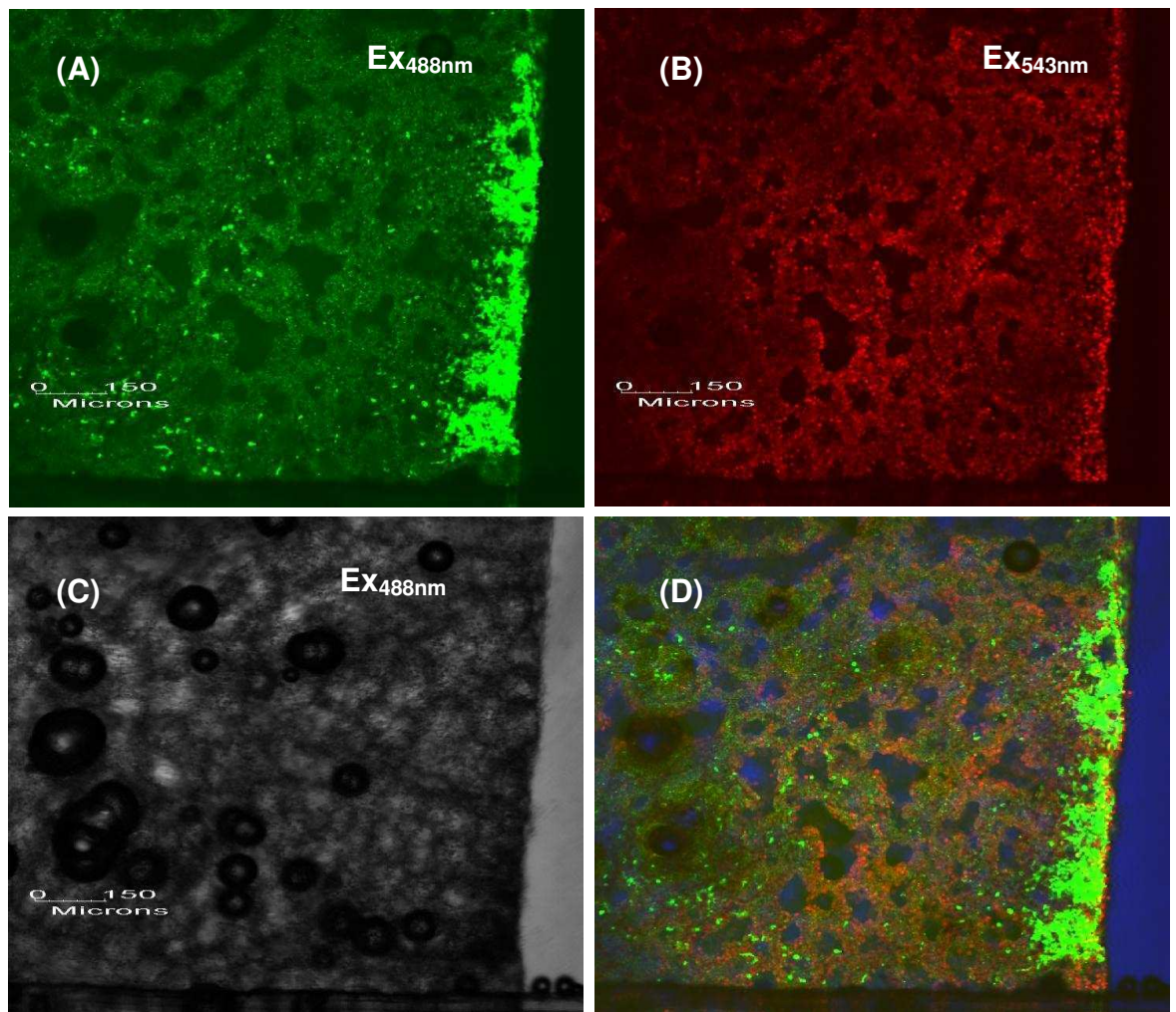


Figure 3.4 PEG 400 backfilled lung slice treated with LIVE/DEAD® cell viability stain.

A 200 μm thickness rat lung slice, imaged on the CellMap IC™ confocal 10x magnification water dipping objective with a PEG 400 backfill. Panel A shows the calcein live stain, demonstrating the live cells in green (Ex488nm). Panel B illustrates the EthD-1 staining which identifies dead cells shown in red when

imaged with the Ex532nm laser line. In panel C is the transmitted light image captured with Ex488nm laser line. Panel D shows the overlay of all three images. In order to reduce optical aberrations, images captured as transmitted light image are given a blue pseudocolour by the CellMap software in the overlay.

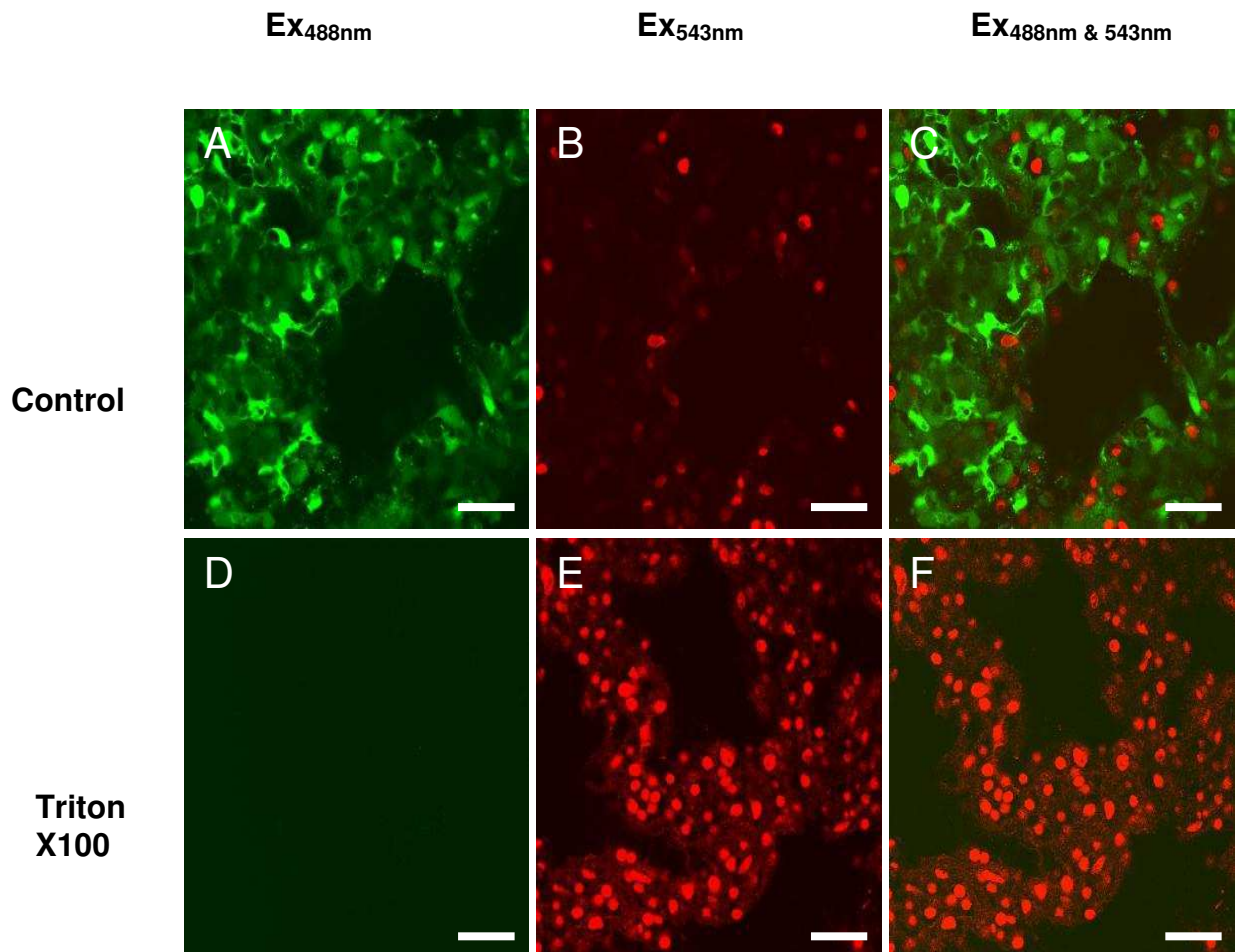


Figure 3.5 Confocal images of unfilled rat lung slice co-stained with LIVE/DEAD® viability/cytotoxicity assay kit for animal cells.

Panel A is a 200µm rat lung slice loaded with 2µM Calcein AM, 4 µM EthD-1 and excited with 488nm laser (green emission) to show viable cells. Panel B is an image taken from the same slice and optical section loaded with 2µM Calcein AM, 4 µM EthD-1 and excited with 532 nm, (red emission) to show the cells with compromised membranes. Panel C is the overlay of image A and B and demonstrates a high level of viability. Panel D is a 200 µm rat lung slice loaded

with 2 μ M Calcein AM4, μ M EthD-1 following a 10 minute treatment with 1% Triton X-100 and then excited with 488nm (green emission) to show viable cells. Panel E is the same slice and optical section loaded with 2 μ M Calcein AM 4 μ M EthD-1 and excited with the 543nm laser to show the cells with compromised membranes. Panel F is the overlay of the images in Panel D and E. White scale bar represents 20 μ m.

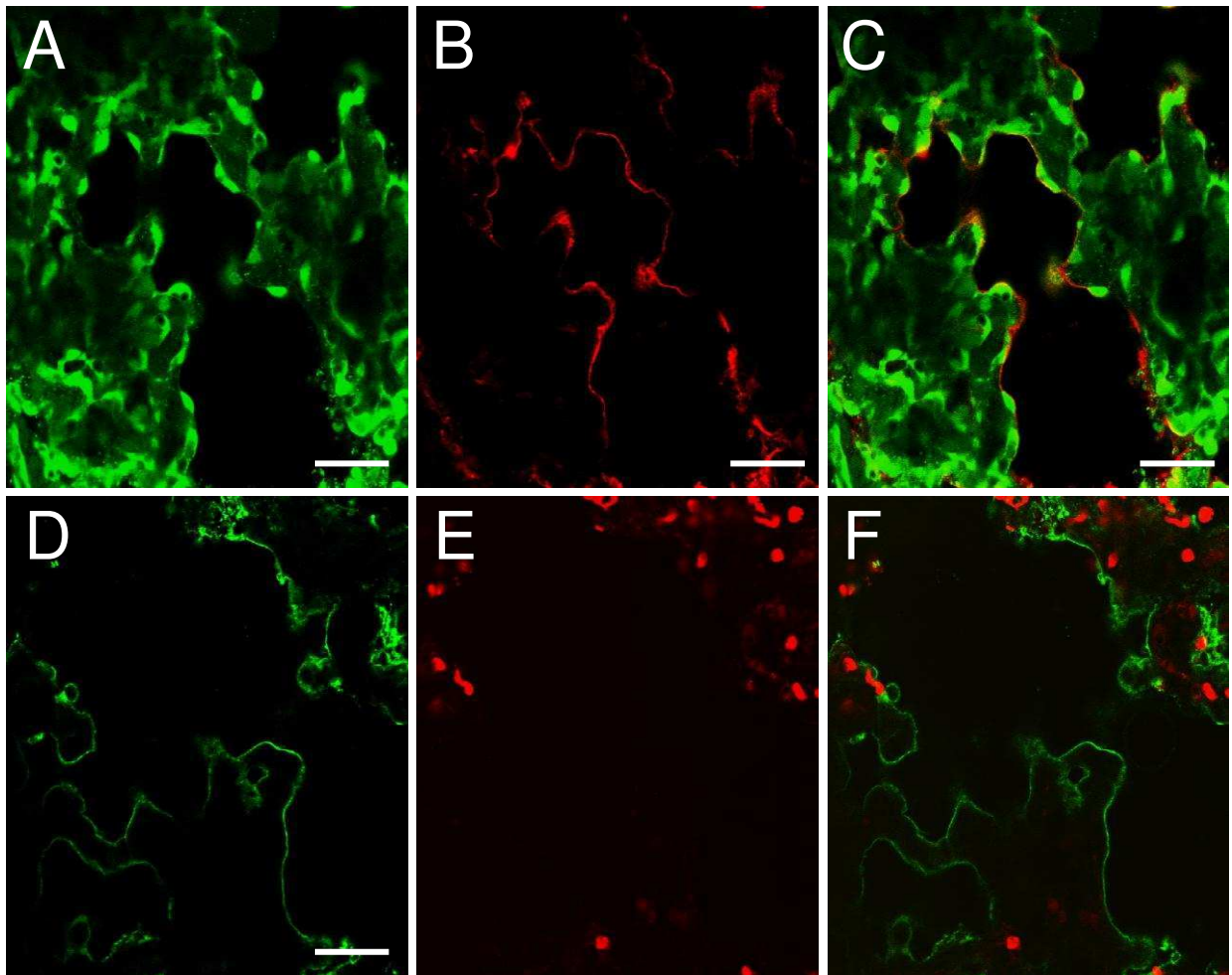


Figure 3.6 Confocal images of rat lung slice co-stained with either live or dead viability stains and specific alveolar epithelial type one cell antibody, VIII B2.

Panel A shows a 200 μ m rat lung slice incubated with the live stain (2 μ M Calcein-AM) following live immunohistochemical staining with VIII B2 primary antibody/Alexa Fluor 532 secondary antibody and excited at 488nm (green emission) to show living cells. Panel B shows the same lung slice incubated with the live stain (2 μ M Calcein-AM) following live immunohistochemical treatment with VIII B2 primary antibody/Alexa Fluor 546 secondary antibody staining at the alveolar epithelium type one cells. Panel C the overlay of images A and B showing that the VIII B2 immunoreactivity is clearly restricted to elongated, thin cells located at the edge of the

alveolar space. Panel D shows a 200 μm rat lung slice incubated with dead stain (4 μM EthD-1) following live immunohistochemical staining with VIIIIB2 primary antibody/Alexa Fluor 488 secondary antibody and excited at 488nm (green emission) to show secondary antibody staining of alveolar epithelial type one cells. Panel E is the same lung slice incubated with the dead stain (4 μM EthD-1) following live immunohistochemical treatment with the primary antibody VIIIIB2/Alexa Fluor 488 secondary antibody and excited at 532nm (red emission) to show the EthD-1 positive, compromised nuclei. Panel F is the overlay of both images. Scale bar 20 μm .

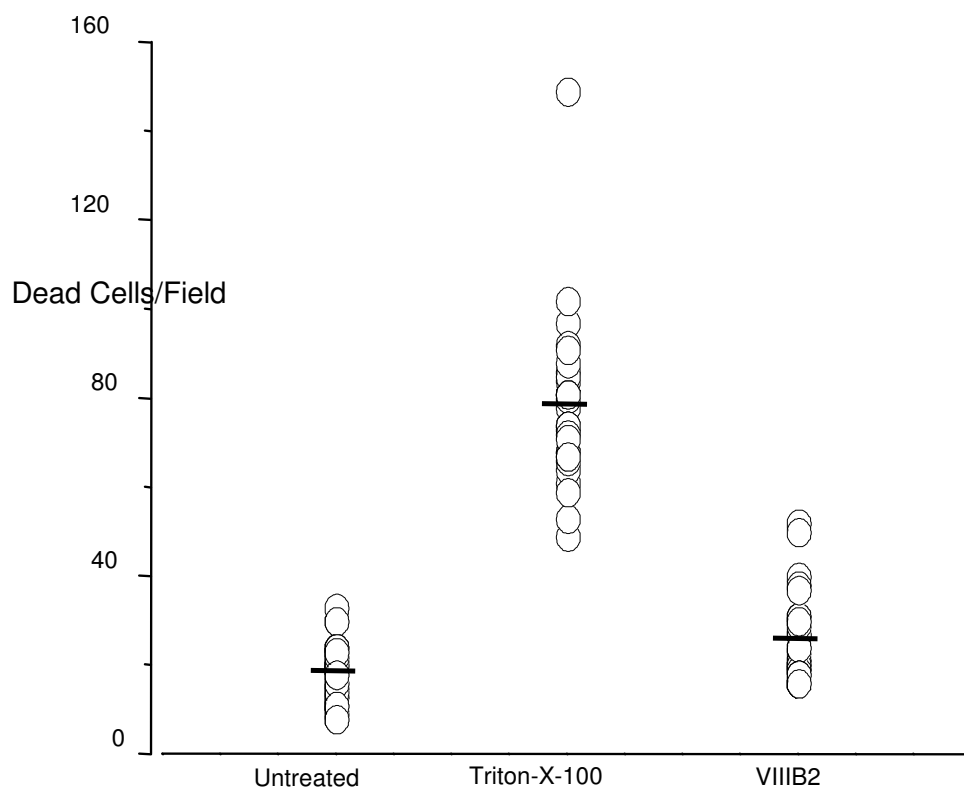


Figure 3.7 Graph showing quantification of dead cells per field of view in unfilled lung slices loaded with LIVE/DEAD® cell viability stain.

Compromised nuclei counted in lung slices from a field of view 105 μm X 105 μm . Three different criteria were examined. Untreated slices loaded with dead viability stain (4 μM EthD-1) and excited with the 543 nm laser, slices treated with 1% Triton X 100 for 10 min. and subsequently loaded with Dead stain (4 μM

EthD-1) and excited via the 543nm and third are slices that have been treated with VIIIIB2 and then incubated with with dead stain (4 μ M EthD-1) see panel F (fig 3.5). The modest, but significant 1.4-fold increase cell death evoked by live immunohistochemistry is quantified, which shows that VIIIIB2 treatment results in 25.3 ± 1.7 dead cells per field (n = 31) compared with 18.0 ± 0.9 in untreated slices (n=23).

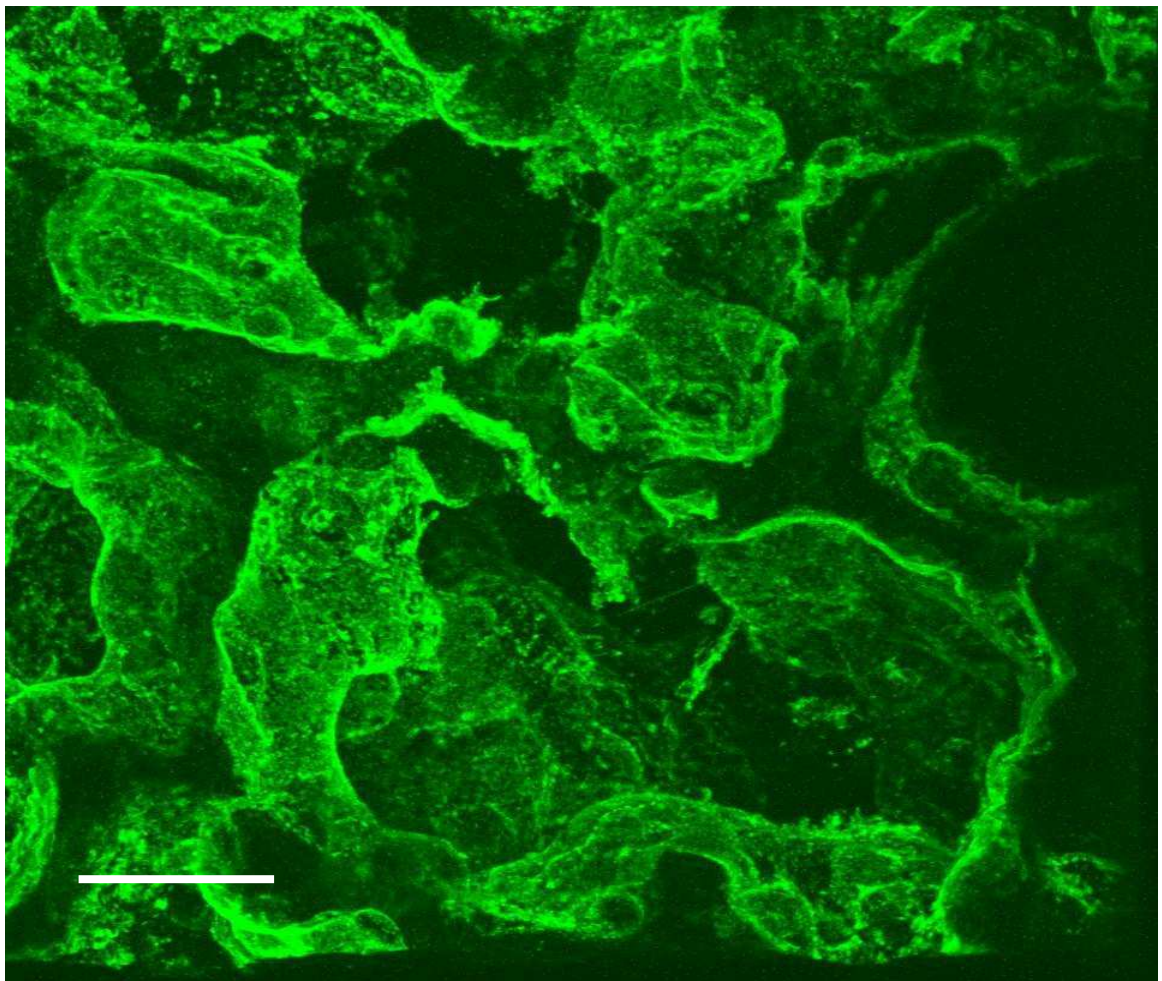


Figure 3.8 Confocal reconstructed stack of alveolar epithelial type one cells identified with VIIIIB2 antibody in 200 μ m thickness lung slice.

A 200 μ m thickness lung slice was cut using the Integraslice® in the unfilled configuration. After slicing was complete, the slice was incubated with the VIIIIB2 antibody followed by addition of the Alexa Fluor 488 anti mouse IgG secondary. The images were captured by exciting via the 488nm laser line of the CellMap

IC™ confocal. The slice was held in an in-house designed specimen bath of a BX50WI Olympus upright microscope with a X 60 water dipping objective. The image shows a reconstructed z stack of confocal images. Each image has a z resolution of 0.55 μ m. The x and y resolutions is 2048 pixels X 2048 pixels and the complete image is the combination of 127 individual optical sections. The white scale bar represents 20 μ m.

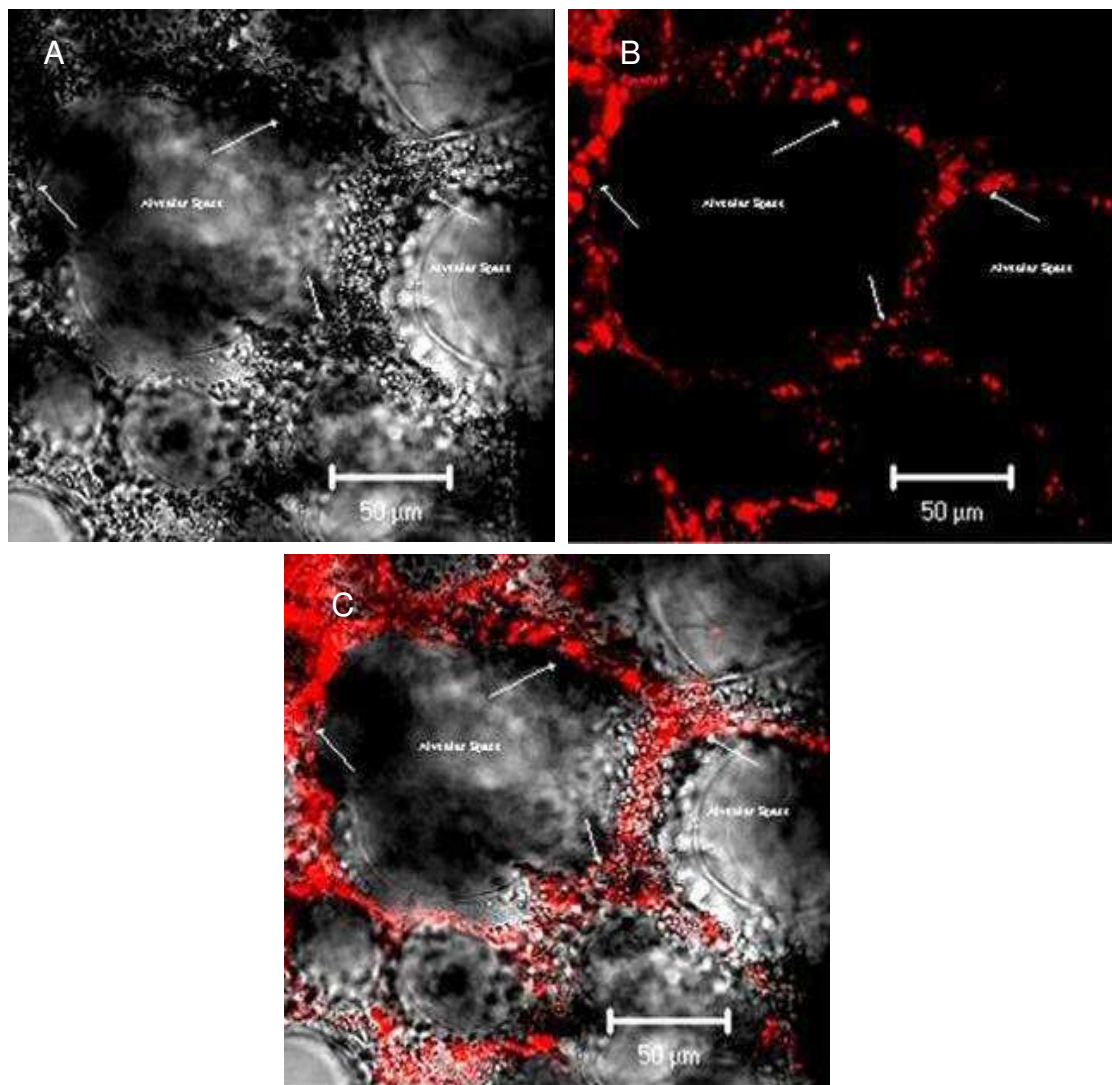


Figure 3.9 Confocal image of lung slice treated with Nile Red vital stain.

A 200 μm thickness agarose filled lung slice was imaged on a Zeiss LSM 410 inverted confocal microscope. Panel A is a transmitted light image of a lung slice treated with 1 $\mu\text{g}.\text{ml}^{-1}$ Nile Red. The image was captured with 543nm laser, no filters were present in the light path. Panel B is a confocal imaged of a lung slice treated with 1 $\mu\text{g}.\text{ml}^{-1}$ Nile Red containing physiological solution. The image was captured by excitation with the 534nm laser and allowed the collection of fluorescence signal by using a long pass 560 nm filter. Panel C is the digital overlay of the images. The alveolar space is also labelled. The white arrows indicate regions of Nile Red accumulation.

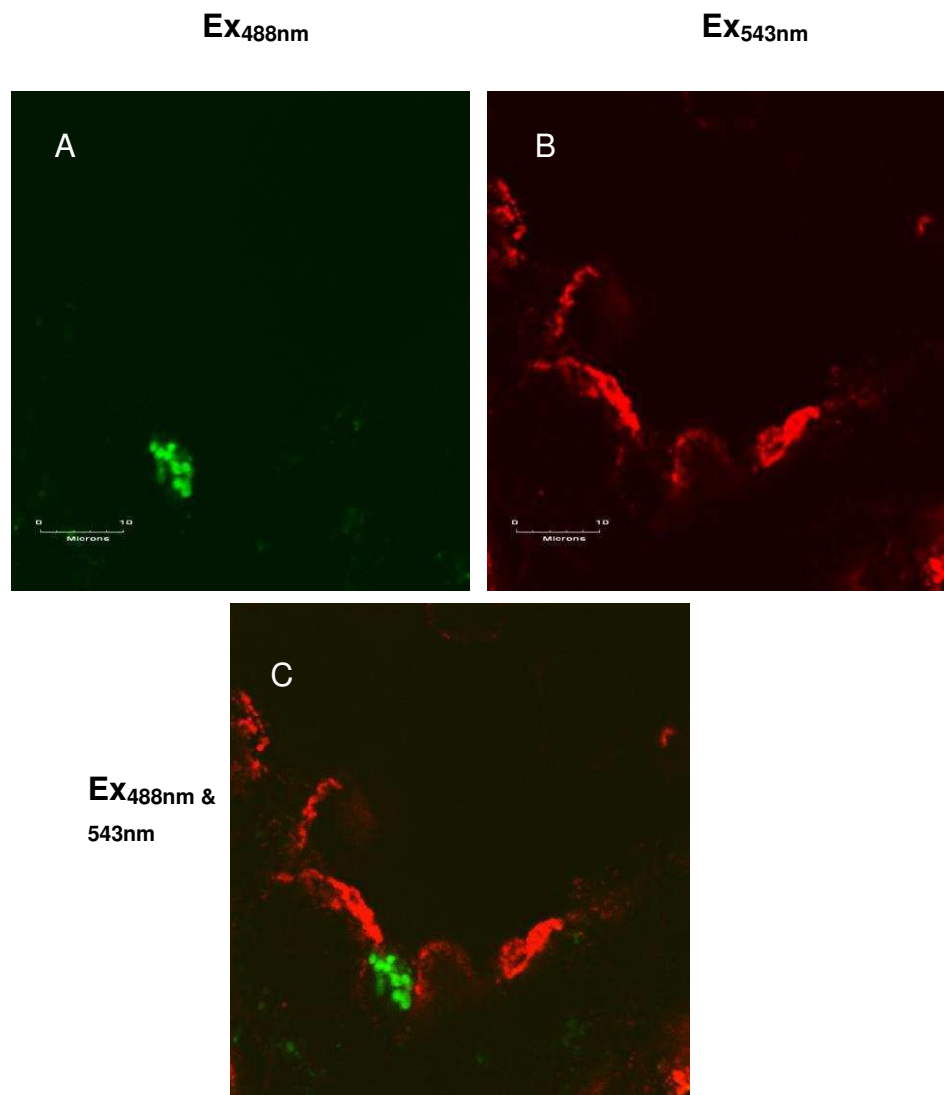


Figure 3.10 A confocal image of live cell identification in a lung slice of alveolar epithelial type one and alveolar epithelial type two cells.

An unfilled rat lung slice of 200 μ m thickness was imaged on an Olympus BX50WI upright microscope with a BioRad/Zeiss Cellmap IC confocal. Panel A shows a slice loaded with lyso tracker green DND-26 stain (50nM) and treated with VIII B2 mouse monoclonal antibody (Alexa Flour 543nm secondary antibody). Excitation with the 488nm laser, showing localisation of DND-26 to alveolar epithelial type two cell. Panel B shows the same slice excited with the 543nm laser, showing the localisation of red signal to the alveolar epithelial type one cell membrane. Panel C is the digital overlay of these images.

Chapter 4

**Electrophysiological investigation of identified
alveolar epithelial type one cells in a lung slice.**

Introduction.

The application of cellular electrophysiology can be described as the investigation of electrical properties of cell membranes and their functional significance. A critical aspect determining the function a cell will play in an organ involve the specific proteins associated with the membrane of the cell. The cellular membrane is composed of a lipid bilayer and its membrane proteins, including ion channels and carriers with highly specific in functions. Ion channels are ubiquitously expressed and provide a very selective route for ions to pass between the extracellular space and the cytoplasm. In order for the cell to function, it must maintain the ionic concentration of the cytoplasm while allowing the transport of specific solutes and ions, back and forth across the membrane. This is achieved with the help of transport proteins which can be split in to three main groups pumps, channels and carriers. Ion channels are subdivided into “channel families” and the criteria are based upon molecular structure.

The patch clamp technique (Hamill *et al.* 1981) requires the formation of a high resistance seal between the glass micropipette and the cellular membrane by careful positioning. In order to obtain useful electrophysiological data the high resistant seal establishes a closed compartment independent of the extracellular solution. This experimental technique allows the investigator to electronically isolate the currents measured across a membrane patch. Although a number of patch clamp configurations exist, the cell-attached configuration was determined the most appropriate configuration to study the single channel activity of the alveolar epithelial type one cell apical membrane.

There has been a rapid advancement in scientific investigation and understanding of the physiology of the alveolar epithelium and the molecular mechanisms over the past 30 years. The investigation into the mechanisms underlying the ion movement and liquid transport in the lung has used a wide range of species and experimental models. With the alveolar epithelium covering 99% of the surface area of the gas exchange region of the lung (Crapo *et a./* 1983), it has an extensive and unique contact with the exterior environment. The recent advances in understanding of the molecular composition of the alveolar

epithelium allows a greater insight into how the fluid in the lung is maintained through out both normal and pathological situations (for review see Dobbs and Johnson 2007; Kemp and Kim 2004; McElroy and Kasper 2004). Previous patch clamp investigations have been restricted to isolated alveolar epithelial type two cells but functional electrophysiological data has been presented from alveolar epithelial type one cells (Bourke *et al.* 2005; Johnson *et al.* 2006; Helms *et al.* 2006; Helms *et al.* 2008).

Direct electrophysiological evidence of functional ion channels present in alveolar epithelial type one cells did not exist in the literature prior to the completion of this study (Bourke *et al.* 2005). There have been a number of difficulties in producing functional ion channel recordings from alveolar epithelial type one cells. Isolated alveolar epithelial type one cells have a fragile membrane. It had been found to be particularly difficult to isolate them directly and they appear unsuitable for patch clamp experiments even if successfully isolated. Considering this, only one paper is contained in the literature reporting electrophysiological recordings from isolated alveolar epithelial type one cell (Johnson *et al.* 2006) the results of that study are discussed below. Furthermore, it has proved difficult to generate electrically tight confluent monolayers of isolated alveolar epithelial type one cells on a permeable supports, making Ussing chamber experiments unreliable (personal communication, Dr KJ Kim, University of Southern California, Los Angeles, U.S.A.). It is only in recent times that alveolar epithelial type one cell specific markers have been used successfully in living cells (Bourke *et al.* 2005; Helms *et al.* 2006; Helms *et al.* 2008), making the electrophysiological measurement of ion channels from identified alveolar epithelial type one and type two cells within a lung slice preparation a reality only in the past 4 years (Bourke *et al.* 2005; Johnson *et al.* 2006; Helms *et al.* 2006; Helms *et al.* 2008).

Evidence for ion channel activity in isolated alveolar epithelial type one cell preparations has been difficult to produce. However improved isolation methods, permitted Johnson *et al.* (2006) to demonstrate directly, via electrophysiological recording, that isolated alveolar epithelial type one cells contain the functional ion channels required to play an important role in fluid homeostasis within the

lung. They identified a highly selective cation channel and a non-selective cation channel with measured unit conductances of 4-5 pS and 21pS respectively; both demonstrating amiloride sensitivity, suggesting the presence of ENaC channels within the apical membrane of alveolar epithelial type one cells. These observations were reinforced by western blot analysis, which demonstrated the presence of α , β , and γ ENaC subunits in alveolar type one cells *in situ*. Furthermore, the presence of the cystic fibrosis transmembrane regulator (CFTR) within alveolar epithelial type one cells was also demonstrated using cell-attached patch-clamp recordings, western blot and immunohistochemistry. In addition, the presence of a cyclic nucleotide-gated cation channel, which had a unitary conductance of 2.9pS, $P_{Na^+} : P_{K^+}$ of 1, was insensitive to amiloride and stimulated (in a Ca^{2+} -free bath solution) by application of analogues of cGMP. A potassium channel was also reported, which had a unitary conductance of 15-16pS, and demonstrated Ba^{2+} sensitivity (Johnson *et al.* 2006).

The use of the lung slice has proved a valuable research model for the study of the alveolar epithelium, as outlined in this chapter (Bourke *et al.* 2005) and the publications by the Helms in 2006 and 2008. Indeed, this preparation has greatly advanced our knowledge of ion channel activity present in both alveolar epithelial type one and alveolar epithelial type two cells. Using the cell-attached configuration of the patch-clamp technique, have demonstrated the presence of two Na^+ channels, a highly selective cation channel and a non-selective cation channel, within the apical membrane of identified alveolar epithelial type one cells (Helms *et al.* 2006). They reported mean unitary conductances of 8.2 ± 2.5 and 22 ± 3.2 pS, respectively, for these channels, which correspond to the published data for ENaC ion channels from other epithelial cells (For example, Jain *et al.* 2001; Chen *et al.* 2005, Anantharam and Plumber 2007) and in a recombinant system (Ruffieux-Daidié *et al.* 2008). Both of these channels demonstrated amiloride sensitivity within the identified cells and measured reductions in channel NP_o following “addition” of 25nM amiloride from 0.481 ± 0.126 to 0.0186 ± 0.003 ; the amiloride-sensitivity was tested using a “pipette diffusion method”, which allowed a control-recording period to be

obtained before the effect of the diffusion of amiloride to the channel was assayed.

Further, Helms *et al* (2008), have demonstrated the first recordings from alveolar epithelial type two cells *in situ* from a lung slice preparation (Helms *et al.* 2008). The biophysical properties of the single channel events recorded from within the slice validate published ion channel activity observed in the primary isolated cell preparation (Jain *et al.* 2001; Chen *et al.* 2002, Anantharam and Plumber 2007). They demonstrated the presence of both highly selective and non-selective cation channel activity and suggested they were important to the net Na⁺ ion transport across the alveolar epithelium. The average conductances were measured as 8.8 ± 3.2 pS and 22.5 ± 6.3 pS, respectively. There was also an apical membrane anion channel with a conductance of 10pS. A difference in the response to nitric oxide (NO) donor, PAPA-NONOate (1.5M), was observed in the ENaC ion channel activity between the alveolar epithelial type one and type two cell populations. The NP_o of the alveolar epithelial type one cell was not effected by this application. However, there was a significant reduction in the NP_o value for alveolar epithelial type two activity, from 1.38 ± 0.26 to 0.82 ± 0.16 . These results provide further evidence that alveolar epithelium plays an important role in maintaining ion fluid balance in the lung.

In previous chapters, the optimisation and viability of the lung slice, along with live cell labelling of alveolar epithelial type one cells and alveolar epithelia type two cells, have been presented. This chapter describes the first recordings of functional ion channels from such identified alveolar epithelial type one cells in an unfilled lung slice model. The culmination of these methods has allowed the measurement of single channel events recorded from the apical membrane of identified alveolar epithelial type one cells from an *in situ* lung slice preparation. The development of this experimental technique will prove to be instrumental in furthering the understanding of the physiological function of the alveolar epithelial type one cell in lung fluid homeostasis in health and disease.

Results.

4.1 Locating and positioning of patch electrodes within the lung slice following identification of alveolar epithelial type one cells.

Figure 4.1 is an image of the patch electrode in contact with the apical membrane of an identified alveolar epithelial type one cell in a live lung slice 200µm thickness. Such a methodology permitted the first ever-reported electrophysiological recordings from alveolar epithelial type one cells *in situ* (Bourke *et al.* 2005). Panel A of figure 4.1 illustrates the use of the mouse monoclonal antibody, VIII B2, to label specifically living alveolar epithelial type one cells. This antibody binds to the apical membrane of alveolar epithelial type one cells exclusively (Danto *et al.* 1992). Visualisation under both epifluorescence and by confocal imaging was clearly detectable. The image seen in panel B is a 1µm z resolution confocal image of the recording electrode; for illustrative purposes, the recording electrode had a bolus of Alexa Fluor 546 antibody included in the solution. The 1µm confocal optical section, when excited via the 534nm laser, assists in demonstrating the contact point at the tip of the recording electrode with the lung slice.

Panel C visually demonstrates the problems encountered when observing a lung slice under transmitted light. Although 95% of the epithelium is covered by alveolar epithelial type one cells, the use of the VIII B2 live labelling serves as an invaluable research tool in positioning the patch electrode. The patch-clamp electrode is clearly visible in the image, along with the microstructure of the lung slice. In this particular image there is no emission or excitation filters present, and the image was captured using the 488nm excitation laser. Panel D represents the overlaid images of panels A, B, and C. This demonstrates clearly that the tip of the patch-clamp electrode is in direct contact with the identified alveolar epithelial type one cell apical membrane. The blue background is

created by the software and represents the transmitted light image seen in panel C. This image visually demonstrates that it is possible to manoeuvre a patch clamp microelectrode to a position where it can make contact with an identified alveolar epithelial type one cell within a lung slice.

Use of the unfilled model increases the opportunity of accessing the alveolar epithelial apical membrane.

4.2 Electrophysiological recordings from identified alveolar epithelial type one cells in the lung slice.

Using the cell-attached patch-clamp configuration, single channel currents could be recorded from VIII B2 immunoreactive cells within a 200 μ m thickness lung slice. Figure 4.2.A and 4.2.B are exemplar recordings from two different animals showing that a variety of ion channels are present within the epithelium. The voltage protocol was as follows: cells were patched-clamped in the cell-attached mode and were held for 40 milliseconds at 0 mV, a step was made to -70 mV and the voltage was increased in a ramp fashion for a time period of two seconds to a value $+90$ mV before being stepped back to -70 mV for 40 milliseconds. These data were recorded using the high K^+ solution (see section 2.3.1). Figure 4.1. C represents the magnified portion of the trace identified by the red lines seen on figure 4.2 panel A. Figure 4.2. panel D represents a magnified portion of the trace identified between the green lines seen on figure 4.2. panel B. The recordings shown here, produced from the ramp protocol, demonstrate that it is possible to record functional ion channel currents from alveolar epithelial type one cells using the lung slice experimental model. This particular ramp protocol was chosen in order to identify the presence of voltage-activated ion channel population within the alveolar epithelium type one cells. These traces have not been leak-subtracted and show the presence of ion channel activity across the entire voltage range.

4.3 Cell-attached, gap-free, patch-clamp recordings from identified alveolar epithelial type one cells in a lung slice.

In order to investigate and characterise the ion channels present in alveolar epithelial type one cells it was necessary to make a change to the recording protocol. A gap-free voltage protocol was undertaken to allow the continuous recording of single channel activity.

Figure 4.3 represents a family of currents recorded in the cell-attached configuration from an identified alveolar epithelial type one cell in a rat lung slice. The holding voltage was changed in a stepwise manner from -100mV to $+30\text{mV}$ and the current was filtered at 200Hz in order to capture the single channel events. Single channel openings could be resolved at the each voltage step. There was a cocktail of channel blockers present in the patch pipette, which aimed to block ENaC, chloride channels and the majority of potassium channels (see section 2.3.1.2 for details). Under these stringent recording conditions, the resultant family of single channel currents are seen in figure 4.3.

The changing of the membrane potential resulted in activation of a small conductance channel (figure 4.4 Panel A). This figure is representative of data recorded from three individual cells from three different lung slices. Figure 4.4 demonstrates that the channel exhibits a voltage-dependence with the reverse potential seen at around -60 to -70 mV, which is close to E_K under the conditions which the records were acquired. The current-voltage relationship for these channels, as shown in figure 4.4, demonstrates this alveolar epithelial type one cell a channel has a mean unitary conductance of 21 ± 3 pS. Figure 4.5 is a plot of the open state probability and channel number (NPo) versus voltage relationship of the same channel and shows that the channel activity was voltage-dependant, activating at potentials more positive than -40mV .

4.4 Discussion.

To date, our understanding of the electrophysiology of the alveolar epithelium has relied almost entirely on the information gathered from either freshly isolated or cultured alveolar epithelia type two cells. The results presented in this chapter represents the first demonstration that it is possible to record successfully functional ion channels from positively identified, living alveolar epithelial type one cells from within an *in situ* unfilled lung slice preparation. The traditional view has been that the alveolar epithelium plays a role in generating the active Na⁺ driving force, which is then harnessed to promote osmotic fluid reabsorption of fluid from the airspaces. Based on my electrophysiological data, and the electrophysiological data from other laboratories over the past 3 years, it is clear that alveolar epithelial type one cells have the potential to play an active role in fluid lung homeostasis. The alveolar epithelial type one cells express β -adrenoreceptors (Liebler *et al.* 2004), the entire family of ENaC ion channel subunits and electrophysiological properties (Borok *et al.* 2002; Johnson *et al.* 2006; Hemls *et al.* 2006) and the picture of how the alveolar epithelial type one cells contribute to alveolar homeostasis is slowly becoming clear.

The unfilled lung slice provides a valuable experimental model for the study of the alveolar epithelium in as close to *in vivo* experimental conditions as is currently possible for electrophysiological investigations. Figure 4.1 provides an elegant example of the strengths provided by the live immunohistochemical labelling of alveolar epithelial type one cells. There can be no question as to the position of the recording electrode tip contact point and the specificity of the VIII B2 mouse monoclonal antibody to label the apical membrane of the alveolar epithelial type one cell. Close inspection of the confocal overlay image in panel D provides the most vivid image of the value of live labelling. A number of technical factors were critical to obtaining these first functional recordings from identified alveolar epithelial type one cells. The use of a long working distance, dipping objective lens was critical as it allow excellent image resolution and

subsequent positioning of the electrophysiological recording electrode onto the alveolar epithelium. Due to the shallow angle of approach of the patch electrode that is required when using a non-inverted microscope, there was a limited area within the slice where recordings could be made. However, the in-house design of the specimen bath allowed straightforward rotation of the slice, thus facilitating good access to numerous regions within the slice.

Resolving single channel electrophysiological events requires very low electrical noise level. The exemplar traces seen in figure 4.2 and 4.3 demonstrate that single channel events could be resolved easily from the baseline noise level, which was < 0.5 pA. Reduction of electrical noise is a culmination of number independent factors. The selection of a high quality borosilicate pipette glass for recording electrodes was essential (Levis and Rae 1993) and made possible the manufacture of high resistance recording electrodes. The electrodes were also coated in Sigmacote[®] (Sigma-Aldrich), a hydrophobic liquid, which reduced the noise associated with liquid rising, via capillary action, up the outside of the electrode. A shallow bath level was maintained throughout the recording and making the recording in the “stop bath” configuration eliminated artefacts associated with perfusion. The choice of amplifier and associated head stage was also a contributing factor. The use of a capacitive feedback headstage (Multiclamp, Axon Instruments) was very useful in this regard as the noise level was very low; as there is a capacitor present in the feedback circuit of the current to voltage converter, this creates a circuit which acts as an integrator. This system can result in up 30% reduction in noise when other sources are minimised (Ogden and Stanfield 1994). It was also essential that the entire electrophysiological set up was properly grounded. This was achieved by a systematic check of each component and connecting each to a central earthing point, which was connected to the patch-clamp amplifier. These measures enabled the recording of cell-attached single channel patch-clamp electrophysiological data.

The exemplar traces shown in figure 4.2 demonstrate the presence of voltage-activated ion channels. There may have been more than one family of ion

channels present since the different amplitudes were present simultaneously (Panels C and D). Channels were activated across the entire voltage range. It was clear that in order to characterise fully the ion channels present, a combination of pharmacology and ion replacement would be required. The cocktail of pharmacological agents was selected to block any ion channel that had been demonstrated via other experimental methods. The inclusion of a TEA at 10mM blocks the majority of K⁺ selective channels, 100µM niflumic acid blocks chloride channels, 10µM amiloride blocks the ENaC Na⁺ channel. Ion replacement (sodium isethionate in place of NaCl) was also employed to reduce the possibility of contamination of chloride channels. The result of these additions is seen in figure 4.3. These data represent the first published ion channel activity recorded from alveolar epithelial type one cells (Bourke *et al.* 2005). The reversal potential of these channels (see figure 3.4) indicates that they are primarily permeable to potassium. However, the contribution of other ions cannot be completely ruled out. This channel, which is expressed at the apical membrane of the alveolar epithelia type one, had a measured mean conductance of 21±3 pS and was a voltage-activated. These characteristics suggest that the most likely potassium channel candidate underlying these cell-attached currents belong to the Kv family, perhaps Kv1.7, KCNA7 (Coetzee *et al.* 1999; Davies and Kozlowski 2002). The Kv1.7 is the most recent member of the Kv 1 voltage-activated potassium ion channel family to be cloned and is highly expressed in skeletal muscle, heart and kidney (Kashuba *et al.* 2001).

Kv 1.7 has also been identified in lung tissue (Coetzee *et al.* 1999; Davies *et al.* 2001). The main physiological function of the potassium channels within the alveolar epithelium is control of membrane potential and maintenance of the driving force for transepithelial ion and liquid transport. The potassium channels are essential in preventing cell depolarization during the periods of Cl⁻ efflux and Na⁺ influx (O'Grady *et al.* 2003). Kv 1.7 has been identified in rat lung pulmonary arteries by PCR, but this particular study did not report or investigate the expression of this channel in the alveolar epithelium. Potassium channels have been identified at the apical and basolateral membranes of both the alveolar epithelial type one and alveolar epithelial type two cells (review see Bardou *et al.*

2009). However, the function of a large number of the identified cells still remains to be elucidated. The presence of a 15-16 pS potassium channel in the isolated type one cells has recently been reported (Johnson *et al.* 2006) and is similar in amplitude (21 ± 3 pS) to the channel reported in this chapter. The exact physiological role of Kv1.7 in alveolar epithelium remains to be elucidated and will require the use of new genetic models to investigate thoroughly.

Conclusion.

The data presented in this chapter demonstrate the first published electrophysiological data obtained from alveolar epithelial type one cells. It further confirms that the unfilled lung slice is a suitable experimental model for understanding of the alveolar epithelium at a functional level. To obtain these data required the optimisation and combination of a number of experimental techniques. The inherent strengths of this experimental technique are that it allows the retention of cell-to-cell interactions and maintains the viability of the alveolar epithelial type one cell and type two cell populations. Patch-clamp cell-attached ramp recordings demonstrated the presence of voltage-activated ion channels in the apical membrane of identified alveolar epithelial type one cells. Recordings made using the gap-free voltage protocol and under stringent recording conditions allowed the characterisation of a K^+ selective voltage activated ion channel with a mean conductance of 21pS. This experimental technique provides the opportunity to characterise fully the ion channels present in the apical membrane of the alveolar epithelium, essential in understanding mechanisms involved in alveolar flooding and lung fluid homeostasis.

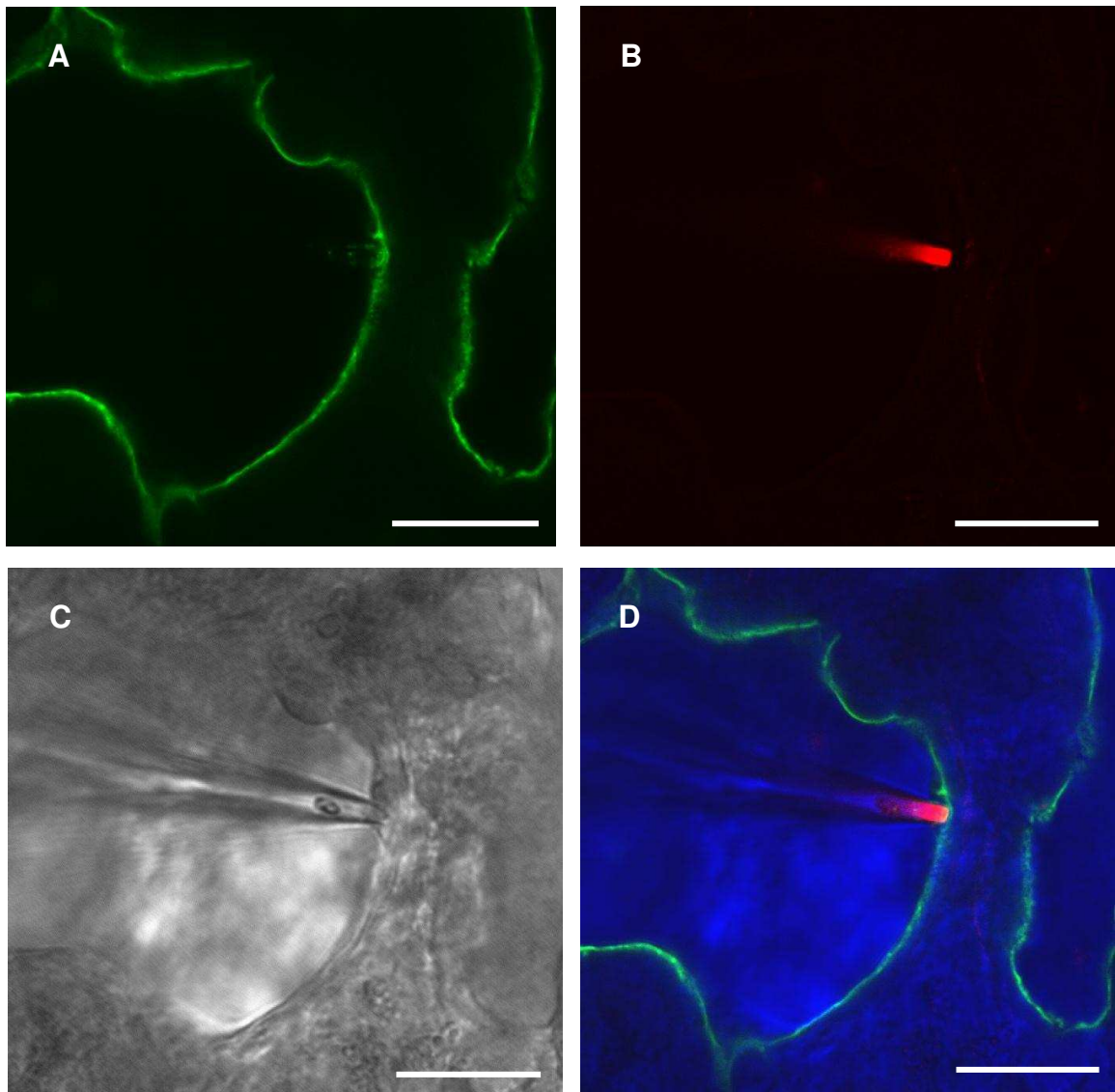


Figure 4.1 Confocal image of a cell-attached patch-clamp recording in a lung slice following identification of alveolar epithelial type one cells with VIII B2.

Panel A shows a $1\mu\text{m}$ z-resolution confocal image of a $200\mu\text{m}$ thickness rat lung slice immunohistologically stained with the VIII B2 antibody and Alexa 488 secondary antibody, excited via the 488nm laser. Panel B shows the same $1\mu\text{m}$ z-resolution confocal image of a patch clamp pipette with a bolus of Alexa Fluor 546 antibody (1:400), excited via the 543nm laser. Panel C is the transmitted

light image of the slice and pipette in contact with the alveolar epithelium. Panel D is the overlay of all images. The slice was imaged on an Olympus BX50WI upright scope with a 63X water dipping objective and CellMap IC confocal attachment. The scale bars represent 20 μ m.

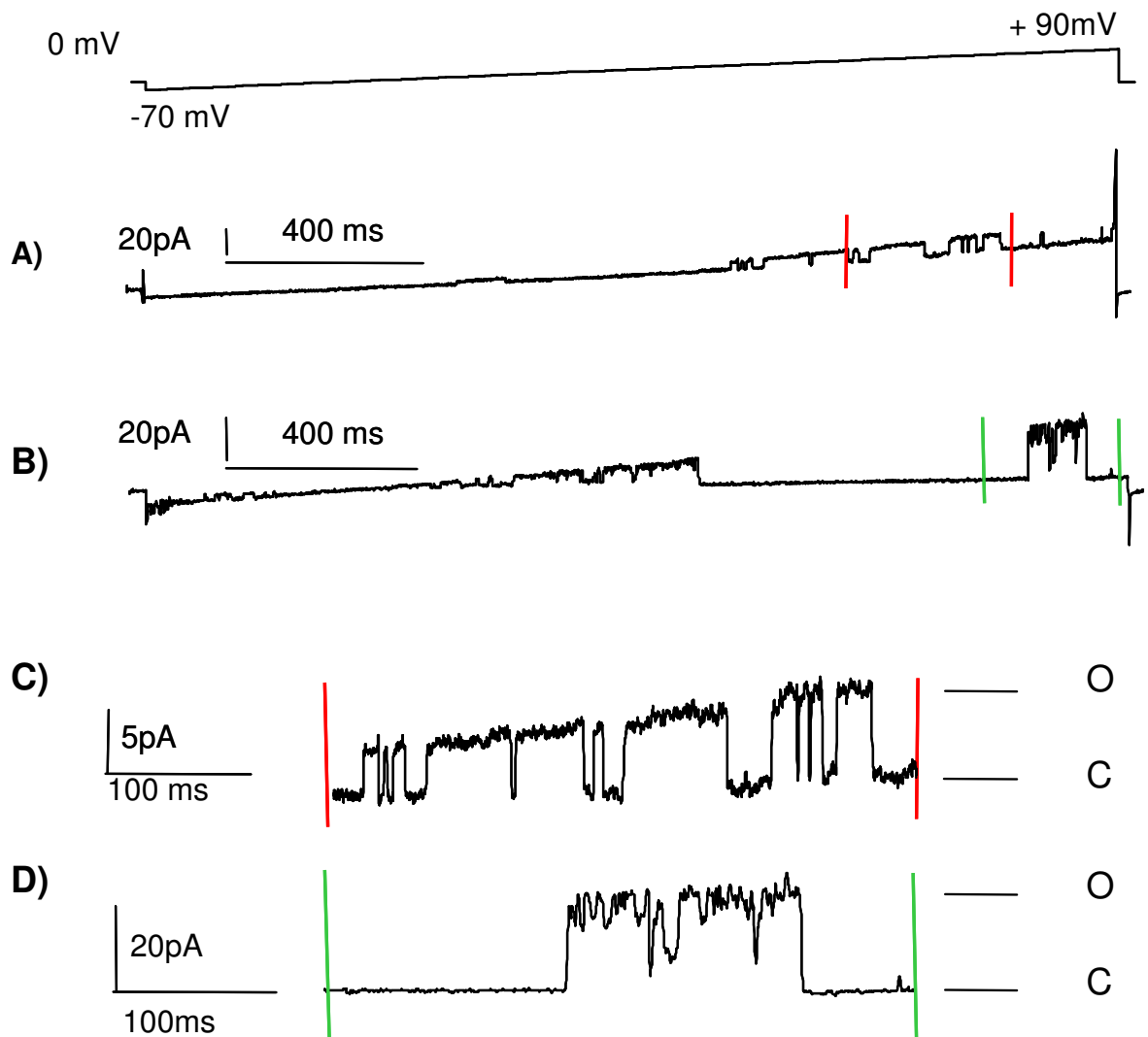


Figure 4.2 Cell-attached recordings from an identified alveolar epithelial type one cell in the lung slice employing high K⁺ solution.

Representative cell-attached patch-clamp data recorded from identified alveolar epithelial type one cells with two distinct conductances. Panels A and B are exemplar traces of voltage activated channel activity. The ramp runs from -70mv to +90mv over a 2 second period. The scale bars represent 20pA and 400ms. Respectively. Panel C and D represent the expanded periods identified by the

red (Panel A) and green (Panel B) lines, respectively. The open and closed states of the channel are shown, upward deflections from the closed state are outward currents. The scale bars associated with panel C represent 5pA and 100ms, and those associated with panel D are 20pA and 100ms.

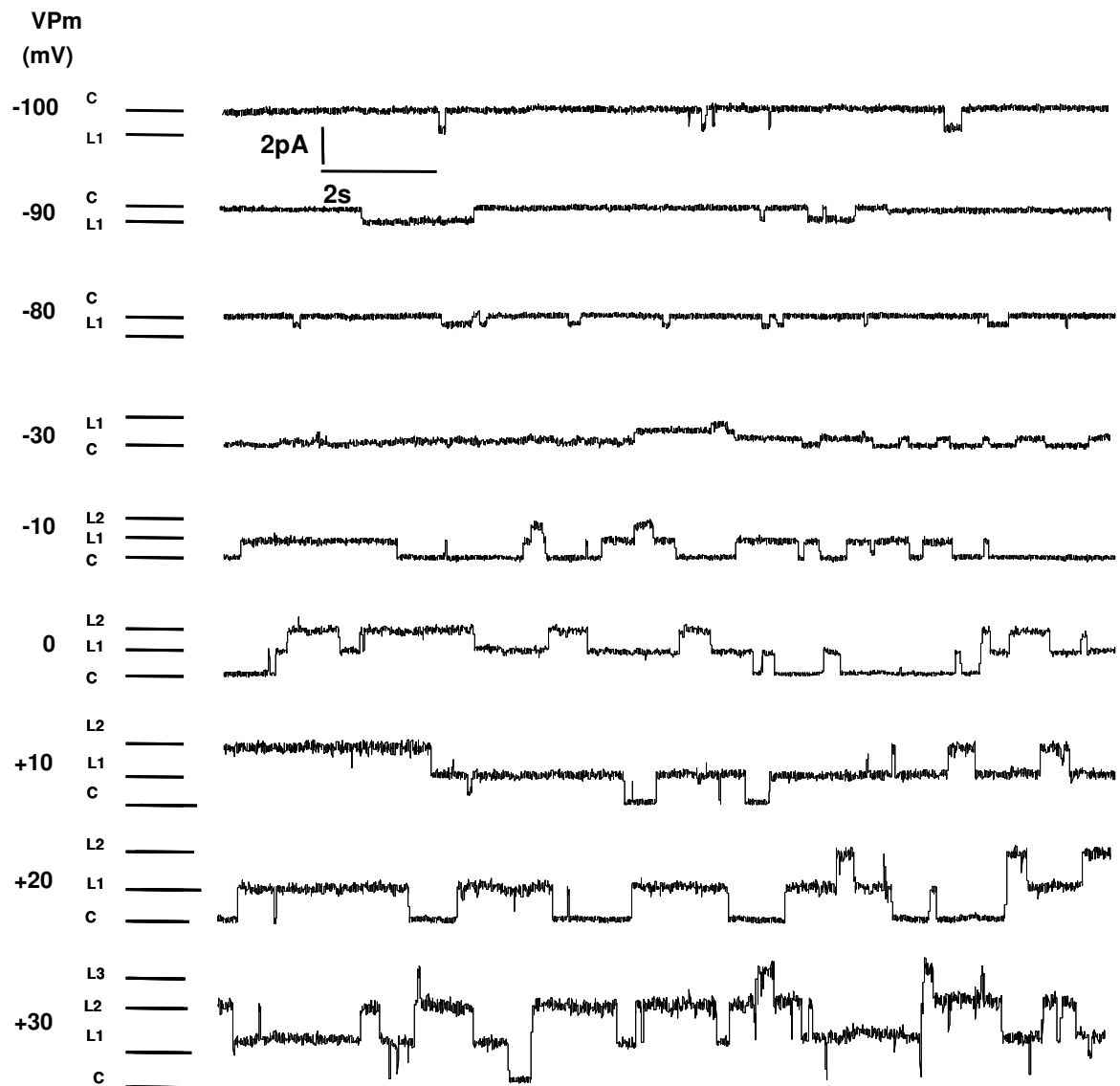


Figure 4.3 Cell-attached single-channel recordings from identified alveolar epithelial type one cells in rat lung slice.

Representative family of cell-attached currents recorded from an alveolar epithelial type one cell, identified by live immunohistochemistry in a rat lung slice. Single channel activity was recorded in the cell-attached configuration of the patch-clamp technique using the high K^+ /low Cl^- pipette solution (see

2.4.1.2) with 10 μ M amiloride, 100 μ M niflumic acid and 10mM TEA. Currents were recorded at -100, -90, -80, -30, -10, 0, +10, +20, +30mV potentials, indicated to the left of each trace and were filtered at 200Hz. L1, L2 and L3 channel open levels 1,2 and 3, respectively, whilst C indicates the channel closed level.

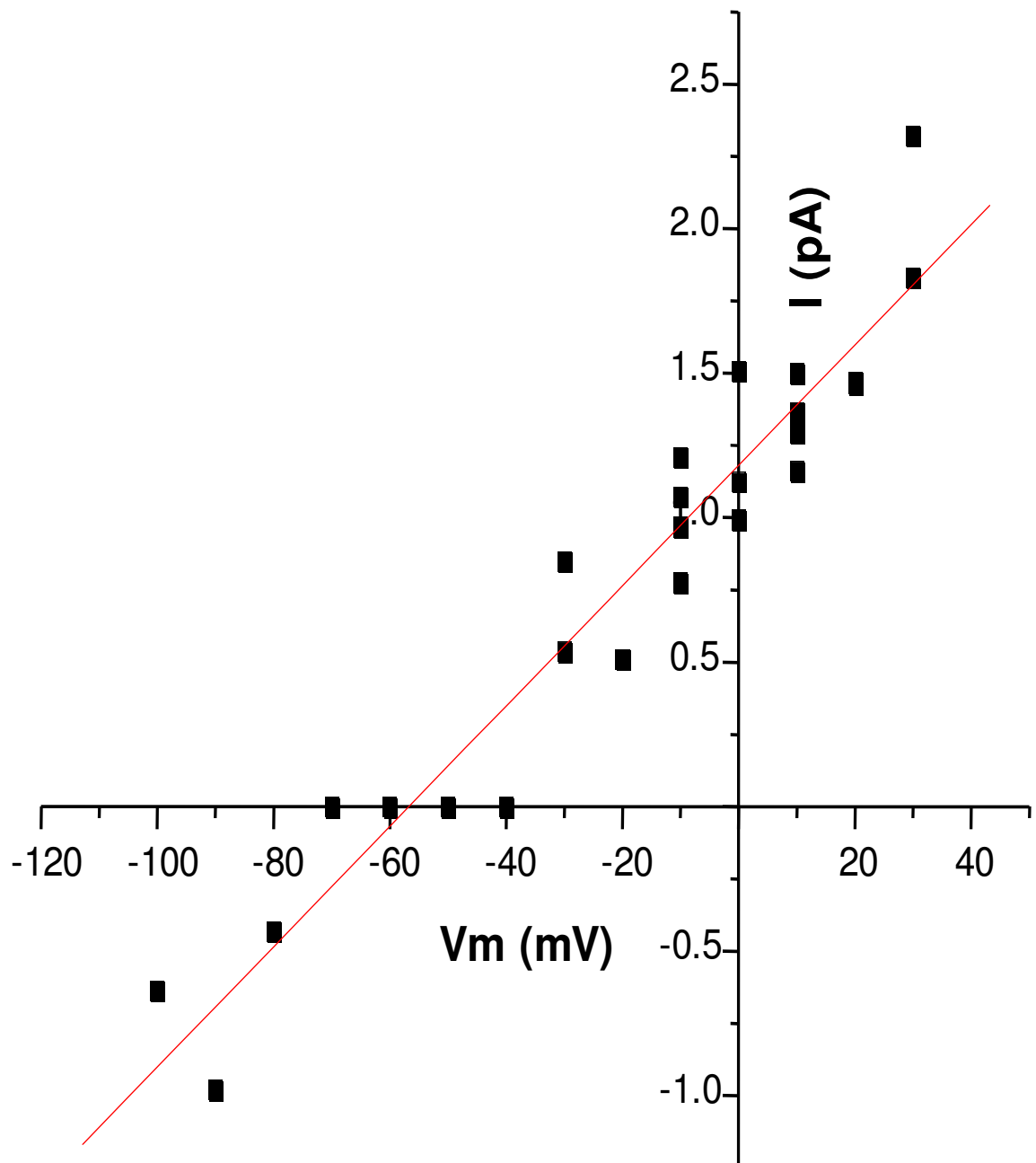


Figure 4.4 Current-voltage relationship from the channels identified in alveolar epithelial type one cells in a rat lung slice.

Graphical representation of the cell-attached single channel current amplitude (y axis) versus membrane voltage (x axis). The values were obtained from three individual cells from three different slice preparations. A mean single channel conductance of 21 ± 3 pS was calculated by regression.

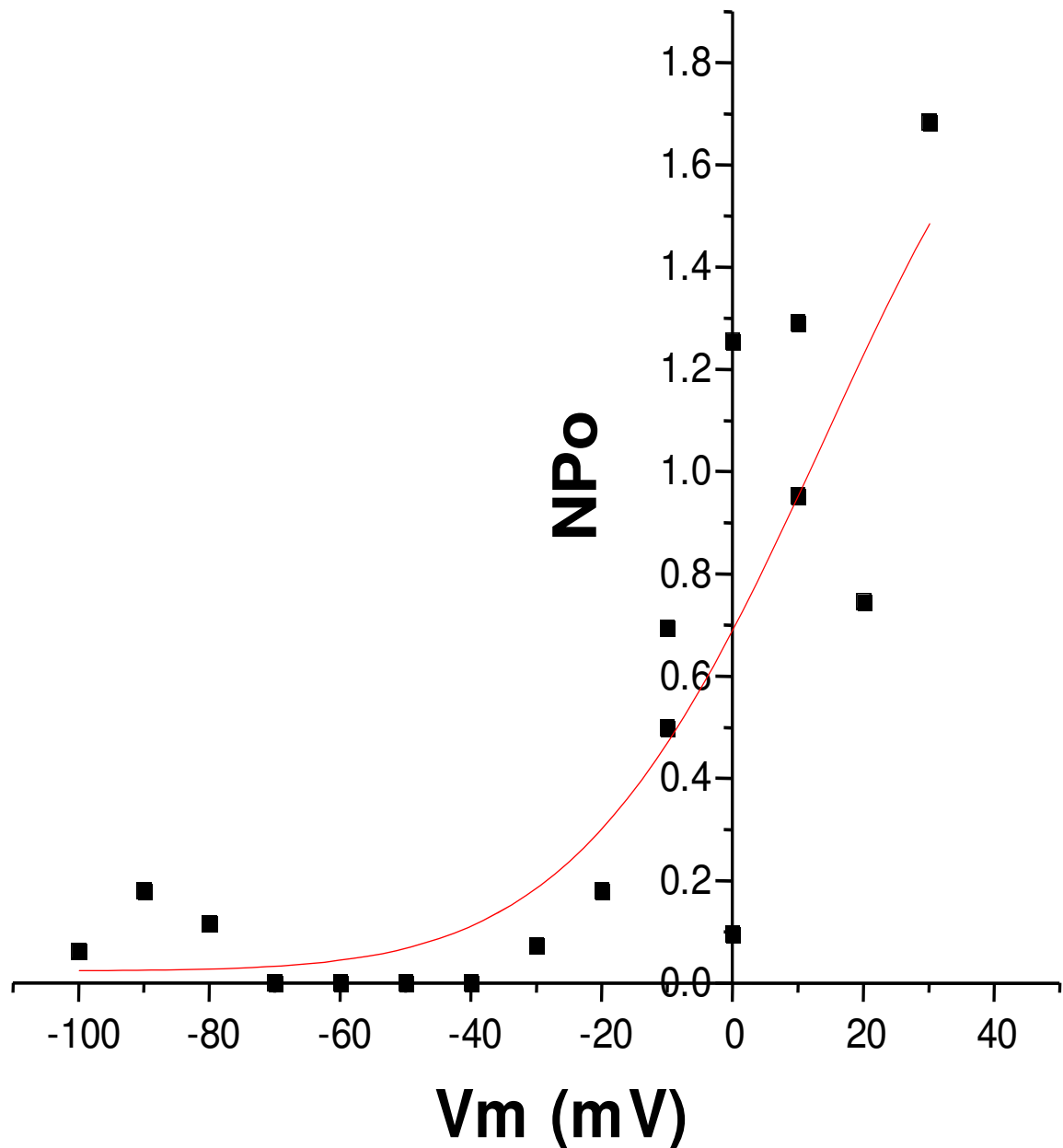


Figure 4.5 Voltage-dependence of the single channels recorded from identified alveolar epithelial type one cells in a lung slice.

NPo plot of the channel recorded from identified alveolar epithelial type one cells three different slice preparations. The NPo values were measured over a range of membrane holding potentials. A graphical representation of NPo (y axis) versus membrane voltage (x axis).

Chapter 5.

**Measuring calcium signals in living rat lung
slices.**

Introduction.

Calcium is a ubiquitous second messenger that regulates a number of cellular processes in both excitable and nonexcitable cells (Berridge 2008; Abraham *et al.* 2001; Ashino *et al.* 2000). A number of key methodological advances has allowed a rapid progress over the past 25 years to our understanding of the mechanisms involving calcium homeostasis. Advances in imaging, both at hardware and software levels, coupled to the introduction of biological fluorescent ion indicator probes e.g. fura 2 and Fluo3 and Fluo4, has made it possible to visualise, in real time, the physiological role played by Ca^{2+} and associated proteins, within an organ (Kuebler *et al.* 2007, Ashino *et al.* 2000), individual cell (Tsien 1983, Clunes and Kemp 1996, Isakson *et al.* 2003, Lee *et al.* 2006), organ slice (Bourke *et al.* 2003, DeProost *et al.* 2008) and cellular organelles (Haller *et al.* 1998, Wang *et al.* 2004). Ca^{2+} indicator dyes have seen significant developments and this has led directly to reliable and convenient indicators of intracellular Ca^{2+} ion concentration that have proved invaluable in the progression of many fields within biomedical research. A number of fluorescent dyes are in mainstream scientific use and this, combined with the increase of affordable imaging systems, has resulted in a greater understanding of the physiological role of Ca^{2+} . The field of respiratory physiology has also benefited, like all other areas of biology, directly from such advancement allowing the demonstration key processes that are calcium dependant such as surfactant release at a cellular level (Haller 1999) and micromechanic studies of alveolar in the whole lung (Lindert *et al.* 2007).

The importance of Ca^{2+} is clear and measured values for Intracellular calcium concentrations in cells range from 10^{-7} to 10^{-5} M. Extracellular concentration of calcium is about 2×10^{-3} M (2 mM). Therefore, there is a chemical gradient for calcium to diffuse into the cell. As with all ion gradients within biology it is coupled with the negative membrane potential of cells therefore Ca^{2+} also is under the control of an electrical driving force that help bring Ca^{2+} into the cell. Ca^{2+} is of course required to be removed from the cell also as a sustained increase would lead to cellular dysfunction.

Calcium is removed from cells by two basic mechanisms. The first mechanism involves an ATP-dependent Ca^{++} pump that actively removes calcium from the cell (see figure at right). The second mechanism is the sodium-calcium exchanger. The exact mechanism by which this exchanger works is unclear. It is known that calcium and sodium can move in either direction across the sarcolemma. Furthermore, three sodium ions are exchanged for each calcium; therefore this exchanger generates an electrogenic potential. The direction of movement of these ions (either inward or outward) depends upon the membrane potential and the chemical gradient for the ions. When the membrane potential is negative (e.g., in resting cells), the exchanger transports Ca^{++} out as Na^+ enters the cell. When the cell is depolarized and has a positive membrane potential, the exchanger works in the opposite direction (i.e., Na^+ leaves and Ca^{++} enters the cell).

We also know that an increase in intracellular sodium concentration leads to an increase in intracellular calcium concentration through this exchange. This has important physiological implications. One example of this occurring is when the activity of the Na^+/K^+ -ATPase pump is decreased. This energy requiring, ATP-dependent pump transports sodium out of the cell and potassium into the cell. When the activity of this pump is reduced, for example, by cellular hypoxia (which causes ATP levels to fall) or by chemical inhibitors of this pump such as digitalis, then intracellular Na^+ concentrations increase. One way to envision how this affects Ca^{++} exchange is that the increased intracellular Na^+ reduces the concentration gradient of Na^+ across the sarcolemma, which reduces the inward movement of Na^+ down its concentration gradient via the exchanger. This, in turn, reduces the outward movement and exchange of Ca^{++} , which leads to an accumulation of intracellular calcium. This is the mechanism by which digitalis increases cardiac inotropy. Under hypoxic conditions, the enhanced calcium concentrations cannot increase inotropy because of the lack of ATP; however, the increased intracellular calcium (termed calcium overload) can damage mitochondria and alter cellular function.

Ca^{2+} signalling contributes to a number of different biological events. A rise in Ca^{2+} concentration is generally a global event and often recruits Ca^{2+} entry from

extracellular fluid as well as Ca^{2+} release from stores (Berridge, M.J. 2008). However, smaller dynamic Ca^{2+} events occur within the cell allowing Ca^{2+} to effect certain biological processes, for example contraction of smooth muscle via the action of Ca^{2+} activated currents. Central to an understanding of Ca^{2+} homeostasis within the cell is an understanding of the structure and function of the Ca^{2+} stores within the cell. The main Ca^{2+} store is the endoplasmic reticulum (ER), an organelle that forms an extensive network believed to be in close apposition with the plasma membrane (Clapham 2007). The ER must rely on Ca^{2+} pumps to transport Ca^{2+} across its membrane, and the sarcoplasmic/endoplasmic reticulum Ca^{2+} ATPase (SERCA) pump pumps Ca^{2+} against the electrochemical gradient. SERCA rely on ATP as their energy source in the transport of Ca^{2+} into the stores. The roles of the ER include Ca^{2+} uptake and storage to maintain a relatively low cytosolic Ca^{2+} concentration but also Ca^{2+} release back into the cytoplasm through specialised release channels, ryanodine receptors (RyR) and IP_3 receptors (IP_3R) channels (Carafoli 2002).

Ryanodine receptors are activated by both micromolar Ca^{2+} and caffeine and blocked by ryanodine and ruthenium red. Release of Ca^{2+} from the RyR can cause a very transient local elevation in Ca^{2+} , which have become known as Ca^{2+} sparks (Carafoli 2002; Berridge 2008; Clapham 2007). The release of Ca^{2+} from the ER by IP_3R channel and the opening of a small cluster of these channels have been implicated in creating a Ca^{2+} idea of the “ Ca^{2+} puff”. The spike-like events of the IP_3R can lead a “ Ca^{2+} waves” in which the Ca^{2+} at the initial site diffuses to nearby stores to activate them to release Ca^{2+} , which in turn diffuses further outward to hit additional stores, this is a form of Ca^{2+} induced Ca^{2+} release. The current thinking suggests that waves rely on RyR for initiation and IP_3R for propagation (Berridge 2008).

Critical to alveolar epithelial function is the release of surfactant from the lamellar bodies of alveolar type two cells, which relies on a Ca^{2+} -dependant step (Haller, *et al.* 1998; Ashino *et al.* 2000). The phospholipid-rich surfactant is critical in reducing the surface tension at the alveoli and preventing collapse of the lung air space, which allows efficient gas exchange at the alveolus. The release of the pulmonary surfactant is brought about by exocytosis of the lamellar bodies within

alveolar epithelial type two cells (Hollingsworth *et al.* 1984). Haller *et al.* (1998) demonstrated directly by imaging rises increase in Ca^{2+} indicator dye, at a single cellular level, that the onset of exocytosis upon agonist stimulation essentially coincides with intracellular Ca^{2+} signal in the majority of isolated primary alveolar epithelial type two rat cells.

Haller (1998) provided practical information in regards to a number of methodological aspects that transfer to the lung slice model directly. The use of LysoTracker® Green (Molecular Probes) was demonstrated as an effective molecular marker of alveolar epithelial type two cell lamellar bodies in the pre-exocytotic stage. The localization of the LysoTracker® Green to the lamellar bodies is a result of the acidic nature of the intralamellar space (Wadsworth *et al.* 1997) and upon exocytosis the shift in pH results in a loss of fluorescence. The use of FM1-43 (Molecular Probes) as a specific lamellar body stain was also investigated and shown to emit a fluorescent signal upon the fusion of the lamellar body with the membrane lipid bilayer (Ashino 2001 *et al.*). It was also possible to measure the speed of exocytosis in the presence and absence of agonists. There was a three-fold increase in fluorescence intensity of FM 1-43, and a similar reduction of in the intensity of LysoTracker® Green upon stimulation. ATP and isoproterenol were added to the bath solution as a means to stimulate exocytosis; simultaneous Ca^{2+} measurements, using fura-2, with and FM 1-43, revealed a rapid increase in Ca^{2+} upon stimulation within a matter of seconds and also that the lamellar body exocytose, which demonstrates the Ca^{2+} -dependant step involved in surfactant release from alveolar epithelial type two cells.

In order to gain a more complete understanding of the molecular physiology of the lung, it is vital to use a number of experimental model systems. Whole organ model systems are a complex and time consuming preparation but provide a valuable tool for understating the entire organ response to particular stimuli and pharmacology. Leading the way in whole lung Ca^{2+} imaging is the Bhattacharya laboratory. Their success in producing whole lung Ca^{2+} imaging studies has demonstrated that there is a pressure-sensitive component within the lung capillaries, and an increase in the Ca^{2+} indicator dye signal could be detected in

the whole lung model upon increasing the pressure in this model (Kuebler *et al.* 2002). Within the literature there is direct evidence demonstrating that the lung slice model can produce functional Ca^{2+} indicator measurements. As described in the previous paragraph, there is a Ca^{2+} dependant process in the exocytosis of surfactant and this was also demonstrated elegantly by Ichimura in 2006 utilizing a real-time digital imaging in conjunction with photo-excited Ca^{2+} uncaging on intact alveoli of isolated, blood-perfused rat lung (Ichimura *et al.* 2006). The development of a model to investigate a number of aspects of the murine lung slice by Professor Sanderson has led to publications on both the ciliary beat frequency and smooth muscle Ca^{2+} signals in the lung slice (Bai and Sanderson 2006; Bergner and Sanderson 2002). Both of these publications, and other studies in other organ slices, demonstrate that important biological and physiological questions can be answered with the optimisation and development of Ca^{2+} imaging in lung slices. More recently, DeProost and colleagues have undertaken investigation into the physiological role of neuroepithelial bodies (NEB) by means of a lung slice. They have demonstrated the ability of the lung slice to respond to a number of bath applied stimuli *e.g.* High K^+ solution and ATP. Their findings clearly demonstrate the importance of studying the pulmonary NEB microenvironment as a functional unit (DeProost *et al.* 2008).

The development of Ca^{2+} sensitive dyes has revolutionized our understanding of physiological role that Ca^{2+} signals play in normal homeostasis. A number of ion sensitive substances have been developed. In this particular study fluo 3 was the probe of choice. It was introduced in 1989 (Kao *et al* 1989) and since the fluo 3 imaging has revealed the spatial dynamics of many elementary processes in Ca^{2+} signaling. The most important properties of fluo 3 is it absorption spectrum that is compatible with excitation at 488nm by argon-ion laser sources and a very large increase in fluorescent intensity upon binding of differences in ionic strength, pH, viscosity and Ca^{2+} buffering by intracellular lipids and proteins. Fluo-3, fluo-4 and their derivatives all exhibit large fluorescence intensity increases on binding Ca^{2+} . Unlike the ultra-violet light-excited indicators fura-2 and indo-1, there is no accompanying spectral shift. The fluorescence intensity increase on Ca^{2+} binding is typically >100-fold (Harkins *et al* 1993). A number of important values have been ascertained for fluo 3, firstly it has dissociation

constant (K_d) from Ca^{2+} as listed by the manufacturer of 350nM. However this value is very variable can the results obtained a biological system are highly variable, K_d in situ varies considerably due to differences in ionic strength, pH, viscosity and Ca^{2+} buffering by intracellular lipids and proteins. Fluo 3 has an absorption maximum value of 506nm in the presence of bound Ca^{2+} and an emission maximum value of 526nm when bound with Ca^{2+} . The development of brighter probes e.g. Fluo 4 has been an advantage to imaging even more challenging experimental models.

The aim of this chapter was to develop a technique to undertake functional Ca^{2+} indicator measurements within a 200 μ m thick agarose filled lung slice and to optimise the acquisition of data by means of a LSM 410 microscope. I aimed to image physiological events within the alveolar epithelium and to manipulate them with addition of pharmacological stimuli in order to understand further the role which Ca^{2+} plays in alveolar epithelial function.

Results

5.1. Confocal scanning microscope line-scan imaging of Fluo-3 in living rat lung slices.

There are a number of scanning protocols available within the of the Zeiss LSM software to obtain physiological data using a Ca^{2+} indicator dye. The first scanning method that was selected in this investigation, to see if functional Ca^{2+} responses could be recorded, was the line scan. The beauty of a line scan is that it can provide a very rapid and easily undertaken measure of Ca^{2+} activity in a time-lapse manner. In simple terms, it is a scan in one dimension over a selected linear region and the resultant signal is captured as a confocal image, with the usual rules of confocal acquisition applying, as described in chapter one. It is suitable for rapid investigation and ideal to provide "first look" information.

Figure 5.1 illustrates the pattern of loading of Fluo-3 dye within the lung slice of 200 μm thickness as described in section 2.6. The Sanderson laboratory has previously demonstrated the ability to measure Ca^{2+} signalling events in a lung slice. Their investigation focused initially on murine airway smooth muscle (Berger and Sanderson 2002) followed by investigation into ciliary beat frequency and intracellular calcium in rabbit lung slice (Zhang. and Sanderson 2003). Direct measurements of Ca^{2+} in the alveolar epithelial type one cells have not been reported in a lung slice model. In order to optimise this technique, the most suitable method of data acquisition needed to be determined. The line scan provides an experimental method to gain rapidly initial information about the speed and size of signalling events. In fig. 5.1 the white arrow defines the area that was imaged, or line of interest (LOI). A critical factor in the collection of Ca^{2+} dye data is the time of acquisition. In order to capture any fast signalling events that may be present, the focus of the initial investigation placed speed of acquisition as a defining factor. A LOI across the entire field of view could be completed in a period of ~ 100 ms. Contrast that time period with the capture of a

full field of view image (512 X 512 pixels) with a scan time of ~1.5 seconds. Images that are sampled at a lower resolution can be gathered more quickly. However, the increase in speed has a trade off in that there is a decrease in the resolution of the images, making these images unsuitable for some types of analysis. In order to gather a useful overview of the physiology, it is essential that quicker events should not be overlooked. As an initial investigation tool, the line scan allowed coverage of a large region of interest without the loss of signal of the fluorophore. Photobleaching of fluorescent signal is a factor that has to be considered when acquiring information from a fluorescent probe. Photobleaching is the photochemical destruction of a fluorophore. In microscopy, photobleaching may complicate the observation of fluorescent molecules, since they will eventually be destroyed by the light exposure. Loss of activity caused by photobleaching can be controlled by reducing the intensity or time of light exposure, by increasing the concentration of fluorophores or by employing more robust fluorophores that are less prone to bleaching. The balance of the above factors is dependant upon the thickness of sample, loading of the fluorophore in the imaging environment, (temperature, pH, etc,) and the experimental procedure to be undertaken.

There are a number of outcomes that should be considered with regard to figure 5.1. Firstly, the staining/loading pattern that is localised to the alveolar capillary or interstitial region of the lung slice is not very cellular in nature and more speckled. However, this was consistent over all slices loaded, the compartmentalisation may be due to the loading procedure and addition of a pluornic acid in helping the diffusion of Fluo-3 to into the cytoplasm. The thickness of the slice may have a bearing on the ability of the dye to load efficiently into the cytoplasm of cells. Fig. 5.1 also demonstrates the complications that a slice provides the investigator in regards identification of the particular cells types that have given a response unless indisputable cell markers can be introduced.

The results of the line scans are shown in fig. 5.2. The duration of this experiment was lengthy as the line scan kept photo damage to a minimum. Fig.

5.2 demonstrates that there are a number of transient Ca^{2+} events occurring in a lung slice and the rise in Ca^{2+} is seen in a number of cells across LOI. Upon binding of intracellular Ca^{2+} with the Fluo-3 dye and excitation with the 488nm laser line there is an increase in the fluorescent signal. This is recorded as a current at the PMT and converted to fluorescence intensity. In fig. 5.2, the brighter the “green” signal the greater the increase of Ca^{2+} present in the cytoplasm.

Fig. 5.3 is essentially the same data as shown in fig. 5.2 panel A except that they are presented as a three dimensional image format. The data are presented in a rainbow pseudo colour chart with red equating to an elevated binding of Ca^{2+} and blue representing no cytoplasmic Ca^{2+} present. The blue areas in fig 5.3, is either alveolar space, which is devoid of loading, or cells that have failed to take up or retain the Fluo-3 dye. The ability to present data in this format clearly demonstrates the presence of spontaneous Ca^{2+} events within a rat lung slice.

5.2. Time-lapse imaging of cropped regions of interest in Fluo-3 loaded rat lung slice.

Precision cut lung slices produce spontaneous physiological intracellular Ca^{2+} transients, which can be measured using laser confocal scanning microscopy. It was also evident that the line scan data were unable to provide the information as to the specific location of the cells that were demonstrating spontaneous Ca^{2+} events and, more importantly, if they were associated with the alveolar epithelium. The population of cells that demonstrated spontaneously active Ca^{2+} oscillations in the lung connective tissue warranted further investigation. In order to acquire data that could illustrate the location of the cells that were oscillating, a change in image acquisition methodology was required. The next step in gaining a clearer understanding of the physiology of the Ca^{2+} signal was to capture complete images over time, *i.e.* full frame time lapse imaging.

A typical example of a data set produced with this acquisition method is shown in figure 5.4. Panel A shows a single confocal z series image of the loading of a

200 μ m lung slice with fluo-3 am as described in the methods 2.6. Attention should be drawn to two important factors. Firstly, all the slices were produced with a low melting point agarose back fill to provide stability during slicing. Secondly, all images were captured at room temperature. The loading of the fluorescent indicator dye is localised in the same pattern to that seen in fig. 5.1. The time required for capturing an image of this field of view is about 1500 ms which creates problems with signal bleaching as the specimen is subjected to long periods of excitation. The extended period of excitation with the laser could also become phototoxic to the specimen causing cell death. In order to provide good image resolution and reasonable capture time it was essential that a cropped region of interest (ROI) be created within the field of view. The advantage of cropping the image was to decrease the scan time and in turn allow longer periods for time-lapse image acquisition. This reduced capture area resulted in a suitable image resolution that demonstrated clearly the location of the Ca²⁺ oscillations as seen in fig. 5.2.

The cropped region could be positioned anywhere in the field of view. Only the regions that demonstrated a suitable level of loading with Fluo-3 probe were selected. In twenty seven slices only three ROI demonstrated no spontaneous activity.

Panel B fig. 5.4 demonstrates the first single time lapse image of the cropped ROI as outlined on panel A. There are a number of “hot spots” within the lung slice cropped region. In this particular example, images were captured once every 5 seconds and continued for 450 seconds. 350 ms was required to capture each image in the time lapse series. At this rate, the signal to noise was adequate to identify the Ca²⁺ oscillatory events. There are 7 numbered white circular regions marked on panel B of fig. 5.4. These represent the ROI which demonstrated oscillations that were identified by offline analysis of the entire time-lapse movie. The data are seen in fig. 5.5 presented as fluorescence vs. time plots.

The four panels contained in fig. 5.5 represent the results of the offline analysis of the regions of interest defined in fig. 5.4 panel B. Fig. 5.5 demonstrated an interesting observation that could not be observed in the line scan data. There is a population of cells that clearly display coupled synchronous Ca^{2+} oscillations both within the alveolar epithelial region of the lung. These data demonstrate that within this population of cells there is very tight synchronisation of Ca^{2+} events. When the data of certain cells is overlaid it shows they are 180° out of synchronisation.). The tightly coupled nature of the events was maintained over large distances. The events also show a reduction in frequency over time (panel D).

5.3 Manipulation of Ca^{2+} oscillations in a lung slice.

In an attempt to understand the physiological function of the coupled Ca^{2+} events demonstrated in fig. 5.5, a set of experiments were undertaken to modulate either the frequency of the oscillations or the coupling of these events. Also, the introduction of pharmacology may provide an insight as to the cell type involved in producing the coupled oscillatory Ca^{2+} events. However, the initial investigation was to manipulate the events by addition of a high K^+ (50mM) solution. The aim was to bring about a depolarisation of cells within the slice and cause a rise in Ca^{2+} thereby causing an increase in fluorescence. Seven slices underwent the following sequential protocol; a two-minute control image capture period, during which slice was perfused with extracellular bath solution (section 2.4.1.1); a three-minute application of high K^+ solution; a two-minute wash period with extracellular bath solution. Cropped ROI images were captured and the mean period of capture was 320 ms (± 66 ms) every five seconds for seven minutes. This protocol allowed suitable capture of images and acceptable resolution and demonstrated a tolerable level of bleaching of the signal. No change in fluorescence signal was observed in any of the seven slices, no change was observed in the frequency or amplitude of the oscillation events.

A number of agents were introduced into the bath solution in an attempt to modulate the calcium oscillations. Application of A23187 (10 μM) Calcimycin

(Alamone Labs, Israel). A23187 is a mobile-carrier Ca^{2+} ionophore (allows Ca^{2+} ions to cross cell membranes) originally isolated as an antibiotic from *Streptomyces chartreusensis*. It is used to increase intracellular Ca^{2+} levels, (Scharff and Foder 1992). The protocol was the same as outlined above (n=5). In the remaining experiments (n=10) after the application of A23187 the slice was perfused with a Ca^{2+} free solution for three minutes. Neither the application of A23187 or the Ca^{2+} free bath solution demonstrated a change in the measured fluorescence signal (N=15). The oscillations were not affected in either amplitude or frequency. Additional experiments included the addition of bath solution containing 100 μM adenosine triphosphate (ATP) (n=15). 50 μM muscarine chloride, a muscarinic acetylcholine receptor agonist; originally isolated from *Amanita muscaria* (Fryer and Jacoby 1998), was applied and time-lapse imaging was carried out (n=11). Neither ATP nor muscarine promoted a shift in fluorescence intensity and they had no effect the coupling of the oscillations or frequency or amplitude of the events.

5.4 Discussion

Confocal microscopy improves imaging of thick specimens by physically removing the out-of-focus light before the final image is formed (Minsky 1961; Petran *et al.* 1968; Brakenhoff *et al.* 1979). In the production of fluorescent three dimensional reconstructions of cellular structure the confocal microscope is an incredibly powerful research tool. The confocal image acquisition method takes advantage of differences in the optical paths followed by in-focus and out-of-focus light, selectively blocking the latter, while allowing the former to pass to the detector. Confocal microscopes differ from conventional (wide-field) microscopes because they do not “see” out-of-focus objects. The hardware and software combine to exclude the out-of-focus light from the final image and this increases the contrast and fine details that would be obscured if the out-of-focus light were included in the final image. The critical element that is present in a confocal light path is the presence of a pinhole aperture, which effectively excludes light from the out-of-focus planes reaching the detector. The incoming illumination is also focused to a point by the use of a second pinhole aperture and the combination of these pinhole apertures increases resolution. The confocal microscope is simply a light microscope in which both the field of view of the objective lens and the region of illumination have been restricted to a single point in the same focal (confocal) plane (Wilson and Sheppard 1984).

The ability to measure reliably physiological Ca^{2+} events in a living lung slice has been shown to be a beneficial research model (Berger and Sanderson 2001 and DeProost *et al.* 2008) and may help in providing answers to a number of questions relating to the homeostasis of the alveolar epithelium and respiratory physiology in general. The aim of this study was to investigate the Ca^{2+} signalling events within the alveolar epithelium. It has been demonstrated that the release of surfactant vesicles from alveolar epithelial type two cells has a

critical Ca^{2+} dependent step (Ichimura *et al.* 2006; Haller *et al.* 1998). The data presented in this study shows that there was a collection of cells within the lung epithelium that demonstrated spontaneous Ca^{2+} oscillatory events. The findings in this study provide further insights towards the strengths and weaknesses of the agarose filled lung slice as a suitable model for real-time cellular imaging of the alveolar epithelium.

The lung slices used in the Ca^{2+} imaging section were cut with a low melting point agarose backfill (section 2.2.2.). This treatment has a direct effect on the lung slice as it causes an increase in alveolar volume and in turn caused a physiological response via stretch receptors. A 200 μm thick lung slice will retain a number of the nervous connections and cell-to-cell communications not available in isolated cells. The effect of stretch on the alveolar region was demonstrated directly by Ashino (2000), using a whole lung imaging protocol. A fifteen second expansion of the alveolus induced thirty-minute exocytosis of surfactant from identified alveolar epithelial type two cells. By employing the Ca^{2+} indicator dye fura-2 in this set of experiments, they demonstrated directly the Ca^{2+} dependent step in exocytosis events within the alveolar epithelium. However, the response seen here in the lung slice model cannot be directly attributed to the alveolar epithelium, as the cell specific markers were not used. The use of a cell specific marker would provide conclusive evidence that events captured are as a direct result of an increase in pressure due to the agarose backfill and are directly associated with alveolar epithelial type two cells or to capillary endothelial cells.

The use of a laser scanning confocal microscopy to collect fluorescence Ca^{2+} indicator dye time-lapse images from an organ slice model has both positive and negative features. The laser scanning confocal microscope provides the user with a means to image deep into an organ slice and is without question a powerful tool. The ability to acquire data from a single 1 μm thick optical slice within a 200 μm thick lung slice and exclude the fluorescence signal from other regions of the slice, would not even have been possible some years ago. There are, however, a number of aspects that must be balanced in order to obtain a

satisfactory time-lapse image series. The acquisition of time-lapse image data requires a suitable signal to noise ratio, the ratio must be such that the signal of interest, in this case a rise in Ca^{2+} and subsequent rise in indicator dye fluorescence signal, is at a level that can be easily discerned from the background signal. The quality of the image must be considered and this is directly associated with the resolution of the image. That is the higher the resolution, the crisper the image. A higher resolution image will provide the researcher with increased detailed information. When using a laser scanning confocal microscope, acquiring images at a higher resolution comes at a cost in live cell preparations, the illumination light source is active for longer periods of time and this can result in both photobleaching of the fluorescence signal and photodamage of the cells. In the case of fixed immunohistochemical samples there are solutions available that prolong the lifetime of the fluorescent signal. In the case of a live sample, the longer the specimen is exposed to a high intensity light, the more phototoxic it becomes. The power of the laser used to excite the fluorescent molecule must be increased to an even greater extent in the case of an organ slice in order to acquire images of high resolution. In capturing the Ca^{2+} indicator dye data for this study it was very important to find a suitable balance between the power of the laser, the period of time required to capture a single frame and phototoxic effects. In order to capture time-lapse images over useful periods it was necessary to sacrifice the resolution of the image. The line scan provided useful insight as to the type of activity present. However, it was the cropped ROI that provided a more complete picture of the coupled Ca^{2+} oscillations observed within the lung slice.

The thickness of the lung slice may well have influenced a number of aspects that proved to be problematic. The punctate staining pattern may well be attributed to the thickness of the slice having a direct effect upon the access of the dye to all regions of the slice. The pattern of loading of Fluo-3 seemed to suggest compartmentalization and this may have been a consequence of the concentration of pluronic acid, which at the concentration used in this study may have caused cell damage. Also, there was no discernible loading into the alveolar type one epithelial cell, the presence of the agarose could have had an effect on the loading of the Ca^{2+} indicator. However, during the period when this

investigation was carried out, the opportunity to label the type two alveolar epithelial cells was not available. Positive identification of the cells that produced oscillations proved difficult. One approach that was considered was undertaking *post hoc* immunohistochemistry. It was, however, not possible to identify the exact region of the slice where imaging had been carried out. The identification was further hampered, as changes in spontaneous activity using pharmacological interventions were not successful. The failure to illicit changes in activity could be attributed to the thickness of the slice and inaccessibility due to agarose backfill. The images were captured with an inverted microscope, hence the plane of image acquisition from the slice was in direct contact with the coverslip, a further possible contributing factor, in failure to observe a change in Ca^{2+} activity. In future studies, it would be advisable to undertake the image acquisition on an up right microscope with a dipping objective lens. Longer application time of the drugs may prove more advantageous in manipulating the observed Ca^{2+} events. The use of unfilled lung slices would provide more access for interaction of physiological stimuli and pharmacological agents.

The temperature of the bath solutions may will directly affected the frequency of oscillations. A temperature controlled perfusion system was not available on the imaging set up and so the images were captured at room temperature. The spontaneous Ca^{2+} activity in whole tissues rabbit smooth muscle urethra preparation demonstrates large temperature sensitivity (unpublished observation). This may account for the slow nature of the event witnessed within the lung slice. In future studies image acquisition should be undertaken solutions that were warmed to 37°C .

The coupled Ca^{2+} events seen in the lung interstitium demonstrated synchronicity, in areas that were close together this is could be attributed to the gap junctions present in the lung (Boitano *et al.* 2004). There is good evidence for the communication in the alveolar epithelial between type one and type two alveolar epithelium cells (Isakson *et al.* 2003; Kuebler *et al.* 2002). The events that were seen to be in synchronisation, e.g. ROI 1,3, and 5 and ROI 6 and 7 were observed in a number of slices and activity was consistent. In the absence of Ca^{2+} bath solution no change in the frequency was observed and this would

suggest that they were mediated via store mediated Ca^{2+} release. However at this stage it would be impossible to suggest if this was via the 1,4,5-trisphosphate receptors or the ryanodine receptors, the two receptors responsible for store release. However, whole lung studies have shown an IP_3 mediated store release of Ca^{2+} underlies the oscillations seen in capillary epithelium cells (Kuebler 2002).

Observations similar to the Ca^{2+} oscillations observed in this study have been demonstrated in whole lung experiments (Ying. *et al.* 1996). The “pacemaker activity” observed in lung endothelial cells located at some of the alveolar vascular branch points could explain the Ca^{2+} activity observed in the agarose filled lung slice. These branch-point endothelial cells regulate cytosolic Ca^{2+} at higher levels than midsegmental cells, and they generate intracellular cytosolic Ca^{2+} waves. An increase of the microvascular pressure markedly increases the amplitude of Ca^{2+} oscillation amplitude, while no observed increase was seen in mean amplitude (Kuebler *et al.* 1999; Ichimura *et al.* 2003). Distinction by molecular markers would have to be undertaken to confirm the identification of the oscillating cells seen in this study.

5.5 Conclusion.

A clearer understanding of molecular mechanisms underlying respiratory physiology is essential if we are to develop effective treatments to pathological lung diseases. The research techniques available to investigate the physiological homeostasis within the lung are vast and range from the whole organ to single protein level. One area that has been immeasurably advanced over the past thirty years is biological real-time imaging. It is clear from the above study, that the combination of high-resolution real-time imaging within a lung slice model has a place in furthering our understanding of respiratory physiology. The above study combines the technical skills of producing viable precision cut lung slice and laser scanning confocal microscope to produce real time Ca^{2+} indicator measurements from a lung slice. From this investigation it is clear that there is a population of cells within the interstium of the lung that develop spontaneous Ca^{2+} oscillations and exhibit tightly coupled events over large distances. The physiological reason for such “pacemaker” events within the lung still remains unanswered. The technical advancements made in this study will provide a strong foundation upon which to carry on further investigation and bring about a clearer understanding of the role that Ca^{2+} plays in the respiratory homeostasis in the alveolar epithelium.

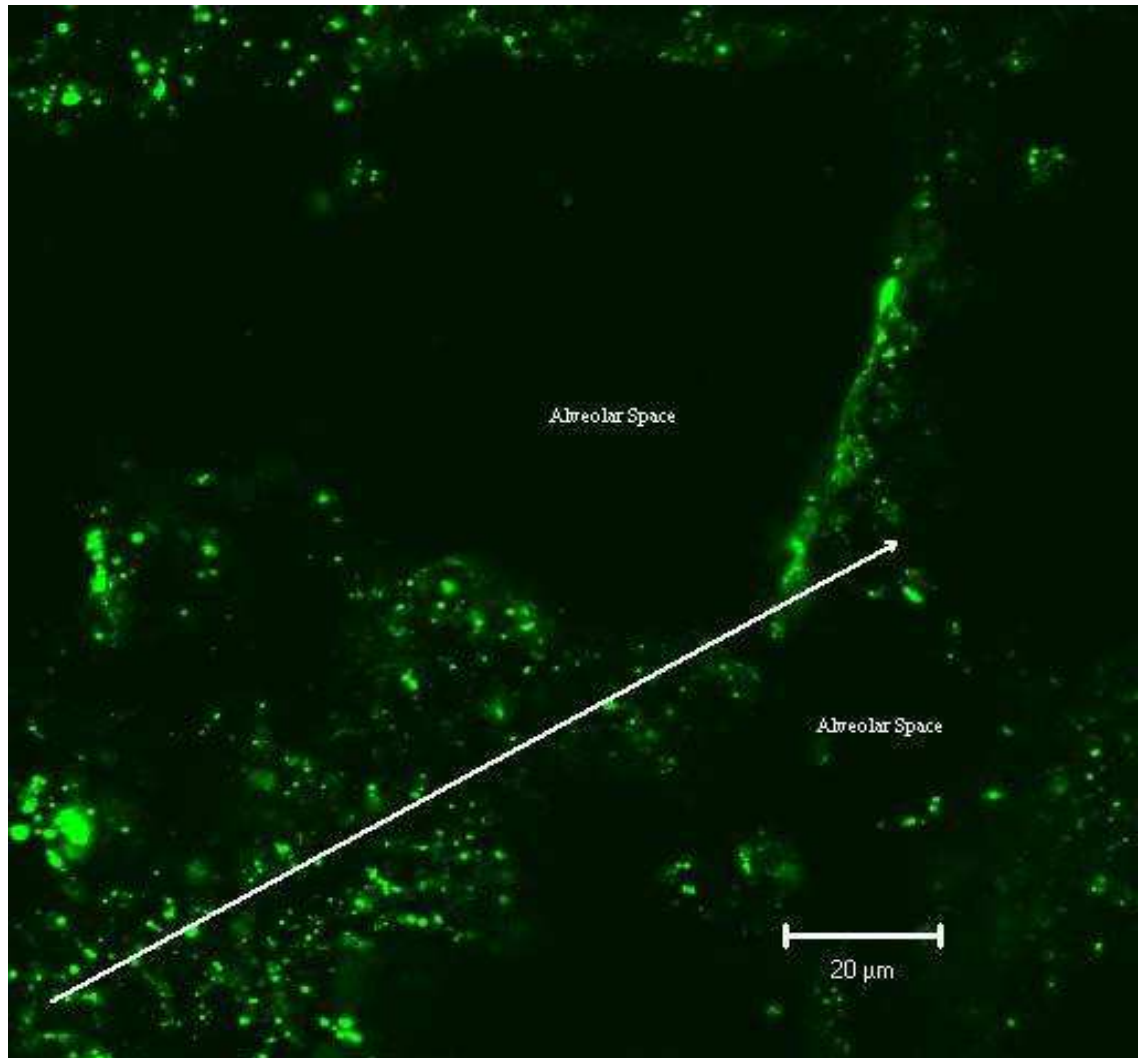


Figure 5.1 Confocal 0.85 μm optical section from a 200 μm live lung slice loaded with 5 μM Fluo-3 Ca^{2+} indicator dye.

The slice was loaded for 30 minutes, at room temperature, with Fluo-3 (5 μM), a physiological calcium indicator dye, in bath physiological solution containing 0.1% (w/v) pluronic acid. The punctate green staining shows the calcium indicator dye localization. The slice was imaged on a Zeiss (Zeiss, Germany) LSM 410 inverted confocal microscope with a 63x oil immersion objective lens.

The white arrow, from left to right, shows the region where a line scan was performed. A scan was performed every 5 seconds and the scan time was 100 ms.

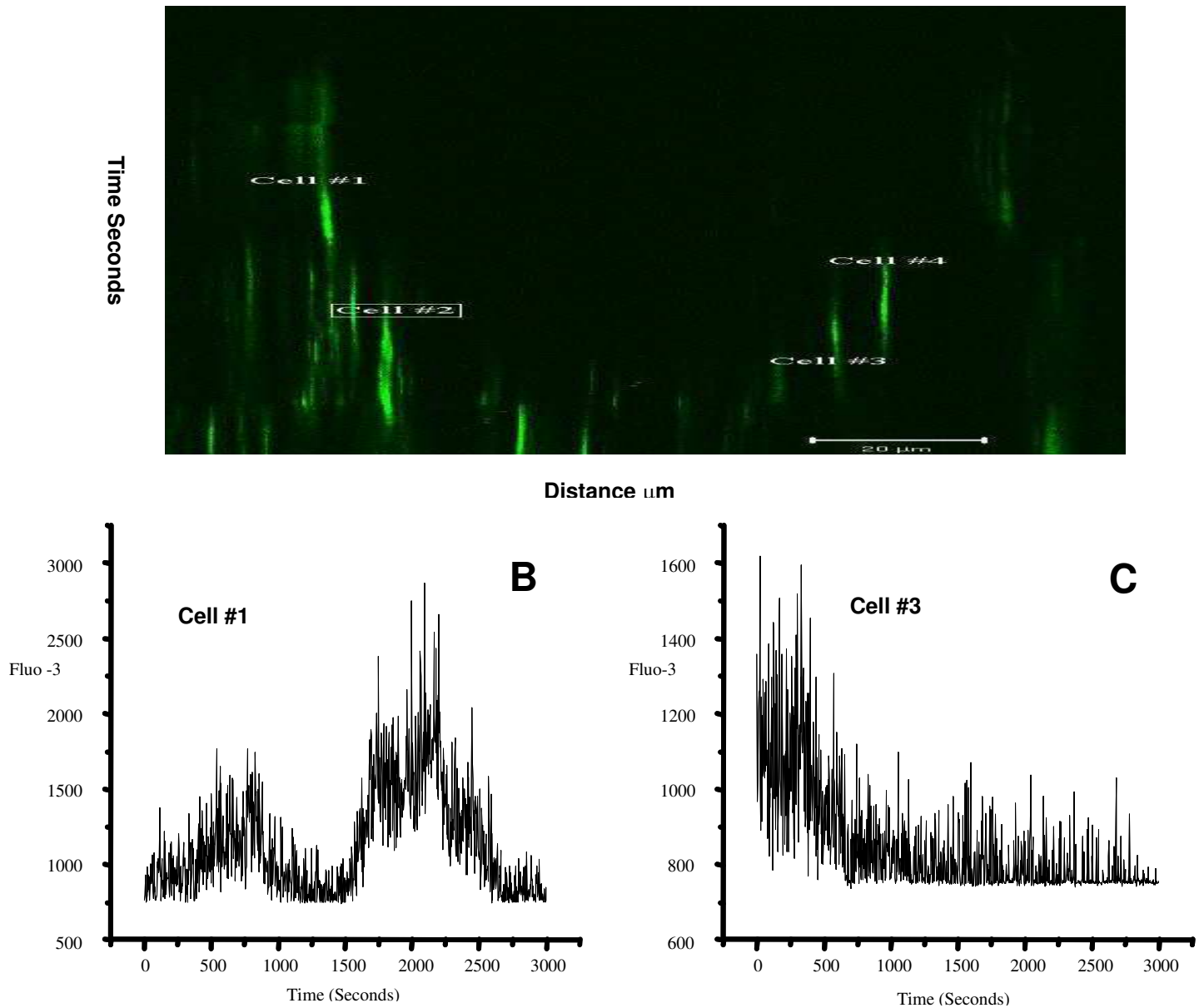
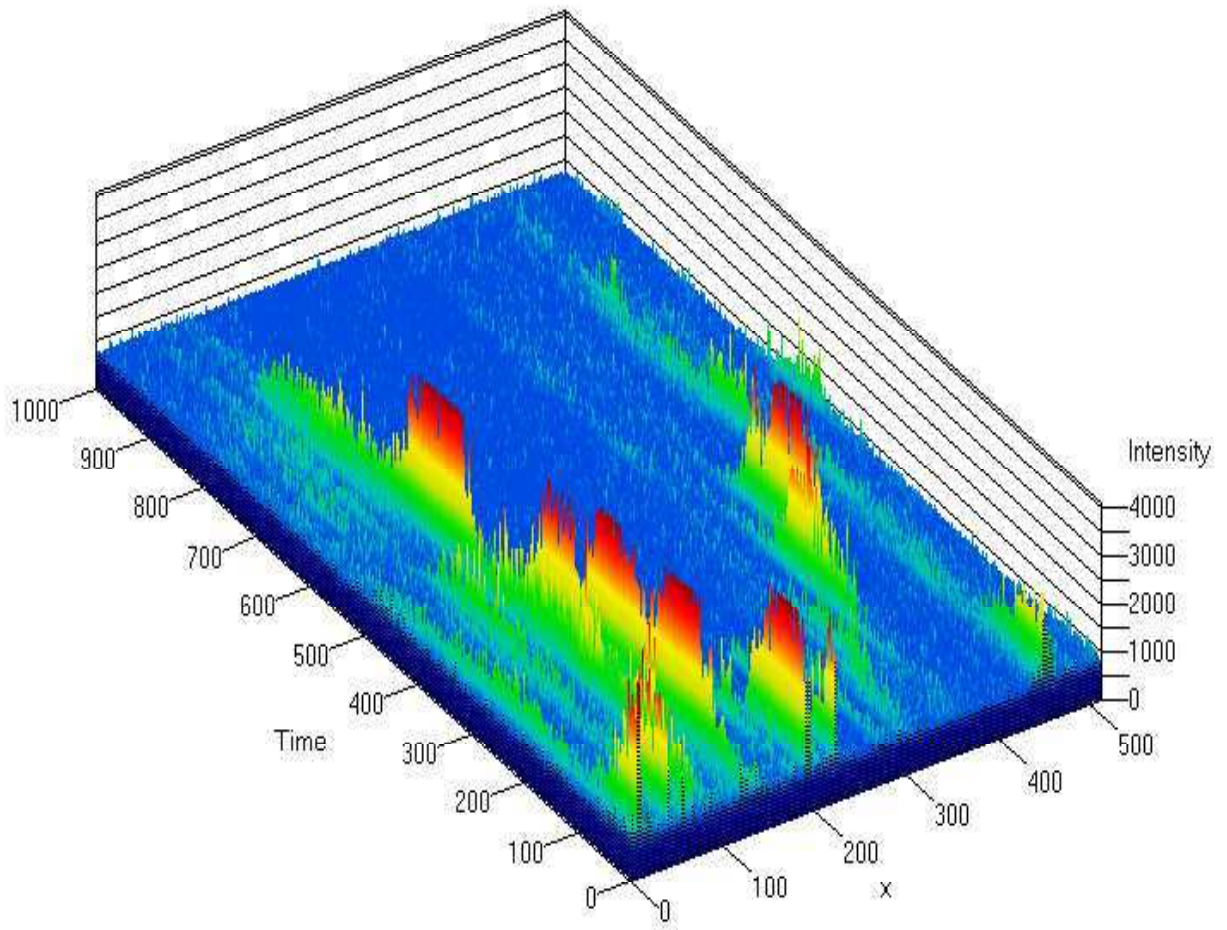


Figure 5.2 Confocal LSM410 linescan of a 200µm thick live lung slice loaded with 5µM Fluo-3 and resultant graphs.

The two dimensional image seen in panel A is the result of a 100ms line scan repeated every two seconds for a total of 3000 seconds across the LOI indicated in fig.5.1. The x-axis of panel A represents distance of the line scan with the reference scale bar showing 20µm. The y-axis of panel A represents the time period of the scan with each line being one pixel scan over the length of the

region of line scan. An increase in green is the result of calcium release or influx, which leads to a rise in fluorescence signal in the presence of Fluo-3. Panel B



and C represent the line scan data as cropped regions of interest excised from the panel A. The graphs demonstrate the fluoresce signal as a function of time.

Figure 5.3 Three-dimensional pseudo color graphical representation of calcium signaling events in a living lung slice.

A three-dimensional illustration of the line scan data collected from the line of interest indicated in fig. 5.1. The x-axis is a measure of distance along the line of interest; the y-axis is a measure of time and the z-axis represents the release of Ca^{2+} and subsequent binding of the Fluo-3 causing an increase in fluorescent

signal, given in arbitrary units of fluorescent. This signal was captured on an LSM 410 confocal microscope, the pseudo color of the z-axis illustrate a increase in signal as a shift from blue towards red with red being a high reading of Ca^{2+} . A sustained upward deflection in the Z-axis can be considered as an increase in the cytosolic Ca^{2+} .

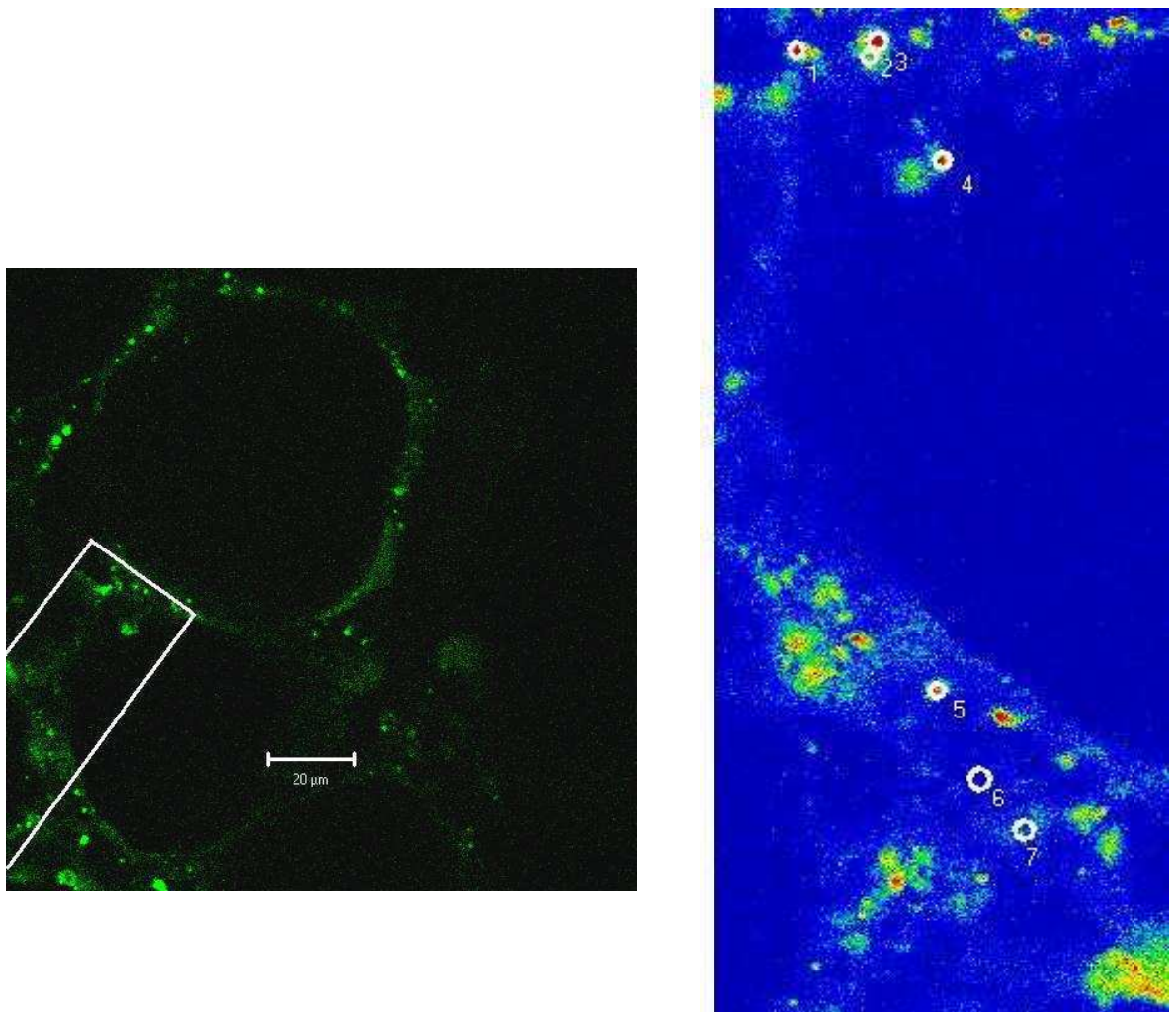


Figure 5.4 Cropped region of interest from Fluo-3 loaded 200µm thickness lung slice.

Panel A shows the full field view of a single image captured by the LSM 410 of a lung slice loaded with 5µm Fluo-3. Slices were loaded as described in methods section 2.6. The area in the lower left corner of panel A, highlighted with a white box, is the region which was cropped for time-lapse imaging at 12 frames per minute. Panel B is single image of a cropped region of interest displayed in a

pseudo color. The Zeiss software repositions the ROI. Within panel B there are a number of small white circles (numbered, one to seven) which represent the ROI identified off-line post capture, which demonstrate an increase in Fluo-3 signal. The pseudo color also demonstrates clearly the edge of the alveolar region. Time-lapse imaging allowed the measurement of specific regions within the ROI over an extended period of time.

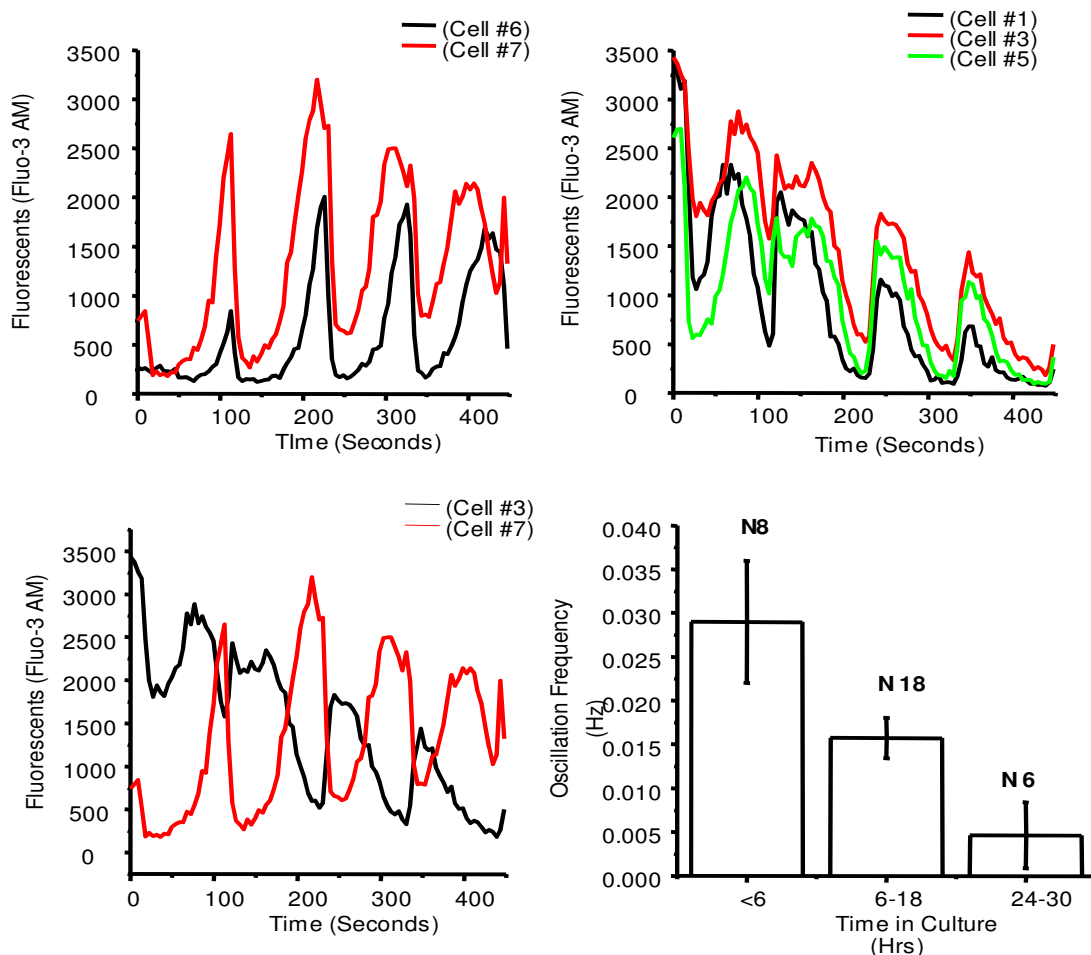


Figure 5.5 Graphical representations of regions of interest from time lapse imaging of 200µm thickness lung slice loaded with Fluo-3 and oscillation frequency as a function of time post slicing.

The graphs in figure 5.5 A B and C above were produced directly from the time-lapse imaging of ROI (1,3,5,6,7) (fig. 5.4 B). The y-axes represent fluorescence intensity and are measured in arbitrary units. Panel A represents the time lapse numerical data of two circular ROI, region 6 and 7 as identified in fig. 5.4.B. This demonstrates that these events oscillate in synchronized fashion. Panel B represents regions 1,3 and 5 as identified in Figure 5.4.B again the events are synchronized with each other. Panel C demonstrates the asynchronous nature of ROI 3 and ROI 7 (as shown in fig. 5.4 B). The

events are a full one hundred and eighty degrees out of synchronization and are not a spatial artifact. Panel D presents the reduction in oscillation frequency as a function of time in culture. These data represent 8 slices that were examined less than 6 hours post sectioning of the slice, 18 slices examined between 6-18 hours post sectioning and 6 slices examined 18-30 hours post sectioning.

Chapter 6

General discussion.

6.1 General Discussion.

The ability of the lung to match gas exchange to the requirements of respiration is maintained by the free movement of O₂ and CO₂ across the pulmonary capillary network and the alveolar epithelium. It is the responsibility of the alveolar epithelium to maintain lung fluid homeostasis and that in turn preserves optimal gaseous exchange. The alveolar epithelium consists of two morphologically distinct cell types: A) alveolar epithelial type one cells, which are squameous cells with a large surface area and which make up 95% of the surface area of the epithelium, and; B) alveolar epithelial type two cells, which are cuboidal and provide only 5% of the surface area but 80% of the volume of the epithelium (Dobbs and Johnson 2007). Vectorial ion transport across the alveolar and distal airway epithelia is the primary determinant of alveolar fluid clearance. The general model is that active Na⁺ and Cl⁻ transport drive net alveolar fluid clearance, the breakdown of this model results in a number of pathological events. Understanding of the physiology of the epithelium has for the most part derived from the isolated alveolar epithelial type two cells. The alveolar epithelial type one cells have proved quite challenging to work with due to their fragile nature. Thus, it was essential to develop an experimental model that would allow the investigation of the ion channel activity within alveolar epithelial type one cell, preferably *in situ*.

I undertook an investigation to optimize the production of precision cut lung slices. The first method I undertook was the agarose backfilling method. This is the traditional method of making precision cut lung slices but it was less than satisfactory for recording functional electrophysiological data from identified alveolar epithelial cells. This model has recently yielded functional ion channel recordings from identified alveolar epithelial type one and alveolar epithelia type two cells (Helms *et al* 2006; Helms *et al* 2008). However, I was unable to gain suitable access to the alveolar epithelial type one cell membrane using this method. With that in mind, I undertook an investigation to identify a substance which would provide the necessary stability required for slicing and could be removed to allow

uninterrupted access the alveolar epithelial type one cells. PEG 400 was chosen due to its unique properties of being liquid at room temperature and solid at 4°C. Although the alveolar airspace was easily cleared of obstructions, the cellular viability was not of a standard required for functional studies. The production of unfilled lung slices was the next progression in the development of a technique to record electrophysiological data from alveolar epithelial type one cells. The success of making unfilled slices was immediate and the cellular viability was unquestionable. The use of the mouse monoclonal antibody VIIIIB2, an alveolar epithelial type one marker, allowed identification of the cell population of interest in an unfilled slice model. Optimization was also undertaken for an alveolar epithelial type two live cell marker in the slice model. The candidates investigated were, the fluorescent lipid dye Nile Red and the fluorescent styryl dye LysoTracker® Green DND26. Both demonstrated lamellar body staining. However, the DND26 was more specific and when imaged in conjunction with VIIB2 showed no fluorescence overlap.

Subsequently, investigations were undertaken to record functional ion channel events from identified alveolar epithelial type one cells within a 200µm thickness living lung slice. Cell-attached patch-clamp recordings were successfully achieved and in the presence of a pharmacological cocktail, K⁺ rich low Cl⁻ recording solution, a voltage activated K⁺ channel was observed. It had a measured unitary conductance of 21±3 pS and close to the equilibrium potential for K⁺ (Bourke *et al* 2005). The most likely was Kv1.7. Kv1.7 is the most recently cloned member of the Kv family of K⁺ channels but its physiological function remains to be explained. The presence of a number of K⁺ channels has been demonstrated in the alveolar epithelium and their function is believed to be in preventing cell depolarization during periods of Cl⁻ and Na⁺ influx (O'Grady and Lee 2003).

The functional data presented in this thesis were the first published from alveolar epithelial type one cells in a lung slice (Bourke *et al* 2005). Since our original publication, there has been a further three publications demonstrating functional ion channels in alveolar epithelia type one cells (Johnson *et al* 2006; Helms *et al* 2006;

Helms *et al* 2008). The observations made in this current study and the alveolar epithelial type one electrophysiological data from Johnson and Helms further strengthen the idea that the alveolar epithelial type one cells play a physiological role in lung fluid homeostasis. It has now been demonstrated that alveolar epithelial type one cells possess the functional molecular machinery to undertake active transport of fluid from the alveolar airspace.

Within the alveolar epithelium a number of observations have been made as to the physiological role for Ca^{2+} . Isolated heterocellular cultures of alveolar epithelial cells demonstrated propagated changes in intracellular Ca^{2+} between type one and type two cells (Isakson *et al* 2003). Slice preparations have also been used to demonstrate Ca^{2+} transients in NEB cells (DeProost *et al* 2008) and smooth muscle contractions in airway smooth muscle (Bergner, A. and Sanderson, M.J. 2002). Whole organ studies have also demonstrated both cell-to-cell communication and Ca^{2+} dependent surfactant release (Ichimura, H. *et al* 2006). An investigation was undertaken to identify the possibility of developing Ca^{2+} imaging measurements in lung slices with particular focus on the alveolar epithelium. This study was undertaken at the beginning of the period of the thesis and the agarose filled lung slice model was the model of choice.

The initial observations were made using a line scan image capture, which was very successful and demonstrated the presence of spontaneous Ca^{2+} transient activity in a population of cells with the lung slice. It was, however, impossible to identify positively the cells that demonstrated this activity using the line scan image capture. A change in acquisition to small regions of interest time lapse imaging clearly demonstrated the location of the cells of interest in the alveolar epithelium. It would require cell specific markers to identify the cells positively.

One further observation within the of cropped regions of interest was that oscillations showed coupled spontaneous activity. The synchronization was either tightly coupled or 180° out of synchronization. In order to investigate further this

population of spontaneously active cells a number of physiological and pharmacological agents were introduced to the perfusion system. However, it was not possible to alter these observed events with any of the substances introduced. A number of reasons were considered to explain the lack of modulation of these events. The agarose backfill interfered with the access of the substances to the alveolar epithelium, the thickness of the slice affected the access of the substances, the duration the substances were present was not long enough for them to have an effect, events were not observed as the sensitivity imaging systems was not suitable. The observed Ca^{2+} transients could be the result of stretch-induced surfactant release due to the agarose back fill, stretch-induced Ca^{2+} oscillations from the endothelial of lung capillaries, both responses have been demonstrated in whole lung studies (Kuebler, W.M. *et al* 2002; Perlmann. C.E and Bhattacharya, J. 2006). Further investigation would be required, and combination of specific cell markers may proved more information as to the identification of the cells demonstrating this response.

The alveolar epithelium is critical in maintaining lung fluid homeostasis and in a breakdown of the mechanism of active clearance of fluid it not treated is fatal. A vast number of studies and wide variety of techniques have been undertaken to investigate and understand the mechanisms that of lung fluid clearance. Our understanding is ever expanding. It is becoming evident that the alveolar epithelia type one cells are not passive in the mechanism of lung fluid clearance. Although suspected by a number of investigators it ahs only been in the recent past that the evidence has come to light (Dobbs and Johnson 2007). One vital piece of in formation has been lacking, ion channel recordings from the alveolar epithelial type one cell population. The ability of manipulates functionally the ion channels present in a cell allow a greater understanding how that cell operates at a physiological level. This projects main aim was to optimize the recording of functional ion channels from an identified alveolar epithelia type one cell in a lung slice model. It was a challenging undertaking as outlined above it required the combination of a number of powerful experimental techniques to arrive at the results presented in

this thesis. The optimization of the techniques for recording of electrophysiological data from the alveolar epithelia type one cells presents an exciting opportunity to further advance our understanding of the physiological function of alveolar epithelial type one cell in health and disease states.

References:

Abraham V, Chou ML, DeBolt KM, Koval M. (1999). Phenotypic control of gap junctional communication by cultured alveolar epithelial cells. *Am J Physiol.* May;276(5 Pt 1):L825-34.

Abraham V, Chou ML, DeBolt KM, Koval M. (2001). Phenotypic control of gap junctional communication by cultured alveolar epithelial cells. *Am J Physiol.* May;276(5 Pt 1):L825-34.

Adams FH, Fujiwara T, Rowshan. (1963). The nature and origin of the fluid in the fetal lamb lung. *G. J Pediatr.* Nov;63:881-8.

Adamson TM, Boyd RD, Platt HS, Strang LB. (1969) Composition of alveolar liquid in the foetal lamb. *J Physiol.* Sep;204(1):159-68.

Addison WHF and How HW. (1913). On the prenatal and neonatal lung. *Am. J. Anat.* 15, 199-241.

Aherne W, Dawkins MJ. (1964). The removal of fluid from the pulmonary airways after birth in the rabbit, and the effect on this of perematurity and prenatal hypoxia. *Biol Neonat.* 7:214-29.

Alberts, B, Johnson, A, Lewis J, Raff M, Roberts K, Walter P (2002). *Molecular Biology of the cell* (4th edition). Garland Science, a member of the Taylor & Francis Group.

Anantharam A, Palmer LG. (2007). Determination of epithelial Na⁺ channel subunit stoichiometry from single-channel conductances.

Andreeva AV, Kutuzov MA, Voyno-Yasenetskaya TA. (2007) Regulation of surfactant secretion in alveolar type II cells. *Am J Physiol Lung Cell Mol Physiol*. Aug;293(2):L259-71.

Ashino Y, Ying X, Dobbs LG, Bhattacharya J. (2000) $[Ca^{2+}]_i$ oscillations regulate type II cell exocytosis in the pulmonary alveolus. *Am J Physiol Lung Cell Mol Physiol*. Jul;279(1):L5-13.

Bai Y, Sanderson MJ. (2006). Airway smooth muscle relaxation results from a reduction in the frequency of Ca^{2+} oscillations induced by a cAMP-mediated inhibition of the IP₃ receptor. *Respir Res*. Feb 23;7:34.

Baines DL, Ramminger SJ, Collett A, Haddad JJ, Best OG, Land SC, Olver RE, Wilson SM. (2001). Oxygen-evoked Na^+ transport in rat fetal distal lung epithelial cells. *J Physiol*. Apr 1;532(Pt 1):105-13.

Balda MS, Matter K. (2008). Tight junctions at a glance. *J Cell Sci*. Nov 15;121(Pt 22):3677-82.

Bardou O, Trinh NT, Brochiero E. (2009). Molecular diversity and function of K^+ channels in airway and alveolar epithelial cells. *Am J Physiol Lung Cell Mol Physiol*. Feb;296(2):L145-55.

Barker PM, Boyd CA, Ramsden CA, Strang LB, Walters DV. (1989). Pulmonary glucose transport in the fetal sheep. *J Physiol*. Feb;409:15-27.

Bartels H. (1979). The air-blood barrier in the human lung. A freeze-fracture study. *Cell Tissue Res*. 1979 May 18;198(2):269-85.

Bartels H, Oestern HJ, Voss-Wermbter G. (1980). Communicating-occluding junction complexes in the alveolar epithelium. A freeze-fracture study. *Am Rev Respir Dis.* Jun;121(6):1017-24.

Bastacky J, Lee CY, Goerke J, Koushafar H, Yager D, Kenaga L, Speed TP, Chen Y, Clements JA. (1995). Alveolar lining layer is thin and continuous: low-temperature scanning electron microscopy of rat lung. *J Appl Physiol.* Nov;79(5):1615-28.

Bastacky J, Lee CY, Goerke J, Koushafar H, Yager D, Kenaga L, Speed TP, Chen Y, Clements J (1995) A. Alveolar lining layer is thin and continuous: low-temperature scanning electron microscopy of rat lung. *J Appl Physiol.* Nov;79(5):1615-28.

Bergner A, Sanderson MJ. (2001). Acetylcholine-induced calcium signaling and contraction of airway smooth muscle cells in lung slices. *J Gen Physiol.* Feb;119(2):187-98.

Bergner A, Sanderson MJ. (2002). ATP stimulates Ca²⁺ oscillations and contraction in airway smooth muscle cells of mouse lung slices. *Am J Physiol Lung Cell Mol Physiol.* Dec;283(6):L1271-9.

Berne RB, Levy MN. (1989). *Physiology*, 4th Edition. Mosby Press.

Berridge MJ. Inositol trisphosphate and calcium signalling mechanisms. (2008) *Biochim Biophys Acta.* Oct 29.

Berthiaume Y, Matthay MA. (2007). Alveolar edema fluid clearance and acute lung injury. *Respir Physiol Neurobiol.* Dec 15;159(3):350-9.

Blaisdell CJ, Gail, and Kiley J. (2008) Respiratory Distress Syndrome: Progress for the New Born. Fall 2008 issue of the ALA Lung Health Magazine.

Boitano S, Safdar Z, Welsh DG, Bhattacharya J, Koval M. (2004). Cell-cell interactions in regulating lung function. *Am J Physiol Lung Cell Mol Physiol*. Sep;287(3):L455-9. Review.

Borok Z, Danto SI, Dimen LL, Zhang XL, Lubman RL. (1998). Na(+)-K(+)-ATPase expression in alveolar epithelial cells: upregulation of active ion transport by KGF. *Am J Physiol*. Jan;274(1 Pt 1):L149-58.

Borok Z, Danto SI, Zabski SM, Crandall ED. (1994) Defined medium for primary culture de novo of adult rat alveolar epithelial cells. *In Vitro Cell Dev Biol Anim*. Feb;30A(2):99-104.

Borok Z, Liebler JM, Lubman RL, Foster MJ, Zhou B, Li X, Zabski SM, Kim KJ, Crandall ED. (2002). Na transport proteins are expressed by rat alveolar epithelial type I cells. *Am J Physiol Lung Cell Mol Physiol*. Apr;282(4):L599-608.

Borok Z, Lubman RL, Danto SI, Zhang XL, Zabski SM, King LS, Lee DM, Agre P, Crandall ED. (1998). Keratinocyte growth factor modulates alveolar epithelial cell phenotype in vitro: expression of aquaporin 5. *Am J Respir Cell Mol Biol*. Apr;18(4):554-61.

Borok Z, Verkman AS. (2002). Lung edema clearance: 20 years of progress: invited review: role of aquaporin water channels in fluid transport in lung and airways. *J Appl Physiol*. Dec;93(6):2199-206.

Bourke S, H.S. Mason HS, Crandall ED, Kim KJ, Borok Z, and Kemp PJ. (2003) Calcium homeostasis in identified alveolar epithelial cells: development of a novel in situ lung slice model. *J Physiol* 552P P119

Bourke S, Mason HS, Borok Z, Kim KJ, Crandall ED, Kemp PJ. (2005) Development of a lung slice preparation for recording ion channel activity in alveolar epithelial type I cells. *Respir Res.* Apr 27;6:40.

Brakenhoff GJ, Blom P, Barends P. (1979). Confocal scanning light-microscope with high aperture immersion lenses. *J. Microsc.* 117: 219-232.

Bucheimer RE, Linden J. (2004). Purinergic regulation of epithelial transport. *J Physiol.* Mar 1;555(Pt 2):311-21.

Canessa CM, Horisberger JD, Rossier BC. (1993). Epithelial sodium channel related to proteins involved in neurodegeneration. *Nature.* Feb 4;361(6411):467-70.

Carafoli E (2002). Calcium signaling: a tale for all seasons. *Proc Natl Acad Sci U S A.* Feb 5;99(3):1115-22. Review.

Carson JL, Reed W, Moats-Staats BM, Brighton LE, Gambling TM, Hu SC, Collier AM. (1998). Connexin 26 expression in human and ferret airways and lung during development. *Am J Respir Cell Mol Biol.* Jan;18(1):111-9.

Chapman DL, Carlton DP, Nielson DW, Cummings JJ, Poulain FR, Bland RD. (1994). Changes in lung lipid during spontaneous labor in fetal sheep. *J Appl Physiol.* Feb;76(2):523-30

Cheek JM, Kim KJ, Crandall ED. (1989). Tight monolayers of rat alveolar epithelial cells: bioelectric properties and active sodium transport. *Am J Physiol.* Mar;256(3 Pt 1):C688-93.

Chen J, Chen Z, Narasaraju T, Jin N, Liu L. (2004). Isolation of highly pure alveolar epithelial type I and type II cells from rat lungs. *Lab Invest.* Jun;84(6):727-35.

Chen J, Chen Z, Narasaraju T, Jin N, Liu L.(2005). Isolation of highly pure alveolar epithelial type I and type II cells from rat lungs. *Lab Invest.* 2004 Jun;84(6):727-35. Erratum in: *Lab Invest.* 2005 Sep;85(9):1181.

Chen Z, Jin N, Narasaraju T, Chen J, McFarland LR, Scott M, Liu L. (2004). Identification of two novel markers for alveolar epithelial type I and II cells. *Biochem Biophys Res Commun.* Jul 2;319(3):774-80.

Clapham DE. (2007). Calcium signaling. *Cell.* Dec 14;131(6):1047-58.

Clements JA.(1997). Lung surfactant: a personal perspective. *Annu Rev Physiol* ;59:1-21.

Clunes MT, Kemp PJ. (1996). P2u purinoceptor modulation of intracellular Ca²⁺ in a human lung adenocarcinoma cell line: down-regulation of Ca²⁺ influx by protein kinase C. *Cell Calcium.* Oct;20(4):339-46.

Coetzee WA, Amarillo Y, Chiu J, Chow A, Lau D, McCormack T, Moreno H, Nadal MS, Ozaita A, Pountney D, Saganich M, Vega-Saenz de Miera E, Rudy B. Molecular diversity of K⁺ channels. (1999). *Ann N Y Acad Sci.* Apr 30;868:233-85. Review.

Colin G (1873). *Traité de physiologie compare des animaux consideree dans ses rapports avec les sciences, naturelles, la medéicine, la zootechnie et l'économie rurale*, second ed Ballière, Paris, p. 109.

Communi D, Painsavoine P, Place GA, Parmentier M, Boeynaems JM. (1999). Expression of P2Y receptors in cell lines derived from the human lung. *Br J Pharmacol.* May;127(2):562-8.

Coyne CB, Gambling TM, Boucher RC, Carson JL, Johnson LG. (2003). Role of claudin interactions in airway tight junctional permeability. *Am J Physiol Lung Cell Mol Physiol.* Nov;285(5):L1166-78.

Crandall ED, Matthay MA. (2001). Alveolar epithelial transport. Basic science to clinical medicine. *Am J Respir Crit Care Med.* Mar;163(4):1021-1029.

Crapo JD, Young SL, Fram EK, Pinkerton KE, Barry BE, Crapo RO. (1983). Morphometric characteristics of cells in the alveolar region of mammalian lungs. *Am Rev Respir Dis.* Aug;128(2 Pt 2):S42-6.

Danto SI, Zabski SM, Crandall ED. (1992) Reactivity of alveolar epithelial cells in primary culture with type I cell monoclonal antibodies. *Am J Respir Cell Mol Biol.* Mar;6(3):296-306.

Daugherty BL, Mateescu M, Patel AS, Wade K, Kimura S, Gonzales LW, Guttentag S, Ballard PL, Koval M. (2004). *Am J Physiol Lung Cell Mol Physiol.* Dec;287(6):L1266-73.

Davies AR, Kozlowski RZ. (2002). Kv channel subunit expression in rat pulmonary arteries. *Lung.* 179(3):147-61.

de Buys Roessingh AS, Dinh-Xuan AT. (2009). Congenital diaphragmatic hernia: current status and review of the literature. *Eur J Pediatr.* Apr;168(4):393-406.

de Graaf IA, de Kanter R, de Jager MH, Camacho R, Langenkamp E, van de Kerkhof EG, Groothuis GM. (2006). Empirical validation of a rat in vitro organ

slice model as a tool for in vivo clearance prediction. *Drug Metab Dispos.* Apr;34(4):591-9.

De Proost I, Pintelon I, Brouns I, Kroese AB, Riccardi D, Kemp PJ, Timmermans JP, Adriaensen D. (2008). Functional live cell imaging of the pulmonary neuroepithelial body microenvironment. *Am J Respir Cell Mol Biol.* Aug;39(2):180-9.

Diamond JM. (1979) Osmotic water flow in leaky epithelia. *J Membr Biol.* Dec 31;51(3-4):195-216.

Ding C, Potter ED, Qiu W, Coon SL, Levine MA, Guggino SE. (1997). Cloning and widespread distribution of the rat rod-type cyclic nucleotide-gated cation channel. *Am J Physiol.* Apr;272(4 Pt 1):C1335-44.

Dobbs LG (1990). Isolation and culture of alveolar type II cells. *Am J Physiol.* Apr;258(4 Pt 1):L134-47.

Dobbs LG, Gonzalez R, Matthay MA, Carter EP, Allen L, Verkman AS. (1998). Highly water-permeable type I alveolar epithelial cells confer high water permeability between the airspace and vasculature in rat lung. *Proc Natl Acad Sci U S A.* Mar 17;95(6):2991-6.

Dobbs LG, Gonzalez R, Matthay MA, Carter EP, Allen L, Verkman AS. (1998). Highly water-permeable type I alveolar epithelial cells confer high water permeability between the airspace and vasculature in rat lung. *Proc Natl Acad Sci U S A.* Mar 17;95(6):2991-6.

Dobbs LG, Johnson MD. (2007). Alveolar epithelial transport in the adult lung. *Respir Physiol Neurobiol.* Dec 15;159(3):283-300.

Dobbs LG, Williams MC, Brandt AE. (1985) Changes in biochemical characteristics and pattern of lectin binding of alveolar type II cells with time in culture. *Biochim Biophys Acta*. Jul 30;846(1):155-66.

Dobbs LG. (1989). Pulmonary surfactant. *Annu Rev Med*. ;40:431-46.

Eaton DC, Helms MN, Koval M, Bao HF, Jain L. (2009) The Contribution of Epithelial Sodium Channels to Alveolar Function in Health and Disease. *Annu Rev Physiol*. 71:10.1-10.21.

Evans MJ, Cabral LJ, Stephens RJ, Freeman G. (1975). Transformation of alveolar type 2 cells to type 1 cells following exposure to NO₂. *Exp Mol Pathol*. Feb;22(1):142-50.

Fehrenbach H. (2001). Alveolar epithelial type II cell: defender of the alveolus revisited. *Respir Res*. 2(1):33-46.

Fesenko EE, Kolesnikov SS, Lyubarsky AL. (1985). Induction by cyclic GMP of cationic conductance in plasma membrane of retinal rod outer segment. *Nature*. Jan 24-30;313(6000):310-3.

Fisher DJ, Heymann MA, Rudolph AM. (1980). Myocardial oxygen and carbohydrate consumption in fetal lambs in utero and in adult sheep. *Am J Physiol*. Mar;238(3):H399-405.

Flynn AN, Buret AG. (2008). Tight junctional disruption and apoptosis in an in vitro model of *Citrobacter rodentium* infection. *Microb Pathog*. Aug;45(2):98-104.

Folkesson HG, Matthay MA. (2006). Alveolar epithelial ion and fluid transport: recent progress. *Am J Respir Cell Mol Biol*. 2006 Jul;35(1):10-9.

Folkesson HG, Norlin A, Baines DL. (1998). Salt and water transport across the alveolar epithelium in the developing lung: correlations between function and recent molecular biology advances (Review). *Int J Mol Med*. Nov;2(5):515-31.

Frömter E, Diamond J. (1972). Route of passive ion permeation in epithelia. *Nat New Biol*. Jan 5;235(53):9-13.

Frömter E. (1972). The route of passive ion movement through the epithelium of Necturus gallbladder. *J Membr Biol*. 8(3):259-301.

Fu XW, Nurse CA, Wang YT, Cutz E. (1999) Selective modulation of membrane currents by hypoxia in intact airway chemoreceptors from neonatal rabbit. *J Physiol*. Jan 1;514 (Pt 1):139-50.

Fu XW, Wang D, Nurse CA, Dinauer MC, Cutz E. (2000). NADPH oxidase is an O₂ sensor in airway chemoreceptors: evidence from K⁺ current modulation in wild-type and oxidase-deficient mice. *Proc Natl Acad Sci U S A*. Apr 11;97(8):4374-9.

Girod CE, Shin DH, Geraci MW, Warren HB, Dobbs LG, Gao B, Rainer JS, Bauer AK, Ikegami M, Shannon JM, Miller YE. (1999). Surfactant protein C promoter-driven expression of T1-alpha induces lung inflammation. *Chest*. Jul;116(1 Suppl):61S.

Gonzalez R, Yang YH, Griffin C, Allen L, Tigue Z, Dobbs L. (2005). Freshly isolated rat alveolar type I cells, type II cells, and cultured type II cells have distinct molecular phenotypes. *Am J Physiol Lung Cell Mol Physiol*. Jan;288(1):L179-89.

Griese M, Gobran LI, Rooney SA. (1991). A2 and P2 purine receptor interactions and surfactant secretion in primary cultures of type II cells. *Am J Physiol.* Aug;261(2 Pt 1):L140-7.

Gumbleton M. (2001). Caveolae as potential macromolecule trafficking compartments within alveolar epithelium. *Adv Drug Deliv Rev.* 2001 Jul 28;49(3):281-300.

Haller EM, Shelley SA, Montgomery MR, Balis JU.(1992). Immunocytochemical localization of lysozyme and surfactant protein A in rat type II cells and extracellular surfactant forms. *J Histochem Cytochem.* Oct;40(10):1491-500.

Haller T, Auktor K, Frick M, Mair N, Dietl P. (1999). Threshold calcium levels for lamellar body exocytosis in type II pneumocytes. *Am J Physiol.* Nov;277(5 Pt 1):L893-900.

Haller T, Ortmayr J, Friedrich F, Völkl H, Dietl P. (1998). Dynamics of surfactant release in alveolar type II cells. *Proc Natl Acad Sci U S A.* Feb 17;95(4):1579-84.

Hamill OP, Marty A, Neher E, Sakmann B, Sigworth FJ. (1981). Improved patch-clamp techniques for high-resolution current recording from cells and cell-free membrane patches. *Pflugers Arch.* Aug;391(2):85-100.

Hamill OP, Marty A, Neher E, Sakmann B, Sigworth FJ. (1981). Improved patch-clamp techniques for high-resolution current recording from cells and cell-free membrane patches. *Pflügers Archiv* 391 (2): 85-100.

Harkins AB, Kurebayashi N, Baylor SM (1983). Resting myoplasmic free calcium in frog skeletal muscle fibers estimated with fluo-3. *Biophys J.* Aug;65(2):865-81.

Helms MN, Jain L, Self JL, Eaton DC. (2008). Redox regulation of epithelial sodium channels examined in alveolar type 1 and 2 cells patch-clamped in lung slice tissue. *J Biol Chem*. 2008 Aug 15;283(33):22875-83.

Helms MN, Self J, Bao HF, Job LC, Jain L, Eaton DC. (2006). Dopamine activates amiloride-sensitive sodium channels in alveolar type I cells in lung slice preparations. *Am J Physiol Lung Cell Mol Physiol*. Oct;291(4):L610-8.

Hollingsworth M, Gilfillan AM. (1984). The pharmacology of lung surfactant secretion. *Pharmacol Rev*. Jun;36(2):69-90. Review.

Hummeler E, Barker P, Gatz J, Beermann F, Verdumo C, Schmidt A, Boucher R, Rossier BC. (1996). Early death due to defective neonatal lung liquid clearance in alpha-ENaC-deficient mice. *Nat Genet*. Mar;12(3):325-8.

Hummeler E, Barker P, Gatz J, Beermann F, Verdumo C, Schmidt A, Boucher R, Rossier BC. (1996). Early death due to defective neonatal lung liquid clearance in alpha-ENaC-deficient mice. *Nat Genet*. Mar;12(3):325-8.

Ichimura H, Parthasarathi K, Lindert J, Bhattacharya J. (2006). Lung surfactant secretion by interalveolar Ca²⁺ signaling. *Am J Physiol Lung Cell Mol Physiol*. Oct;291(4):L596-601.

Isakson BE, Evans WH, Boitano S. (2001). Intercellular Ca²⁺ signaling in alveolar epithelial cells through gap junctions and by extracellular ATP. *Am J Physiol Lung Cell Mol Physiol*. Feb;280(2):L221-8.

Isakson BE, Seedorf GJ, Lubman RL, Evans WH, Boitano S. (2003). Cell-cell communication in heterocellular cultures of alveolar epithelial cells. *Am J Respir Cell Mol Biol*. Nov;29(5):552-61.

Jain L, Chen XJ, Ramosevac S, Brown LA, Eaton DC. (2001). Expression of highly selective sodium channels in alveolar type II cells is determined by culture conditions. *Am J Physiol Lung Cell Mol Physiol.* Apr;280(4):L646-58.

Johnson MD, Bao HF, Helms MN, Chen XJ, Tigue Z, Jain L, Dobbs LG, Eaton DC. (2006). Proc Natl Acad Sci U S A. Functional ion channels in pulmonary alveolar type I cells support a role for type I cells in lung ion transport. Mar 28;103(13):4964-9.

Johnson MD, Widdicombe JH, Allen L, Barbry P, Dobbs LG. (2002). Alveolar epithelial type I cells contain transport proteins and transport sodium, supporting an active role for type I cells in regulation of lung liquid homeostasis. *Proc Natl Acad Sci U S A.* 2002 Feb 19;99(4):1966-71.

Jost A, Policard A. (1948). Contribution experimentale a l'etude du developpement prenatal du poumon chez le lapin. *Arch. Anat. Microsc.* 32:323-332.

Junor RW, Benjamin AR, Alexandrou D, Guggino SE, Walters DV. (1999). A novel role for cyclic nucleotide-gated cation channels in lung liquid homeostasis in sheep. *J Physiol.* Oct 1;520 Pt 1:255-60.

Junor RW, Benjamin AR, Alexandrou D, Guggino SE, Walters DV. (2000). Lack of a role for cyclic nucleotide gated cation channels in lung liquid absorption in fetal sheep. *J Physiol.* Mar 1;523 Pt 2:493-502.

Kaarteenaho-Wiik R, Soini Y. (2008). Claudin -1, -2, -3, -4, -5, and -7 in Usual Interstitial Pneumonia and Sarcoidosis. *J Histochem Cytochem.* Mar;57(3):187-95.

Kao JP, Harootunian AT, Tsien RY (1989). Photochemically generated cytosolic calcium pulses and their detection by fluo-3. *J Biol Chem.* May 15;264(14):8179-84.

Kashuba VI, Kvasha SM, Protopopov AI, Gizatullin RZ, Rynditch AV, Wahlestedt C, Wasserman WW, Zabarovsky ER. (2001). Initial isolation and analysis of the human Kv1.7 (KCNA7) gene, a member of the voltage-gated potassium channel gene family. *Gene.* May 2;268(1-2):115-22.

Katyal SL, Singh G, Locker J. (1992). Characterization of a second human pulmonary surfactant-associated protein SP-A gene. *Am J Respir Cell Mol Biol.* 1992 Apr;6(4):446-52.

Kemp PJ, Boyd CA. (1992). Pathways for glucose transport in type II pneumocytes freshly isolated from adult guinea pig lung. *Am J Physiol.* Nov;263(5 Pt 1):L612-6.

Kemp PJ, Kim KJ, Borok Z, Crandall ED. (2001). Re-evaluating the Na(+) conductance of adult rat alveolar type II pneumocytes: evidence for the involvement of cGMP-activated cation channels. *J Physiol.* 2001 Nov 1;536(Pt 3):693-701.

Kemp PJ, Kim KJ. (2004). Spectrum of ion channels in alveolar epithelial cells: implications for alveolar fluid balance. *Am J Physiol Lung Cell Mol Physiol.* Sep;287(3):L460-4. Review.

Kemp PJ, MacGregor GG, Olver RE. (1993). G protein-regulated large-conductance chloride channels in freshly isolated fetal type II alveolar epithelial cells. *Am J Physiol.* Oct;265(4 Pt 1):L323-9.

Kemp PJ, Olver RE. (1996). G protein regulation of alveolar ion channels: implications for lung fluid transport. *Exp Physiol*. May;81(3):493-504. Review.

Kemp PJ, Peers C. (2007). Oxygen sensing by ion channels. *Essays Biochem*. 2007;43:77-90. Review.

Khakh BS, North RA. (2006). P2X receptors as cell-surface ATP sensors in health and disease. *Nature*. Aug 3;442(7102):527-32.

Kim KJ, Borok Z, Ehrhardt C, Willis BC, Lehr CM, Crandall ED. (2005). Estimation of paracellular conductance of primary rat alveolar epithelial cell monolayers. *J Appl Physiol*. Jan;98(1):138-43.

Koefoed-Johnsen V and Ussing HH. (1958). The nature of the frog skin potential. *Acta Physiol Scand*. Jun 2;42(3-4):298-308.

Koval M. (2002). Sharing signals: connecting lung epithelial cells with gap junction channels. *Am J Physiol Lung Cell Mol Physiol*. Nov;283(5):L875-93.

Krogh A (1919). The supply of oxygen to the tissues and the regulation of the capillary circulation. *J Physiol*. May 20;52(6):457-74.

Kuebler WM, Ying X, Singh B, Issekutz AC, Bhattacharya J. (1999). Pressure is proinflammatory in lung venular capillaries. *J Clin Invest*. Aug;104(4):495-502.

Kuebler WM, Ying X, Bhattacharya J. (2002). Pressure-induced endothelial Ca(2+) oscillations in lung capillaries. *Am J Physiol Lung Cell Mol Physiol*. May;282(5):L917-23.

Kuebler WM, Parthasarathi K, Lindert J, Bhattacharya J. (2007). Real-time lung microscopy. *J Appl Physiol*. 2007 Mar;102(3):1255-64. Review.

Lagercrantz H, Bistoletti P. (1977). *Pediatr Res*. Catecholamine release in the newborn infant at birth. Aug;11(8):889-93.

Langbein L, Grund C, Kuhn C, Praetzel S, Kartenbeck J, Brandner JM, Moll I, Franke WW. (2002). Tight junctions and compositionally related junctional structures in mammalian stratified epithelia and cell cultures derived therefrom. *Eur J Cell Biol*. Aug;81(8):419-35.

Lee B, Yoon SY, Fissore RA. (2006). Regulation of fertilization-initiated $[Ca^{2+}]_i$ oscillations in mammalian eggs: a multi-pronged approach. *Semin Cell Dev Biol*. Apr;17(2):274-84.

Leslie CC, McCormick-Shannon K, Shannon JM, Garrick B, Damm D, Abraham JA, Mason RJ. (1997). Heparin-binding EGF-like growth factor is a mitogen for rat alveolar type II cells. *Am J Respir Cell Mol Biol*. Apr;16(4):379-87.

Levis RA, Rae JL. (1993). The use of quartz patch pipettes for low noise single channel recording. *Biophys J*. Oct;65(4):1666-77.

Liebler JM, Borok Z, Li X, Zhou B, Sandoval AJ, Kim KJ, Crandall ED. (2004). Alveolar epithelial type I cells express beta2-adrenergic receptors and G-protein receptor kinase 2. *J Histochem Cytochem*. Jun;52(6):759-67.

Li T, Folkesson HG. (2006). RNA interference for alpha-ENaC inhibits rat lung fluid absorption in vivo. *Am J Physiol Lung Cell Mol Physiol*. Apr;290(4):L649-L660.

Lindert J, Perlman CE, Parthasarathi K, Bhattacharya J. (2007). Chloride-dependent secretion of alveolar wall liquid determined by optical-sectioning microscopy. *Am J Respir Cell Mol Biol*. Jun;36(6):688-96.

Liu L, Wang M, Fisher AB, Zimmerman UJ. (1996). Involvement of annexin II in exocytosis of lamellar bodies from alveolar epithelial type II cells. *Am J Physiol.* Apr;270(4 Pt 1):L668-76.

Liu X, Driskell RR, Engelhardt JF. (2006). Stem cells in the lung. *Methods Enzymol.* 2006;419:285-321. Review.

Low FN. (1952). Electron microscopy of the rat lung. *Anat Rec.* Aug;113(4):437-49

Lu Q, Harrington EO, Rounds S. (2005). Apoptosis and lung injury. *Keio J Med.* Dec;54(4):184-9. Review.

Lubman RL, Danto SI, Crandall ED. (1989). Evidence for active H⁺ secretion by rat alveolar epithelial cells. *Am J Physiol.* 1989 Dec;257(6 Pt 1):L438-45.

Lumb A. (2005). *Nunn's Applied Respiratory Physiology*, 6th edition. Butterworth-Heinemann

MacGregor GG, Olver RE, Kemp PJ. (1994). Amiloride-sensitive Na⁺ channels in fetal type II pneumocytes are regulated by G proteins. *Am J Physiol.* Jul;267(1 Pt 1):L1-8.

Mairbäurl H, Mayer K, Kim KJ, Borok Z, Bärtsch P, Crandall ED (2002). Hypoxia decreases active Na transport across primary rat alveolar epithelial cell monolayers. *Am J Physiol Lung Cell Mol Physiol.* Apr;282(4):L659-65.

Martín-Padura I, Lostaglio S, Schneemann M, Williams L, Romano M, Fruscella P, Panzeri C, Stoppacciaro A, Ruco L, Villa A, Simmons D, Dejana E. (1998). Junctional adhesion molecule, a novel member of the immunoglobulin

superfamily that distributes at intercellular junctions and modulates monocyte transmigration. *J Cell Biol.* Jul 13;142(1):117-27.

Mason HS, Bourke S, Kemp PJ. Pharmacol. Selective modulation of ligand-gated P2X purinoceptor channels by acute hypoxia is mediated by reactive oxygen species. (2004). *Mol Pharmacol.* Dec;66(6):1525-35.

Mason RJ, Williams MC. (1977). Type II alveolar cell. Defender of the alveolus. *Am Rev Respir Dis.* 1977 Jun;115(6 Pt 2):37-47.

Matalon S, Kirk KL, Bubien JK, Oh Y, Hu P, Yue G, Shoemaker R, Cragoe EJ Jr, Benos DJ. (1992). Immunocytochemical and functional characterization of Na⁺ conductance in adult alveolar pneumocytes. *Am J Physiol.* May;262(5 Pt 1):C1228-38.

McElroy MC, Kasper M. (2004) The use of alveolar epithelial type I cell-selective markers to investigate lung injury and repair. *Eur Respir J.* Oct;24(4):664-73. Review.

Mills JW, Ernst SA, DiBona DR. (1977). Localization of Na⁺-pump sites in frog skin. *J Cell Biol.* Apr;73(1):88-110.

Minsky M. (1961). "Microscope apparatus." U.S. Patent #3,013,476 -----1988. Memoir on inventing the confocal scanning microscope. *Scanning* 10: 128-138.

Moessinger AC, Harding R, Adamson TM, Singh M, Kiu GT. (1990). Role of lung fluid volume in growth and maturation of the fetal sheep lung. *J Clin Invest.* Oct;86(4):1270-7.

Molecular Probes, technical notes MP0525, April 2001 revisions.

Morita K, Tsukita S, Miyachi Y. (2004). Tight junction-associated proteins (occludin, ZO-1, claudin-1, claudin-4) in squamous cell carcinoma and Bowen's disease. *Br J Dermatol.* Aug;151(2):328-34.

Mukhopadhyay S, Dutta-Roy AK, Fyfe GK, Olver RE, Kemp PJ. (1998). G protein-coupled prostaglandin receptor modulates conductive Na⁺ uptake in lung apical membrane vesicles. *Am J Physiol.* Apr;274(4 Pt 1):L567-72.

Murer H, Hopfer U, Kinne R. (1976). Sodium/proton antiport in brush-border-membrane vesicles isolated from rat small intestine and kidney. *Biochem J.* Mar 15;154(3):597-604.

Nagle JF, Mathai JC, Zeidel ML, Tristram-Nagle S. (2008). *J Gen Physiol.* Jan;131(1):77-85. Theory of passive permeability through lipid bilayers.

Nicholas TE, Barr HA. (1983). The release of surfactant in rat lung by brief periods of hyperventilation. *Respir Physiol.* Apr;52(1):69-83.

Nitta T, Hata M, Gotoh S, Seo Y, Sasaki H, Hashimoto N, Furuse M, Tsukita S. (2003). Size-selective loosening of the blood-brain barrier in claudin-5-deficient mice. *J Cell Biol.* May 12;161(3):653-60.

Norlin A, Folkesson HG. (2001). Alveolar fluid clearance in late-gestational guinea pigs after labor induction: mechanisms and regulation. *Am J Physiol Lung Cell Mol Physiol.* Apr;280(4):L606-16.

North RA, (2002). Molecular physiology of P2X receptors. *Physiol Rev* 82: 1013-1067.

O'Brodovich H. (1996) Immature epithelial Na⁺ channel expression is one of the pathogenetic mechanisms leading to human neonatal respiratory distress syndrome. *Proc Assoc Am Physicians*. Sep;108(5):345-55. Review.

O'Brodovich H. (2001). Pulmonary edema fluid movement within the lung. *Am J Physiol Lung Cell Mol Physiol*. Dec;281(6):L1324-6. Review.

Ogden, D. and Stanfield, P. (1994) Chapter 4 Patch clamp techniques for single channel and whole-cell recording. *Microelectrode techniques: The Plymouth Workshop handbook* . page 52-78.

O'Grady SM, Lee SY. (2003). Chloride and potassium channel function in alveolar epithelial cells. *Am J Physiol Lung Cell Mol Physiol*. May;284(5):L689-700.

Olivera W, Ridge K, Wood LD, Sznajder JI. (1994). Active sodium transport and alveolar epithelial Na-K-ATPase increase during subacute hyperoxia in rats. *Am J Physiol*. May;266(5 Pt 1):L577-84.

Olver RE, Robinson EJ. (1986). Sodium and chloride transport by the tracheal epithelium of fetal, new-born and adult sheep. *J Physiol*. Jun;375:377-90.

Olver RE, Strang LB. (1974). Ion fluxes across the pulmonary epithelium and the secretion of lung liquid in the foetal lamb. *J Physiol*. Sep;241(2):327-57.

Olver RE, Walters DV, Wilson SM. (2004). Developmental regulation of lung liquid transport. *Annu Rev Physiol*. 66:77-101.

Palmer LG. (1984). Voltage-dependent block by amiloride and other monovalent cations of apical Na channels in the toad urinary bladder. *J Membr Biol*. 80(2):153-65.

Panos RJ, Rubin JS, Csaky KG, Aaronson SA, Mason RJ. (1993). Keratinocyte growth factor and hepatocyte growth factor/scatter factor are heparin-binding growth factors for alveolar type II cells in fibroblast-conditioned medium. *J Clin Invest.* Aug;92(2):969-77.

Papadopoulos NG, Dedoussis GV, Spanakos G, Gritzapis AD, Baxevanis CN, Papamichail M. (1994). An improved fluorescence assay for the determination of lymphocyte-mediated cytotoxicity using flow cytometry. *J Immunol Methods.* Dec 28;177(1-2):101-11.

Park DS, Cohen AW, Frank PG, Razani B, Lee H, Williams TM, Chandra M, Shirani J, De Souza AP, Tang B, Jelicks LA, Factor SM, Weiss LM, Tanowitz HB, Lisanti MP. (2003). Caveolin-1 null (-/-) mice show dramatic reductions in life span. *Biochemistry.* Dec 30;42(51):15124-31.

Parrish AR, Gandolfi AJ, Brendel K. (1995). Precision-cut tissue slices: applications in pharmacology and toxicology. *Life Sci.* ;57(21):1887-901.

Pattle RE. (1955). Properties, function and origin of the alveolar lining layer. *Nature.* Jun 25;175(4469):1125-6.

Pediani JD, McGrath JC, Wilson SM. (1999) P2Y receptor-mediated Ca²⁺ signalling in cultured rat aortic smooth muscle cells. *Br J Pharmacol.* Apr;126(7):1660-6.

Perlman CE, Bhattacharya J. (2007) Alveolar expansion imaged by optical sectioning microscopy. *J Appl Physiol.* Sep;103(3):1037-44.

Petran M, Hadravsky M, Egger M D, Galambos R. (1968). Tandem scanning reflected light microscope. *J. Opt. Soc. Am. A.* 58: 661-664.

Pickard L, Noël J, Duckworth JK, Fitzjohn SM, Henley JM, Collingridge GL, Molnar E. (2001) Transient synaptic activation of NMDA receptors leads to the insertion of native AMPA receptors at hippocampal neuronal plasma membranes. *Neuropharmacol* Nov;41(6):700-13.

Pitkänen O, Tanswell AK, Downey G, O'Brodvich H. (1996). Increased Po₂ alters the bioelectric properties of fetal distal lung epithelium. *Am J Physiol.* Jun;270(6 Pt 1):L1060-6.

Possmayer F. (1988). A proposed nomenclature for pulmonary surfactant-associated proteins. *Am Rev Respir Dis.* 1988 Oct;138(4):990-8.

Potter EL, Bohlender GP. (1941). Intrauterine respiration in relation to development of fetal lung. *Am. J. Obstet. Gynecol.* 42:14-22.

Qiao R, Zhou B, Liebler JM, Li X, Crandall ED, Borok Z. (2003). Identification of three genes of known function expressed by alveolar epithelial type I cells. *Am J Respir Cell Mol Biol.* 2003 Jul;29(1):98-105.

Ramminger SJ, Baines DL, Olver RE, Wilson SM. (2000). The effects of PO₂ upon transepithelial ion transport in fetal rat distal lung epithelial cells. *J Physiol.* Apr 15;524 Pt 2:539-47.

Rajasekaran SA, Beyenbach KW, Rajasekaran AK. (2008). Interactions of tight junctions with membrane channels and transporters. *Biochim Biophys Acta.* Mar;1778(3):757-69.

Ralevic V, Burnstock G. (1998). Receptors for purines and pyrimidines. *Pharmacol Rev.* 1998 Sep;50(3):413-92.

Ramirez MI, Millien G, Hinds A, Cao Y, Seldin DC, Williams MC. (2003). Alterations in gene expression in T1 alpha null lung: a model of deficient alveolar sac development. *Dev Biol.* Apr 1;256(1):61-72.

Ramsden CA, Markiewicz M, Walters DV, Gabella G, Parker KA, Barker PM, Neil HL. (1992). Liquid flow across the epithelium of the artificially perfused lung of fetal and postnatal sheep. *J Physiol.* Mar;448:579-97.

Razani B, Wang XB, Engelman JA, Battista M, Lagaud G, Zhang XL, Kneitz B, Hou H Jr, Christ GJ, Edelmann W, Lisanti MP. (2002). Caveolin-2-deficient mice show evidence of severe pulmonary dysfunction without disruption of caveolae. *Mol Cell Biol.* Apr;22(7):2329-44.

Rice WR, Burton FM, Fiedeldey DT. (1995). Respiratory distress syndrome for the practicing pediatrician. *Am J Respir Cell Mol Biol.* Jan;12(1):27-32.

Richmond SA, Irving AJ, Molnar E, McIlhinney RA, Michelangeli F, Henley JM, Collingridge GL. (1996). Localization of the glutamate receptor subunit GluR1 on the surface of living and within cultured hippocampal neurons. *Neuroscience.* Nov;75(1):69-82.

Saleeby MG, Vustar M, Algren J. (2003) Tracheal agenesis: a rare disease with unique airway considerations. *Anesth Analg.* Jul;97(1):50-2,

Foder B, Scharff O. (1992) Solitary calcium spike dependent on calmodulin and plasma membrane Ca²⁺ pump. *Cell Calcium.* Oct;13(9):581-91.

Schlüter H, Moll I, Wolburg H, Franke WW. (2007). The different structures containing tight junction proteins in epidermal and other stratified epithelial cells, including squamous cell metaplasia. *Eur J Cell Biol.* Dec;86(11-12):645-55.

Schmidt-Nielsen, B. (1995) August and Marie Krogh: Lives in Science, American Physiological Society Book.

Schneeberger EE, McCarthy KM. (1986). Cytochemical localization of Na⁺-K⁺-ATPase in rat type II pneumocytes. *J Appl Physiol*. May;60(5):1584-9.

Schneeberger EE, Walters DV, Olver RE. (1978). Development of intercellular junctions in the pulmonary epithelium of the foetal lamb. *J Cell Sci*. Aug;32:307-24.

Schneider GT, Cook DI, Gage PW, Young JA. (1985). Voltage sensitive, high-conductance chloride channels in the luminal membrane of cultured pulmonary alveolar (type II) cells. *Pflugers Arch*. 1985 Aug;404(4):354-7.

Schwiebert EM, Potter ED, Hwang TH, Woo JS, Ding C, Qiu W, Guggino WB, Levine MA, Guggino SE. (1997). cGMP stimulates sodium and chloride currents in rat tracheal airway epithelia. *Am J Physiol*. Mar;272(3 Pt 1):C911-22.

Shin K, Fogg VC, Margolis B. (2006). Tight junctions and cell polarity. *Annu Rev Cell Dev Biol*. 22:207-35. Review.

Skou JC. (1957). The influence of some cations on an adenosine triphosphatase from peripheral nerves. *Biochim Biophys Acta*. Feb;23(2):394-401.

Skou JC. (1974). The influence of some cations on an adenosine triphosphatase from peripheral nerves. *Biochim Biophys Acta*. Feb;23(2):394-401.

Skou JC, Esmann M. (1992). The Na,K-ATPase. *J Bioenerg Biomembr*. Jun;24(3):249-61.

Spitz L. (2007). Oesophageal atresia. *Orphanet J Rare Dis.* May 11;2:24. Review.

Spring KR. (1983). Fluid transport by gallbladder epithelium. *J Exp Biol.* Sep;106:181-94. Review.

Spring KR. (1999) Epithelial Fluid Transport--A Century of Investigation. *News Physiol Sci.* Jun;14:92-98.

Stone KC, Mercer RR, Gehr P, Stockstill B, Crapo JD. (1992). Allometric relationships of cell numbers and size in the mammalian lung. *Am J Respir Cell Mol Biol.* Feb;6(2):235-43.

Tortora GJ, Graaboski S. (1996). *Principles of Anatomy and Physiology*, 8th Revised Edition. John Wiley & Sons Inc.

Tsien RW. (1983). Calcium channels in excitable cell membranes. *Annu Rev Physiol.* 45:341-58. Review

Tsukita S, Furuse M. (2000). The structure and function of claudins, cell adhesion molecules at tight junctions. *Ann N Y Acad Sci.* 2000;915:129-35. Review.

Tsukita S, Furuse M, Itoh M. (2001). Multifunctional strands in tight junctions. *Nat Rev Mol Cell Biol.* Apr;2(4):285-93.

Umachandran M, Howarth J, Ioannides C. (2004). Metabolic and structural viability of precision-cut rat lung slices in culture. *Xenobiotica.* Aug;34(8):771-80.

Van Itallie CM, Anderson JM. (2006). Claudins and epithelial paracellular transport. *Annu Rev Physiol.* 68:403-29.

Verkman AS. (1998). Role of aquaporin water channels in kidney and lung. *Am J Med Sci.* Nov;316(5):310-20.

Vickers AE, Fisher RL. (2004). Organ slices for the evaluation of human drug toxicity. *Chem Biol Interact.* Nov 1;150(1):87-96. Review.

Vornov JJ, Tasker RC, Coyle JT. (1991). Direct observation of the agonist-specific regional vulnerability to glutamate, NMDA, and kainate neurotoxicity in organotypic hippocampal cultures. *Exp Neurol.* Oct;114(1):11-22.

Wadsworth SJ, Spitzer AR, Chander A. (1997). Ionic regulation of proton chemical (pH) and electrical gradients in lung lamellar bodies. *Am J Physiol.* Aug;273(2 Pt 1):L427-36.

Walters DV, Olver RE. (1978). The role of catecholamines in lung liquid absorption at birth. *Pediatr Res.* 1978 Mar;12(3):239-42.

Walters DV. (2002) Lung lining liquid -the hidden depths. The 5th Nils W. Svenningsen memorial lecture. *Biol Neonate.* 2002;81 Suppl 1:2-5.

Wang F, Daugherty B, Keise LL, Wei Z, Foley JP, Savani RC, Koval M. (2003). Heterogeneity of claudin expression by alveolar epithelial cells. *Am J Respir Cell Mol Biol.* Jul;29(1):62-70.

Wang SQ, Wei C, Zhao G, Brochet DX, Shen J, Song LS, Wang W, Yang D, Cheng H. (2004). Imaging microdomain Ca²⁺ in muscle cells. *Circ Res.* Apr 30;94(8):1011-22. Review.

Weibel E R, Taylor C R (1988) Design and structure of the human lung. In: *Pulmonary Diseases and Disorders, Vol 1.* Ed: AP Fishman, McGraw-Hill Book Company, New York 11-60, second edition

West JB. (2000). *Respiratory Physiology: The Essentials* 6th edition. Lippincott Williams and Wilkins.

Whittam R, Ager ME. (1964). Vectorial aspects of adenosine-triphosphatase activity in erythrocyte membranes. *Biochem J*. Nov;93(2):337-48.

Williams MC. (2003). Alveolar type I cells: molecular phenotype and development. *Annu Rev Physiol*. ;65:669-95.

Wilson SM, Olver RE, Walters DV. (2007). Developmental regulation of luminal lung fluid and electrolyte transport. *Respir Physiol Neurobiol*. Dec 15;159(3):247-55.

Wilson T, Sheppard CJR, (1984). *Theory and practice of scanning optical microscope*. Academic Press, London.

Ying X, Minamiya Y, Fu C, Bhattacharya J. (1996) Ca²⁺ waves in lung capillary endothelium. *Circ Res*. Oct;79(4):898-908. Erratum in: *Circ Res* 1996 Dec;79(6):1218.

Youngson C, Nurse C, Yeger H, Cutz E. (1993). Oxygen sensing in airway chemoreceptors. *Nature*. Sep 9;365(6442):153-5.

Zhang L, Sanderson MJ. (2003). The role of cGMP in the regulation of rabbit airway ciliary beat frequency. *J Physiol*. Sep 15;551(Pt 3):765-76.

Zhang XL, Danto SI, Borok Z, Eber JT, Martín-Vasallo P, Lubman RL. (1997) Identification of Na(+)-K(+)-ATPase beta-subunit in alveolar epithelial cells. *Am J Physiol*. Jan;272(1 Pt 1):L85-94.

Appendix

Publications and awards.

Articles.

Bourke S, Mason HS, Borok Z, Kim KJ, Crandall ED, Kemp PJ. (2005). Development of a lung slice preparation for recording ion channel activity in alveolar epithelial type I cells. *Respir Res.* Apr 27;6:40.

Mason HS, Bourke S, Kemp PJ. (2004). Selective modulation of ligand-gated P2X purinoceptor channels by acute hypoxia is mediated by reactive oxygen species. *Mol. Pharmacol.* Dec; 66(6): 1525-35.

Abstracts.

Bourke S, Mason HS, Crandall ED, Kim KJ, Borok Z, Kemp PJ. (2003). Calcium homeostasis in identified alveolar epithelial cells: development of a novel *in situ* lung slice model. *J Physiol*; 552P, P119.

Mason HS, Bourke S, North RA, Kemp PJ. (2003). Hypoxia inhibits the ligand-gated rat P2X₂ receptor cation channel. *J Physiol*; 548P, S15.

Bourke S, Mason HS, Kim KJ, Crandall ED, Borok Z, Kemp PJ. Recording ion channel in alveolar type I cells utilizing a novel *in situ* lung slice model. *FAESB* D538;(496.1)

Mason HS, Bourke S, Kemp PJ. (2004). Hypoxic inhibition of the ligand-gated P2X₂ receptor cation channels is mediated by mitochondrial-dependant production of reactive oxygen species. *FASEB* D467;(691.9).

Awards.

1st year graduate poster prize. Leeds University, School of biomedical sciences, September 2003.

Graduate Award. Highlight in respiratory physiology, American physiological society. April 2004.